EARTHQUAKE-INDUCED INELASTIC DISPLACEMENT RATIO IN REINFORCED CONCRETE BOX GIRDER BRIDGES IN CALIFORNIA

A Thesis
Submitted to the Graduate Faculty
of the
North Dakota State University
of Agriculture and Applied Science

By

Bigya Gyawali

In Partial Fulfillment of the Requirements
for the Degree of
MASTER OF SCIENCE

Major Program:
Civil Engineering

April 2024

Fargo, North Dakota

North Dakota State University
Graduate School

Title

EARTHQUAKE-INDUCED INELASTIC DISPLACEMENT RATIO IN REINFORCED CONCRETE BOX GIRDER BRIDGES IN CALIFORNIA

By

Bigya Gyawali

The Supervisory Committee certifies that this ***disquisition*** complies with North Dakota State University's regulations and meets the accepted standards for the degree of

MASTER OF SCIENCE

SUPERVISORY COMMITTEE:

Mijia Yang, Ph.D., P.E.
Co-Chair

Zhili (Jerry) Gao, Ph.D.
Co-Chair

Long Jiang, Ph.D.

Surya Sarat Chandra Congress, Ph.D.

Approved:

04/10/2024
Date

Achintya N. Bezbaruah
Department Chair

ABSTRACT

In conventionally designed bridges, the inelastic displacement is estimated using an amplification factor (R_d) suggested by AASHTO which was developed based on Single-Degree-of-Freedom system. This study models the nonlinear behavior in different components of bridge and presents an equation of inelastic displacement ratio, C_μ, that can better predict the inelastic displacement. While AASHTO R_d closely matches C_μ corresponding to average response of different earthquakes, it does not give a reliable estimation for a wide range of earthquakes. Two equations are developed based on mean + standard deviation (SD) and mean + 3×SD to incorporate the variability in C_μ due to dynamic nature of bridge and wide range of earthquakes. Additionally, it examines the influence of connection of columns to the ground, column height, deck width, number of spans, and damping ratio on C_μ. Contrary to AASHTO suggestion, C_μ was found to be increasing with increase in damping ratio.

ACKNOWLEDGMENTS

I would like to express my sincere gratitude to my advisor, Dr. Mijia Yang, for his continuous support, guidance, and encouragement throughout the entire process of completing this thesis. His expertise, patience, and constructive feedback have been invaluable in completing this work. I am also thankful to my co-advisor, Dr. Jerry Gao, for his insightful contributions and assistance to complete this thesis work.

I also want to thank Prof. Long Jiang and Dr. Surya Sarat Chandra Congress for the interest they have shown in this study by being the examining committee members and for the helpful comments.

I am grateful to my advisor, co-advisor and the department of Civil, Construction and Environmental Engineering for providing me graduate teaching assistantship as a financial support for my master's study.

Special thanks to my family members including my sister and brother-in-law for their constant support, love, and understanding throughout this journey. Their encouragement has been a constant source of strength.

Lastly, I would like to acknowledge my friends and colleagues for their encouragement and support during the ups and downs of this academic endeavor. This thesis would not have been possible without the collective support and guidance of all those mentioned above.

DEDICATION

In loving memory of my dear father,

Throughout my life, you were my source of motivation. Your wisdom, encouragement, and belief in my abilities have shaped the person I am today. Though you are no longer with us, your spirit continues to inspire me every day. This thesis is dedicated to you, Dad. Your memory will forever live on in my heart.

TABLE OF CONTENTS

ABSTRACT iii

ACKNOWLEDGMENTS iv

DEDICATION v

LIST OF TABLES x

LIST OF FIGURES xii

1. INTRODUCTION AND LITERATURE REVIEW 1

1.1. Overview 1

1.2. Literature Review 4

1.3. State of Practice 8

1.4. Research Gap and Objective of Current Work 11

1.4.1. Research Gap 11

1.4.2. Limitation of the Current Approach 11

1.4.3. Objective of the Current Work 12

1.5. Structure of Thesis 13

2. BRIDGE MODELING 15

2.1. Super Structure Modeling 15

2.2. Bent Caps 16

2.2.1. Integral Bent Caps 17

2.2.2. Non-Integral Bent Caps 17

2.3. Columns 17

2.3.1. Column Effective Section Properties 18

2.3.2. Column Nonlinear Behavior 19

2.3.3. Analytical Plastic Hinge Length for Column 22

2.3.4. Column Modeling Approach 22

2.4. Boundary Conditions 23
2.4.1. Soil-Structure Interaction 23
2.4.2. Column Support 24
2.4.3. Superstructure End Restraints 26
2.5. Abutment Modeling 26
2.5.1. Significance 26
2.5.2. Types of Abutments 27
2.5.3. Abutment Model 29
2.6. Abutment Stiffness 36
2.6.1. Longitudinal Stiffness 36
2.6.2. Transverse Stiffness 39
2.6.3. Vertical Stiffness 40
2.7. Damping 40
2.7.1. Definition 40
2.7.2. Recommended Damping Ratio 41
2.7.3. Modeling of Damping in CSiBridge 42
2.8. P-Delta Effects 42
2.9. Time History Analysis 43
2.9.1. Purpose 43
2.9.2. Implementation 44
3. MODELING MATRIX 46
3.1. Bridges 46
3.1.1. OSB1 Bridge 47
3.1.2. OSB2 Bridge 56
3.1.3. R14L Bridge 60

3.1.4. R14R Bridge 65
3.1.5. Adobe Bridge 69
3.1.6. La Veta Bridge 73
3.2. Earthquake Ground Motion 79
3.3. Parametric Study 86
4. MODEL VALIDATION AND ANALYSIS 87
4.1. Model Validation 87
4.1.1. SDOF System 87
4.1.2. MDOF System 88
4.2. Analysis 90
4.2.1. OSB1 Bridge 90
4.2.2. OSB2 Bridge 92
4.2.3. R14L Bridge 94
4.2.4. R14R Bridge 97
4.2.5. Adobe Bridge 99
4.2.6. La Veta Bridge 101
5. RESULTS AND DISCUSSION 103
5.1. Comparison with AASHTO $\boldsymbol{Rd}$ Equation 103
5.2. Parametric Study 106
5.2.1. Influence of Connection of Column to the Ground 106
5.2.2. Influence of Column Height 107
5.2.3. Influence of Deck Width 108
5.2.4. Influence of Number of Spans 110
5.2.5. Influence of Damping 112
6. CONCLUSION 116

7. FUTURE WORKS 119

REFERENCES 120

LIST OF TABLES

Table		Page
2.1.	Capabilities and limitation of nonlinear models for column plastic hinge in SAP2000[34]	19
2.2.	Nonlinear models for column plastic hinge in SAP2000[34]	20
3.1.	Geometry and material strength of six different bridges	77
3.2.	Calculation of Longitudinal stiffness of the abutment	78
3.3.	Calculation of Transverse stiffness and Vertical stiffness	78
3.4.	List of 28 earthquake ground motion and their characteristics	81
3.5.	Horizontal component of earthquake obtained from PEER Ground motion Database	84
4.1.	Comparison of time period of first six modes of OSB1 bridge with literature	89
4.2.	Comparison of inelastic displacement of center of mass of OSB1 bridge with literature	89
4.3.	Maximum inelastic and elastic displacement of OSB1 bridge with pinned boundary condition	91
4.4.	Maximum inelastic and elastic displacement of OSB1 bridge with fixed boundary condition	92
4.5.	Maximum inelastic and elastic displacement of OSB2 bridge with pinned boundary condition	93
4.6.	Maximum inelastic and elastic displacement of OSB2 bridge with fixed boundary condition	94
4.7.	Maximum inelastic and elastic displacement of R14L bridge with pinned boundary condition	95
4.8.	Maximum inelastic and elastic displacement of R14L bridge with fixed boundary condition	96
4.9.	Maximum inelastic and elastic displacement of R14R bridge with pinned boundary condition	97
4.10.	Maximum inelastic and elastic displacement of R14R bridge with fixed boundary condition	98

4.11. Maximum inelastic and elastic displacement of Adobe bridge with pinned boundary condition 99

4.12. Maximum inelastic and elastic displacement of Adobe bridge with fixed boundary condition 100

4.13. Maximum inelastic and elastic displacement of La Veta bridge with pinned boundary condition 101

4.14. Maximum inelastic and elastic displacement of La Veta bridge with fixed boundary condition 102

LIST OF FIGURES

Figure		Page
2.1.	Seat-type abutment (side view)[45]	28
2.2.	Diaphragm abutment (side view)[45]	28
2.3.	Roller abutment model[34]	30
2.4.	Simplified abutment model scheme[34]	31
2.5.	Series of elements for the longitudinal response in simplified abutment model[34]	32
2.6.	General scheme of spring abutment model[34]	35
2.7.	Nonlinear Abutment model[46]	36
2.8.	Effective area of Seat and Diaphragm Abutment (SDC 2.0[46])	39
3.1.	Schematic Plan View of OSB1 bridge (drawing provided by Caltrans)	48
3.2.	Schematic Elevation view of OSB1 (Caltrans)	48
3.3.	Cross-Section detail of OSB1 bridge deck (Caltrans)	49
3.4.	Cross-section detail of column of OSB1[38]	49
3.5.	Three-dimensional model of OSB1 bridge created in CSiBridge	50
3.6.	Spine model of OSB1 bridge created in CSiBridge	51
3.7.	Simplified abutment model created in CSiBridge for OSB1 bridge	51
3.8.	Properties of OSB1 abutment link in longitudinal direction (kips-in)	53
3.9.	Properties of OSB1 abutment link in transverse direction (kips-in)	53
3.10.	Assignment of plastic hinge in column with pinned connection to the ground in CSiBridge	54
3.11.	Assignment of plastic hinge in column with fixed connection to the ground in CSiBridge	55
3.12.	Schematic Plan view of OSB2 bridge (drawing provided by Caltrans)	57
3.13.	Schematic Elevation view of OSB2 bridge (Caltrans)	57
3.14.	Cross-Section detail of OSB2 bridge deck (Caltrans)	57

3.15. Cross-section detail of OSB2 bridge column (Caltrans) 58
3.16. Spine model of OSB2 bridge created in CSiBridge 58
3.17. Properties of OSB2 abutment link in longitudinal direction (kips-in) 59
3.18. Properties of OSB2 abutment link in transverse direction (kips-in) 60
3.19. Schematic Plan view of R14L bridge (drawing provided by Caltrans) 61
3.20. Schematic Elevation view of R14L bridge (Caltrans) 61
3.21. Cross-Section detail of R14L bridge deck (Caltrans) 62
3.22. Cross-section detail of R14L bridge column (Caltrans) 62
3.23. Spine model of R14L bridge created in CSiBridge 63
3.24. Nonlinear property of R14L bridge abutment in longitudinal direction (kips-in) 64
3.25. Nonlinear property of R14L bridge abutment in transverse direction (kips-in) 64
3.26. Schematic Plan view of R14R bridge (drawing provided by Caltrans) 65
3.27. Cross-section detail of R14R bridge column (Caltrans) 66
3.28. Cross-Section detail of R14R bridge deck (Caltrans) 66
3.29. Spine model of R14R bridge created in CSiBridge 67
3.30. Nonlinear property of R14R bridge abutment in longitudinal direction (kips-in) 68
3.31. Nonlinear property of R14R bridge abutment in transverse direction (kips-in) 68
3.32. Schematic Plan view of Adobe bridge (drawing provided by Caltrans) 69
3.33. Schematic Elevation view of Adobe bridge (Caltrans) 70
3.34. Cross-Section detail of Adobe bridge deck (Caltrans) 70
3.35. Cross-section detail of Adobe bridge column (Caltrans) 70
3.36. Spine model of Adobe bridge created in CSiBridge 71
3.37. Nonlinear property of Adobe bridge abutment in longitudinal direction (kips-in) 72
3.38. Nonlinear property of Adobe bridge abutment in transverse direction (kips-in) 72
3.39. Schematic Plan view of La Veta bridge (drawing provided by Caltrans) 73

3.40. Cross-Section detail of La Veta bridge deck (Caltrans) 74

3.41. Cross-section detail of La Veta bridge column..... 74

3.42. Spine model of La Veta bridge created in CSiBridge..... 75

3.43. Nonlinear property of La Veta bridge abutment in longitudinal direction (kips-in) 75

3.44. Nonlinear property of La Veta bridge abutment in transverse direction (kips-in) 76

3.45. Three-dimensional model of OSB1 bridge with three spans for parametric study..... 86

4.1. Comparison of the inelastic displacement ratios of 5% damping SDOF system with Chopra[41] under El Centro ground motion..... 88

5.1. Inelastic displacement ratio vs. time period of first mode of two span bridges for damping ratio of 5%..... 105

5.2. Influence of boundary condition of column on inelastic displacement ratio for damping ratio of 5%..... 107

5.3. Influence of column height on inelastic displacement ratio for damping ratio of 5% 108

5.4. Influence of deck width on inelastic displacement ratio for damping ratio of 5% 110

5.5. Influence of number of spans on inelastic displacement ratio for damping ratio of 5% 111

5.6. Inelastic displacement ratio for all bridges with 1% of damping ratio 113

5.7. Inelastic displacement ratio for all bridges with 3% of damping ratio 114

5.8. Inelastic displacement ratio for all bridges with 7% of damping ratio 114

5.9. Influence of factor a with damping ratio..... 115

1. INTRODUCTION AND LITERATURE REVIEW

1.1. Overview

The earthquake-induced inelastic displacement ratio is defined as the ratio of the maximum lateral inelastic displacement demand of a structure to the maximum lateral elastic displacement demand when subjected to earthquake loading. If the structural element undergoes elastic deformation, then the corresponding deformation is called elastic displacement and the maximum deformation in the lateral direction among different components of the structure gives the maximum lateral elastic displacement. Similarly, if a structure undergoes inelastic deformation, then the respective deformation is called inelastic displacement and the maximum value among all the deformations in the horizontal direction of the structure is called the maximum lateral inelastic displacement. Seismic design guidelines generally allow structures to undergo inelastic deformations when subjected to severe earthquake ground motion. The availability of adequate earthquake time histories recorded in the past and different nonlinear analysis techniques have made the estimation of the inelastic response of structures easier. Among different nonlinear analysis methods, nonlinear time history analysis gives a better estimation of inelastic response since it is a nonlinear dynamic analysis method that considers the nonlinear behavior of the structures as well as its dynamic behavior. However, in most practical design situations, it is impractical to perform nonlinear time history analysis to determine the maximum inelastic response of a structure as the analysis itself is complicated and time-consuming. Therefore, it is necessary to use a simplified method to determine the maximum inelastic response of a structure in the event of strong earthquake ground motions.

Bridges are a critical part of the transportation system. Therefore, ensuring their structural integrity and functionality after major earthquakes is essential. However, past seismic events

have revealed their vulnerabilities since many of them were either severely damaged or collapsed. Under strong earthquakes, most bridges will inevitably exhibit nonlinear behavior[1]. The displacement, rather than force, directly impacts the damage, stability, and functionality of bridges, therefore, the explicit consideration of lateral displacement demands can improve the seismic design of new bridges and seismic assessment of the existing ones. Consequently, displacement-based or advanced performance-based design and evaluation methods are preferred over strength-based approaches[2]. To achieve predefined performance levels under the given earthquake intensities, a simple yet reliable displacement demand model is necessary to predict the maximum displacement accurately. Implementing such a model is crucial for successful performance-based design and evaluation methodologies.

Seismic framing systems should be capable of consistently absorbing and dissipating energy over numerous cycles of deformation without degradation. In conventional construction practices, the plastic hinge zones in the structural frames are the region where energy dissipation occurs. This energy dissipation is accompanied by nonlinear responses, often defined as ductility, and indicates damage to the seismic framing system. The seismic events like the 1989 Loma Prieta and 1994 Northridge earthquakes showed that the structural damage caused by earthquakes is often costly and complicated to repair[3]. The considerable economic losses resulting from these earthquakes have encouraged the earthquake engineering community to accept the principles of performance-based earthquake engineering. While the principal objective of performance-based earthquake engineering is to create structures that respond more reliably during seismic events, many engineers associate it with achieving overall enhanced performance, particularly in terms of damage control[3]. Damage control to structural elements in a building frame can be done by limiting the displacement to a predetermined level for a specified intensity

of earthquake ground motion. Since damage control is a fundamental aspect of performance-based earthquake engineering, it is essential to establish procedures for accurately estimating displacements.

In the last 30 years, the earthquake-resistant design philosophy has changed significantly. The displacement-based design has gained importance because of performance-based engineering and for economic reasons, structures were designed to perform inelastically without collapse during severe earthquake ground motions. The structures were assumed to have sufficient ductility to undergo inelastic displacement during ground motion. ATC 3-06[4] and ATC-19[5] justified this approach by proposing to estimate the design strength of a structure by scaling down the elastic strength using a response reduction factor. This factor considers the available ductility in the structure apart from its overstrength and level of redundancy. For more ductile structures, a larger value of this factor has been defined. Although this “strength-based” approach sufficiently considers the performance in severe ground motion, it fails to control the damage in a structure during less-than-severe ground motion. There is a consensus that both structural and nonstructural damage sustained during an earthquake is produced by the lateral displacement or drift of the structure[6], thus, it became important to control the drift at less-than-severe ground motions[7]. Because of this reason, this displacement-based design philosophy has gained more attention and has become an integral part, along with the strength-based design, of the fast-emerging performance-based design (PBD) approach. In PBD philosophy, structures are engineered to achieve various performance (damage) levels, corresponding to different earthquake hazard intensities[8].

1.2. Literature Review

The main objective of a displacement-based approach is to estimate the maximum displacement of the structure or its component when subjected to a given seismic event. Nonlinear time history analysis is the most accurate process for the determination of inelastic displacement while it is considered inconvenient for most design applications. Therefore, different indirect methods have been proposed to estimate the maximum displacement. Rosenblueth and Herrera[9], Gulkan and Sozen[10], Iwan[11], and so forth have proposed the equivalent linear viscous damping factor and stiffness to be used in an equivalent linearization technique. In this method, the maximum displacement is estimated as the maximum displacement of a linear elastic system with lower lateral stiffness and with higher damping coefficient than that of an inelastic system.

The displacement coefficient method and capacity spectrum method were two commonly used methods in the past to estimate the maximum inelastic displacement demand of structures, as they combine the nonlinear static analysis method with the results from the linear dynamic analysis. The capacity spectrum method is an iterative scheme to determine the demand in the nonlinear static procedure (NSP) and has been implemented in ATC-40[12]. It is based on the equivalent linearization technique developed by the researchers[9-11]. The capacity spectrum method was initially developed as a rapid assessment method for a seismic risk project at the Puget Sound Naval Shipyard for the U.S. Navy in the early 1970s[13]. Over time, this method has undergone various changes while the fundamental principles have remained unchanged. The description of the development and details of the capacity spectrum method can be found in the literature[14]. In ATC-40, the estimation of maximum inelastic displacement involves iterative analysis of a series of equivalent linear elastic systems characterized by an equivalent viscous

damping ratio and lateral stiffness equal to the secant stiffness. Both the secant stiffness and equivalent viscous damping ratio depend on the inelastic deformation.

The displacement coefficient method is based on the principle that the inelastic displacement of a yielding structure can be obtained by multiplying the spectral displacement of a linear elastic SDOF system with the displacement modification factor(s) provided that the SDOF system has the same initial stiffness and damping coefficient as the original nonlinear system. This displacement modification factor, C, also known as "inelastic displacement ratio" has been proposed by many researchers including Newmark and others ([3, 6, 14-19]. The design guidelines FEMA 273[20] FEMA 356[21], and FEMA 440[22] are also based on this displacement coefficient method to determine the displacement demand in the NSP.

The first studies on the displacement coefficient method were carried out by Veletsos and Newmark[23] and Veletsos et. al.[24] who observed that for the flexible oscillators the ratio of maximum deformation (displacement) in a nonlinear system to that in the respective linear system is unity which leads to the "equal displacement rule" and for stiff oscillators, the ratio exceeds unity. In 1971, Veletsos and Vann[25] extended the applicability of the "equal-displacement rule" to the medium frequency zone. Newmark and Hall[15] and Riddell[26] proposed a period independent of the ductility demand, above which the "equal-displacement rule" could be applied. Miranda[6] performed the study on a single degree of freedom system considering 124 earthquake ground motions recorded on rock, alluvium, and soft soil sites and found that for the short-period structures, the inelastic displacement ratio is not only period and ductility dependent, but also it is significantly influenced by site conditions. The study was performed for different levels of ductility demand μ (inelastic displacement ratio represented as C_μ). In another study, Miranda[16] found that for the sites with average shear-wave velocities

higher than 180m/s, the soil conditions have a relatively small influence on the inelastic displacement ratio.

Several researchers have proposed different equations to estimate the inelastic displacement ratio in the past. Miranda[16] computed the inelastic displacement ratios for a single-degree-of-freedom (SDOF) system with a damping ratio of 5% and subjected to 264 acceleration time histories recorded on firm sites in California. Considering three types of soil conditions with a shear-wave velocity greater than 180m/s, the author studied the effect of soil conditions, the effect of earthquake magnitude, and the effect of distance to rupture on the inelastic displacement ratio. Using the nonlinear regression analysis, the author[16] has suggested the following simplified expression: $C_\mu = \left[1 + \left(\frac{1}{\mu} - 1\right)\exp(-12T\mu^{-0.8})\right]^{-1}$ that can be used in design to estimate the mean inelastic displacement ratio for structures on firm sites where μ= displacement ductility ratio; and T= period of vibration and C_μ=inelastic displacement ratio.

Ruiz-Gracia and Miranda [27] performed a detailed study on constant relative strength inelastic displacement ratio, C_R, to estimate the maximum lateral inelastic displacement demands on existing structures from maximum lateral elastic displacement demand. A single-degree-of-freedom system was considered in the study with different levels of lateral strength normalized to the strength required to be in an elastic state when the system is subjected to earthquake ground motion. Three types of soil conditions were considered with shear wave velocity higher than 180m/s. The authors developed the following equation to estimate the constant relative strength inelastic displacement ratio which is also the ratio of maximum inelastic displacement to maximum elastic displacement: $C_R = 1 + \left[\frac{1}{a(T/T_s)^b} - \frac{1}{c}\right](R - 1)$; where R is the lateral strength ratio, T is the period of vibration of the system, T_s is the characteristic period at the site and a, b

and c are constants that also depend on the site conditions. The values of and a, b, c and T_s are given in the literature [27]. The author also studied the influencing factors on C_R including the period of vibration, level of lateral yielding strength, site conditions, earthquake magnitude, and distance to source.

In another study, Hatzigeorgiou and Beskos[28] proposed a simple and effective method to estimate inelastic displacement ratio (represented as IDR by authors) of a bilinear elastoplastic model of a single degree of freedom system subjected to repeated or multiple earthquakes. 112 real earthquake ground motions were considered and four types of soil conditions were considered in the study. The authors developed a relation between inelastic displacement ratio vs. time period, force reduction factor and also considered the effect of viscous damping ratio and the post-elastic stiffness ratio, type of the soil, and the case of seismic sequence in the developed expression. The equation of inelastic displacement ratio was $IDR = 1 + a\left(\frac{R-1}{R}\right)(T^b + R^c + d)$; where a, b, c and d are the coefficients that considers influence of damping ratio ξ, post-yield stiffness ratio H and soil type. The empirical equations for the coefficients a, b, c and d are given in the paper[28]. The author found that repeated earthquake signals have a significant influence on the inelastic displacement ratio which ultimately affects the inelastic displacement of the SDOF system. Wu et. al.[29] has also proposed an equation to determine the inelastic displacement demand of Chinese highway bridges, where the bridge was modeled as a bilinear single-degree-of-freedom system.

Bozorgnia et. al.[30] performed deterministic and probabilistic predictions of inelastic response spectra based on a comprehensive ground motion prediction equation (GMPE). This analysis showed that the scaling magnitude for an inelastic system is higher than that for an elastic system over a wide structural period range, particularly when the ductility is greater than

2 and magnitude of earthquake is greater than 6.5. The “equal displacement rule” to estimate inelastic displacement was found to be valid for small to moderate magnitude and /or for low ductility level, however, it underestimated the inelastic displacement even for the longer period structure when the earthquake magnitude was large.

Most of the studies regarding inelastic displacement ratio were done in a single degree of freedom system either considering elastic-perfectly plastic behavior or bilinear elastoplastic model. Limited studies were done by modeling the real structure of the bridge which is in fact a multiple degree freedom system and shows nonlinear behavior at different structural component levels. When a bridge is subjected to earthquake signals in multiple directions, the reinforced concrete column shows complex hysteretic behavior because of the combined action of shear, bending moment, and axial force. To study the shear-flexure interaction in bridge columns when subjected to multi directional shaking, Zhang et. al.[1] modeled 24 full-size columns and used a set of near-fault ground motions. Using nonlinear time history analysis method, the authors developed a simple yet reliable model to calculate the inelastic displacement and ductility of the bridge columns. However, this study did not consider the nonlinear behavior in abutment and the deck on the top was modeled as a rigid element to restrain it against rotation while in reality, the deck behaves elastically. Therefore, a more detailed study by modeling the complete bridge geometry including its nonlinear behavior at different component levels is needed.

1.3. State of Practice

Current code methods are based on the equal displacement rule at long periods, with ductility-dependent amplification factors used at short periods. The seismic design approach to determine the inelastic demands according to *AASHTO Guide Specifications for LRFD Seismic Bridge Design* [31] is based on the elastic analysis to estimate the inelastic demand using the

"equal displacement approximation" when the time period is longer than a characteristic site period , T^*. For the short period structures (periods shorter than T^*), AASHTO suggests that the design displacement is obtained by multiplying the displacement demand Δ_D, obtained from elastic analysis with the amplification factor, R_d.

$$R_d = \left(1 - \frac{1}{\mu}\right)\frac{T^*}{T_i} + \frac{1}{\mu} \geq 1.0 \; for \; \frac{T^*}{T_i} > 1.0 \tag{1. 1}$$

$$R_d = 1.0 \; for \frac{T^*}{T_i} \leq 1.0 \tag{1. 2}$$

in which

$$T^* = 1.25T_s = 1.25\frac{S_{D1}}{S_{DS}} \tag{1. 3}$$

μ= maximum local member displacement ductility demand

S_{DS}= the short-period acceleration coefficient and can be obtained from the design response spectrum

S_{D1}= 1-sec period acceleration coefficient and can be obtained from the design response spectrum

The design response spectrum has not been explained here. For more information about design response spectrum, AASHTO[31] can be referred. If the elastic response spectrum acceleration at time period T_i, $(SA_{EL})_{T_i}$, is known (can be obtained from design response spectrum), the inelastic displacement demand, $(SD_{INEL})_{T_i}$, can be determined using the following equation.

$$(SD_{INEL})_{T_i} = R_d\,(SD_{EL})_{T_i} = R_d\left(\frac{T_i}{2\pi}\right)^2 . g . (SA_{EL})_{T_i} \tag{1. 4}$$

where $(SD_{EL})_{T_i}$= elastic response spectrum displacement at time T_i.

The inelastic displacement demand is one of the important parameters in seismic design philosophy and is compared with displacement capacity of the structure which is as one of the

requirements in seismic design criteria. The inelastic displacement demand, $(SD_{INEL})_{T_i}$, is equivalent to maximum inelastic displacement, u_m, and $(SD_{EL})_{T_i}$ is equivalent to maximum elastic displacement, u_e. The ratio of maximum inelastic displacement and maximum elastic displacement is C_μ which is similar to AASHTO R_d. The inelastic displacement ratio has been represented by C_μ in the present research work.

Several values of μ has been suggested by AASHTO for different Seismic Design Categories [31]. For detailed analysis, $\mu = 6$ may be used[31], thus the same value has been used in this research work. And considering the upper bound value of T^*, $T^* = 1.25$ [32], R_d can be written as

$$R_d = 0.167 + \frac{1.042}{T_i} \quad (1.5)$$

The specified ground motion spectra suggested by AASHTO[31] are for 5% viscous damping; which is a reasonably conservative value. If bridges have other damping ratio, ζ, AASHTO suggests a reduction factor, R_D, to be applied to the five percent damped design spectrum coefficient used to estimate the displacement demand. The damping reduction factor R_D is expressed as.

$$R_D = \left(\frac{0.05}{\zeta}\right)^{0.4} \quad (1.6)$$

AASHTO[31] suggests that the displacement demands for bridges whose abutments are designed to fuse shall be based on a 5% damped spectrum curve unless the abutments are particularly designed for sustained soil mobilization.

1.4. Research Gap and Objective of Current Work

1.4.1. Research Gap

AASHTO R_d was developed based on single degree of freedom system. Single degree of freedom system has only one degree of freedom, however, bridge is a complex system having multiple degrees of freedom and nonlinearities at different structural component. Single degree of freedom system cannot represent those nonlinearities in bridge and displacement at the different joints of the bridge adequately. Therefore, a more reliable equation needs to be developed to accurately estimate the inelastic displacement ratio in bridges. Furthermore, limited research has been done to model the complete geometry of the bridge as well as nonlinear behavior in different structural components. Thus, a detailed study on the modeling of real bridge structures with their linear and nonlinear behavior at the structural level is necessary. This research was performed to address this research gap.

1.4.2. Limitation of the Current Approach

Huff [33] carried out a study to assess the validity of the current method i.e. AASHTO R_d for the bridges subjected to ground motions of varying duration. The author used three different methods from the literature: inelastic response history analysis, the substitute structure method, and a recent ground motion prediction model and found that each method agreed that the inelastic displacement amplification factor is strongly dependent upon the various intensity measures of ground shaking, while the current code methods from bridge design specification do not consider for this dependence.

While current seismic design methods, such as those outlined in AASHTO guidelines, provide methodologies for estimating inelastic displacement ratios, they may not fully capture the complexities of real bridge structures. Single-degree-of-freedom (SDOF) systems, upon

which current methods are based, cannot represent the multi-degree-of-freedom (MDOF) nature of bridges and the nonlinear behavior of their components. Also, AASHTO R_d does not consider the influence of various intensity measures of ground shaking on the inelastic displacement ratio. These limitations may lead to underestimation of inelastic displacement ratios, particularly for bridges subjected to a wide range of earthquake ground motions.

1.4.3. Objective of the Current Work

One of the main answers that this research is trying to respond to is how reliable the inelastic displacement ratio given by AASHTO, also known as amplification factor, R_d for the real bridge structure which is, in fact, a multi degree of freedom system (MDOF) while AASHTO R_d was developed based on single degree of freedom (SDOF) system. Also, this research is focused on suggesting a more reliable equation to predict the inelastic displacement ratio on bridges subjected to a wide range of earthquake ground motion.

This study aims to compute the inelastic displacement ratio for different bridges undergoing inelastic deformation when subjected to a relatively large number of recorded earthquake ground motions. This study aims to apply 28-time history records of earthquake signals that were recorded in California in last 55 years since the focus is on the response of bridges subjected to earthquakes that happened in recent years. Each time history records have two components and thus, those signals will be applied in the longitudinal and transverse direction of the bridge during the analysis. This study does not consider the influence of site class including type of soil, shear wave velocities, etc. Using nonlinear regression analysis, a simplified expression will be developed that allows an estimation of maximum inelastic displacement demand in bridges provided that the maximum elastic displacement demand is

known, which can be obtained from linear analysis or response spectrum curve as suggested in AASHTO.

To sum up, the primary objective of this research work is to address the limitations of the current method and propose a more reliable approach for estimating inelastic displacement ratios in bridges. The specific objectives of this research work are listed below.

- Demonstrating the potential underestimation of inelastic displacement ratio by current AASHTO R_d method across a wide range of earthquake ground motion
- Propose an alternative method to estimate inelastic displacement ratio in box girder bridges.
- Recommending an appropriate amplification or reduction factor for different damping ratios of bridges
- Performing a detailed parametric study to investigate the factors influencing the inelastic displacement ratio in bridges
- Considering a range of bridge geometries and earthquake events in California to enhance the applicability and robustness of the proposed method.

1.5. Structure of Thesis

The structure of this thesis is organized as follows:

- Chapter 1 provides an overview of the inelastic displacement ratio, its significance, the current method for estimating displacement ratio, its limitation, the research gap, and the objectives of this thesis work
- Chapter 2 outlines a detailed explanation of modeling methods for different component of the bridges. It further explains the approach to model the nonlinear

behavior in columns and abutments which are the main structural components to undergo inelastic excursion during a seismic event.

- Chapter 3 explains about the type of bridges considered in this study, selection of earthquake ground motions and the parametric study performed to investigate the parameters that influence the inelastic displacement ratio.
- Chapter 4 presents the model validation using single degree of freedom system and Ordinary Standard bridge (OSB1) model previously developed by Caltrans.
- Chapter 5 discusses the results of the research and discussion on the parametric studies.
- Chapter 6 is about the conclusion made from this research study.

2. BRIDGE MODELING

This chapter discusses the modeling method for different components of the bridges including superstructure deck section, bent cap, column, abutment modeling, boundary condition of column support, and damping. The guidelines for nonlinear analysis of bridge structures in California[34] and the guidelines for nonlinear seismic analysis of ordinary bridges: version 2.0[35] were referred to model the bridge structure as well as its linear and nonlinear behavior.

2.1. Super Structure Modeling

The guideline[35] suggests that the superstructure elements (deck and bent-cap) are modeled as linear-elastic beam-column elements, reflecting the material properties of uncracked reinforced concrete (typical for prestressed concrete). During the analysis the nonlinearities are not considered in the superstructure elements which is because the elements like columns and abutments are designed to experience inelastic behavior, whereas the superstructure is protected by capacity design principles, thus it is anticipated to remain in the elastic region[34]. The superstructure frame properties for a box-girder cross section can be directly modeled in CSiBridge as a superstructure deck section. The drawing of several bridges has been obtained from Caltrans and the bridges were modeled as per the as-built drawings.

The guideline[35] suggests that the deck is modeled as a three-dimensional spine model which comprises a series of elastic beam-column elements, defined along the centerline of the bridge deck. To represent the width of the deck section, two nodes at the end of the spine model are assigned by a transverse rigid bar whose length is equal to the width of the deck. This approach allows the consideration of the passive resistance of backfill soil distributed along the width of the deck. Based on the abutment skew angle, the orientation of the rigid bars and their widths are assigned.

Lightly reinforced sections are represented by the lower bound while heavily reinforced sections are represented by the upper bound. SDC 2004[36] suggests that the location of the prestressing steel's centroid and the direction of bending considerably influence how cracking affects the stiffness of the prestressed members and thus, stiffness reduction is not recommended for prestressed concrete box girders. In the present research, no flexural stiffness reduction has been considered for the superstructure deck section.

2.2. Bent Caps

The cap beam is a concrete element that links the superstructure with the column bents, enabling a multi-column bent bridge to withstand lateral loads or displacements, primarily applied in the transverse direction, through frame action. In the case of single-column bent bridges, the cap beam is constructed to ease the connection between the bent and the superstructure while reinforcing the joint. In case of multi-column bent bridges, the cap beam should be modeled as an elastic frame element with a solid rectangular cross section using the dimensions provided in the plan of the bridge.

The cap beam is typically joined to the superstructure through rigid or moment connections, as both elements are commonly constructed monolithically without any joints. Given that the concrete superstructure and cap beam are cast simultaneously to form a single unit, the flexural stiffness of the superstructure enhances the torsional stiffness of the cap beam. Consequently, the effective dimensions of the cap beam-superstructure system resisting torsion exceed the individual cross-sectional dimensions of the cap beam element[34].

The bent cap can be categorized into two different types: integral bent cap and non-integral bent cap.

2.2.1. Integral Bent Caps

Integral bent cap is monolithically casted with the superstructure deck section and generally has the same depth as the superstructure depth[37]. Therefore, it responds monolithically with the girder system/ deck system during dynamic excitation. The girder superstructure deck is framed into the bent cap and is supported indirectly by the bent cap. This kind of bent cap is generally used in the construction of cast-in-place concrete box girder. It can also be used in steel girder bridge to provide a longitudinal frame action. The reinforcement detailing in this type of bent cap could be challenging because of the monolithic connection of the members, therefore, the bar reinforcement should be considered carefully. Since this research is focused on reinforced concrete box girder bridges, integral bent connection has been considered in this research. The guideline[35] suggests that integral cap beam is modeled with elastic beam-column elements with very large torsional and bending (out-of-plane of bent) rigidities. Also, its connection with the central node of deck spine model is rigid. In this research work, the connection of bent with deck, and bent with column top were modeled as rigid connection by providing joint constraints.

2.2.2. Non-Integral Bent Caps

The superstructure deck section might be simply supported at the bent cap or span continuously with a separation detail such as elastomeric pad or isolation bearing between bent cap and the superstructure.

2.3. Columns

The foundation of the column is defined at the level of base fixity. Since columns are designed to undergo inelastic excursions, they are modeled as ductile element. The nonlinear material response of beam or column members can be modeled using two groups of finite

element models: 1) concentrated or lumped plasticity and 2) Distributed plasticity[34]. In the concentrated or lumped plasticity approach, the nonlinear behavior can be represented along the length L_p, which is located at the ends of the linear elastic region. The second technique is based on the displacement- or force-based formulation where the nonlinear behavior can be distributed along the length of the beam/ column element.

The guideline suggests that [34] when load is applied in the transverse direction of the bridge, the plastic hinge is expected to form at both the column top and bottom, given that rotational restraint detailing is provided at the base of the column, because of the frame action in multi-column bent bridges. The guideline further suggests that in case of the bridge with single-column bent with long-span superstructure, the plastic hinge is more likely to form at the column bottom because of the cantilever action in the transverse direction. Depending upon the boundary conditions and the torsional restraint of the superstructure ends provided by the abutment, double curvature might be developed in single-column bent when the loading is applied in the transverse direction. This could lead to the formation of plastic hinges at both the top and bottom of the column. According to the guideline[34], when the load is acting in longitudinal direction of the bridge, the nature of single and multi-column bent bridges is same and is evenly governed by the degree of foundation fixity and the frame action through the superstructure. The plastic hinge zone is assigned in the inelastic region while the rest of the element is assigned an elastic region with a solid cross-section as per the geometry and effective section properties.

2.3.1. Column Effective Section Properties

SDC 2004 section 5.6[36] suggest that the cracked flexural stiffness I_{eff} should be considered when modeling the ductile elements. The use of effective cross-sectional properties is a usual practice suggested by the ACI 318-2005 building code, considering the development of

crack in reinforcement concrete girders and column because of the gravity loads and wind loads. Due to the lateral loads including wind pressure and earthquake ground motion, column undergoes several cycles of motion and the inflection point in the column bents oscillates with respect to its original position. Because of this reason, the effective inertia of column should be considered for the entire length of the element for seismic analysis.

2.3.2. Column Nonlinear Behavior

In the current research work, discrete plastic hinge models have been used to model the nonlinearity and hysteretic behavior in columns. An approximate plastic hinge length is needed in order to convert the plastic curvature to the plastic rotation and Section 7.6.2 of SDC 2004[36] has been referred.

Different nonlinear models like Uncoupled Hinge M2,M3, Interaction PMM Hinge, Fiber PMM Hinge, NL-link-Plastic Wen, NL-Link-Multi-Linear Plastic etc. to model the column plastic hinge are explained in [34] including their capabilities and limitations are summarized in Table 2.1 and Table 2.2 below.

Table 2.1. Capabilities and limitation of nonlinear models for column plastic hinge in SAP2000[34]

Nonlinear Option	Coupled behavior M2-M3	Axial-moment interaction: P-M2-M3	Degrading behavior	Ductility estimation	Numerical stability	Low computational effort
Uncoupled Hinge M2, M3			×	×		×
Interaction PMM Hinge	×	×	×	×		×
Fiber PMM Hinge	×	×	×		×	
NL-link- Plastic Wen					×	×
NL-link-Multi-Linear Plastic			×	×	×	×

Based on the features shown in Table 2.1 and the observation in the guideline [34], it suggests the application of these nonlinear models for the following type of analysis.

Table 2.2. Nonlinear models for column plastic hinge in SAP2000[34]

Nonlinear Option	2D Pushover Analysis (L or T directions)	3D Pushover Analysis (Simultaneous L and T directions)	Dynamic 2D (THA with L, V or T, V components)	Dynamic 3D (THA-Simultaneous L, T and V components)
Uncoupled Hinge M2, M3	×			
Interaction PMM Hinge	×	×		
Fiber PMM Hinge	×	×	×	×
NL-link- Plastic Wen	×		×	
NL-link-Multi-Linear Plastic	×		×	

The authors[34] found that a fiber model (Fiber PMM in SAP2000) for different axial load levels is capable for the determination of the column behavior under an applied curvature and the cross-section's axial strain. Also, as observed in Table 2.2, among all of the nonlinear models listed, Fiber PMM Hinge is suitable for the dynamic 2D and dynamic 3D static and dynamic analysis, thus, Fiber PMM hinge has been used in the current research work to model the nonlinear behavior in column and perform the nonlinear time history analysis.

The fiber hinge calculates a relation between the moment and curvature in any bending direction for different levels of axial load throughout the static or dynamic analysis. This interaction among the biaxial moment and axial force, and distribution of the nonlinear behavior throughout the section can be generated automatically by allocating a particular stress-strain $\sigma - \varepsilon$ relationship to the individual discretized fibers in the cross-section. This stress-strain relationship corresponds to the confined concrete, unconfined concrete, and the longitudinal steel reinforcement.

The fiber hinge model is a lumped plasticity model having a characteristic length L_p, and it is assigned to an elastic/linear element at a particular point. This model can be implemented in

modal analysis, nonlinear static (pushover), and the nonlinear time history analysis with the direct integration. The concrete undergoes cracking and reinforcing steel undergoes yielding because of the flexural yielding and strain hardening which results in decrease in the stiffness, and this loss of stiffness can be represented by the fiber hinge modeling approach. This model considers the shear and torsion behavior of the cross section elastically and it can represent the degradation and softening after yielding; however, it does not consider the pinching and bond slip[34].

Each fiber in the cross-section of column and shaft is defined using the area, centroid coordinates, and the material type where the stress-strain relationship for the material is already defined. In reinforced concrete column of bridge, stress-strain relationship with degrading material strength is defined separately for the confined and unconfined concrete and the steel reinforcement. The detailed fiber hinge modeling approach has been described in the guideline[34].

In fiber section model in column, the column stiffness and strength were found to be different between CSiBridge and OpenSees, specifically, the CSiBridge model showed a greater reduction in initial stiffness than anticipated [38]. To resolve this initial column stiffness/strength issue for fiber section in CSiBridge, Caltrans has introduced a specialized column modeling approach[38] explained in section 2.3.4. In this approach, plastic regions are assigned at the rigid connection of column with the bent and ground. The plastic hinge region defines the portion of the column, pier or shaft that needs enhanced lateral confinement. The plastic hinge length can be calculated based on Seismic Design criteria (SDC) 1.7[39]. In addition, the effective flexural stiffness for column is used as $0.35I_g$ for elastic region and $3I_g$ for the plastic hinge region.

2.3.3. Analytical Plastic Hinge Length for Column

Section 7.6.2 of SDC 2004[36] gives an expression for the analytical plastic hinge length (L_p) for column. It is the equivalent length of column over which the plastic curvature is assumed constant for determining the plastic rotation[36-39].

$$L_p = \begin{cases} 0.08L + 0.15f_{ye}d_{bl} \geq 0.3f_{ye}d_{bl} & (in, ksi) \\ 0.08L + 0.022f_{ye}d_{bl} \geq 0.044f_{ye}d_{bl} & (mm, Mpa) \end{cases} \quad (2.\ 1)$$

L=column height (inch)

f_{ye}=steel yield strength (ksi)

d_{bl}= longitudinal bar size (inch)

2.3.4. Column Modeling Approach

The column modeling approach proposed by Caltrans and discussed in the work of Lu et. al. [38] has been followed in the present research work. The procedure involves the following steps:

- The column is discretized into a minimum of two elements, with one element assigned for the hinge length centered at the hinge position, and the other(s) allocated for the remaining portion of the column.
- The hinge is positioned at the midpoint of the hinge length element.
- A stiff section modifier is applied to the hinge length element by increasing its Moment of Inertia, thereby preventing the double counting of elastic deformation across the hinge length.
- Cracked section modifiers are assigned to all elements in the column except for those within the hinge region.

2.4. Boundary Conditions

2.4.1. Soil-Structure Interaction

The earthquake-induced response on bridges is significantly influenced by the dynamic response between the soil and the pile shaft of the bridge foundation. Such soil-interaction can be generally categorized into kinematic and inertial effects. The kinematic interaction is caused by the change of free-field ground motion because of the massless foundation; however, the inertial interaction is caused by the deformation of the soil due to time-variant inertia forces generated in the substructure.

It might not be feasible to consider all of the influences of the soil on the seismic response of a bridge. However, it should be well understood that soil-structure interaction creates flexibility and energy dissipation into the bridge as compared with the rigid or pinned connection assumption. The stiffness and damping of a foundation are influenced by the properties of the soil, piles and interaction between pile and pile cap. And large number of piles in bridge substructure can greatly influence the dynamic properties (section 4.2.2 of ATC 32)[40].

Following the geotechnical specifications, for Ordinary Standard bridge structures constructed in normal soil condition, the soil can be considered as rigid and thus, the soil-structure interaction can be ignored. However, in such case if a reduction in the cross section is outlined for the column base, the column base may be modeled to have semi-rigid behavior by assigning a rotational spring[34]. In case of non-conventional soil conditions in Ordinary Standard bridges, the guideline[34] suggests to define a semi-rigid connection at the column base. While performing the analysis of non-standard and important bridges like very rigid structure and with short natural time periods, the guideline suggests considering the soil-structure interaction effects. For such cases, the modal damping ratio of the soil might notably differ from

the rest of the structure, with the value ranging between 15-20% compared to 3-5%. Therefore, the classical damping is not enough and thus, not applicable for the combined soil-structure system with different damping levels and adjustment is needed in the modal damping through substructure method[41]. For considering the soil-structure interaction while modeling the bridges structures, the guidelines given in section 4.2.2 of ATC 32 can be followed.

In the present research work, the normal soil condition has been assumed for the bridges considered, thus, the underlying soil is assumed to be rigid and the soil-structure interaction has been neglected.

2.4.2. Column Support

In structural system, the definition of the boundary conditions is an important factor that influences the stiffness matrix which ultimately affects the static and dynamic response of the structure. The boundary condition should be assigned using the simplified and realistic models of the abutment and the foundation system of the bridge such that it correctly estimated the ductility capacity and the seismic demand on the major structural elements. In a dynamic analysis of the structure, the selection of boundary conditions significantly influences its modal periods, mode shapes, and other related properties.

Based on the detailing provided to the foundation, column base can be assigned with a pinned, semi-rigid, or fixed connection. Pinned connection has restraints on degrees of freedom U1, U2 and U3 corresponding to the translation while fixed connection has restraints of the degrees of freedom U1, U2, U3, R1, R2, R3 corresponding to both translation and rotation. The guideline[34] suggests that a pinned connection can be defined at the column base if a reduction in the column base (built hinge) is detailed in the multi-column bent bridge plan and in such case a rigid connection between the column top and the superstructure is also defined to ensure the

stability of the bridge under transverse loads. In case of the single-column bent bridges, the guideline[34] suggests that an idealized fixed support at the base of the column and a rigid connection between superstructure and column bent top ensures the stability of the structure in the transverse direction. The guideline further suggests verifying the boundary conditions with the geotechnical parameters of the site and assign the boundary condition to the model through joint restraint at the base of the column.

Bridge is a complex system and its displacement capacity is influenced by the elements other than the ductile members within the frame, importantly the flexibility of the column bent foundations. If the bridge shows the flexible foundations with suitable lateral restraint, a pinned connection is assigned at the column base providing the joint restraint at degrees of freedom U1, U2 and U3 corresponding to lateral and vertical translation, however the elastic or inelastic behavior of foundation is assigned at the degree of freedoms corresponding to rotations R2 and R3[34].

Whenever there is an increase in rotational stiffness, the respective degree of semi-rigidity at the base of column causes the upward movement of the point of inflection in the column when subjected to lateral load or displacement. This relocation of inflection point changes and redistributes the rotational demand on the column between top and bottom part. This results in an increase in base shear, lowers the displacement ductility of the bridge and greatly influences the other response of the bridge[34]. Because of this reason, the degree of semi-rigidity at the base of the column must be determined carefully. To model the semi-rigid connection at the column base, linear or nonlinear springs can be used[34], and geotechnical specification of the particular site is used to define the parameters. During modeling it is

necessary that the boundary conditions or the spring models should promise the stability of the bridge model in any direction during the analysis.

2.4.3. Superstructure End Restraints

The superstructure end restraint is another important boundary condition to be considered. The property of the restraint is selected and defined based on the type and characteristics of abutment provided to the bridge system. The selection of the deck end restraint will significantly influence the displacement demand on bridges; therefore, it should be selected wisely when modeling the bridge structure. There are different abutment modeling approaches available in the literature and some of them are discussed in the following section.

2.5. Abutment Modeling

2.5.1. Significance

Abutments are the type of earth-retaining structures that serve to provide unhindered traffic flow throughout the bridge. They also resist the bridge inertial loads that are developed when a bridge is subjected to an earthquake ground motion. Conventionally, the abutments are designed based on the principles of free-standing retaining walls using active and passive earth pressure theory. Although these pressure theory for abutment wall hold for most of the cases, it is not valid when an earthquake happens and the inertial load from the huge bridge system generates higher passive earth pressure than expected[42].

The post-earthquake reconnaissance reports have found out that the abutment behavior, soil-structure interaction and the embankment flexibility greatly affect the response of the bridge structure during moderate to severe seismic events[34]. Particularly, for the Ordinary Standard Bridges having short span and comparatively high superstructure stiffness, the embankment mobilization and the inelastic nature of the soil when subjected to high shear deformation control

the response of the bridge and the intermediate column bent[43]. The systematic evaluation and the dynamic behavior and response of abutment under the lateral ground motion is also important.

An appropriate abutment model should illustrate all the main resistance components and the mechanics including an accurate assessment of their mass, stiffness, and the nonlinear hysteretic behaviors. To quantify the embankment mobilization, values of embankment critical length and the mass participation have been suggested by many researchers including Kotsoglou and Pantazopouloi[43] and Werner[44]. The abutment mass participation significantly affects the mode shape and ultimately the dynamic behavior of the bridge. Also, the soil-structure interaction behind the wall of abutment and the abutment foundation also influences the abutment response[34].

2.5.2. Types of Abutments

In general, two different types of abutments are used in California: seat abutments and diaphragm abutments.

2.5.2.1. Seat abutment

Seat-type abutments provide support to bridge superstructure on a stemwall or seat. Short seat-type abutment consists of a backwall which holds the structure backfill material above seat[45] as shown in Figure 2.1 . Seat abutment is a non-integral type of abutment in which the superstructure and the abutment itself are not monolithically constructed.

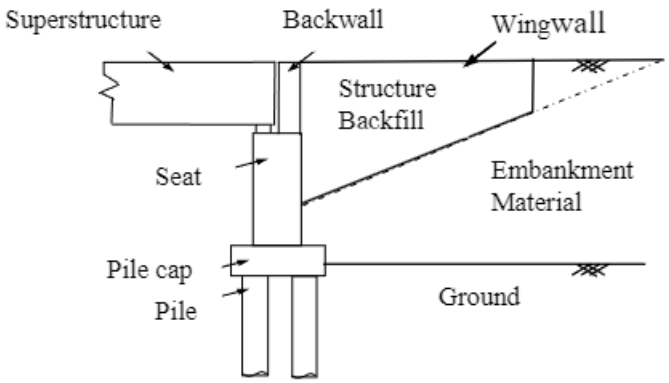

Figure 2.1. Seat-type abutment (side view)[45]

2.5.2.2. Diaphragm abutment

Diaphragm abutment is an integral type of abutment in which the superstructure and the abutment are monolithically constructed. It includes an end diaphragm which is monolithically constructed with the deck section and the abutment stemwall as shown in Figure 2.2. The abutment approach fill is supported by diaphragm under service conditions, and the diaphragm mobilizes the passive pressure longitudinally during an earthquake event[45].

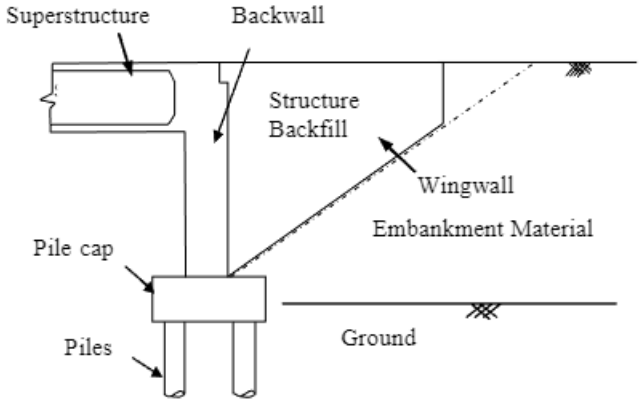

Figure 2.2. Diaphragm abutment (side view)[45]

Since all the bridge drawings considered in this research work have seat type of abutment, this research work is only for seat-type abutment.

2.5.3. Abutment Model

The selection of the abutment model has a significant influence of the bridge response, particularly, the end spans that are close to the abutment. Different modeling and design of the foundation types comprising abutment, pile footing, spread footing, cast-in-place column shaft and cast-in-place pile shaft has been presented in Chapter 5 of ATC 32[40]. Section 6.3 of SDC 2019[46] explains the guideline for developing the backbone curve for the abutments in longitudinal and transverse direction.

2.5.3.1. Roller abutment model

A roller boundary condition is a simplified abutment modeling approach in which a simple vertical support is provided at the end of deck as shown in Figure 2.3 and it provides vertical restraint at degree of freedom U3 i.e. displacement in the vertical direction. No torsional and lateral restraints are provided. This modeling approach can be implemented to determine a lower-bound estimate of the longitudinal and transverse resistance of the bridge[34]. The response of the bridge is controlled by the formation of plastic hinges and the ductility of the column bents. In this modeling approach, a single-column bent bridge resists lateral loads or deformation in the transverse direction of the bridge. The small torsional resistance at the deck end has negligible influence on the transverse response of a multi-column bent bridge, this is because the frame action is developed between column bents and the cap beam, and the double curvature is formed in the column which causes formation of the plastic hinges at the top and base of the column[34].

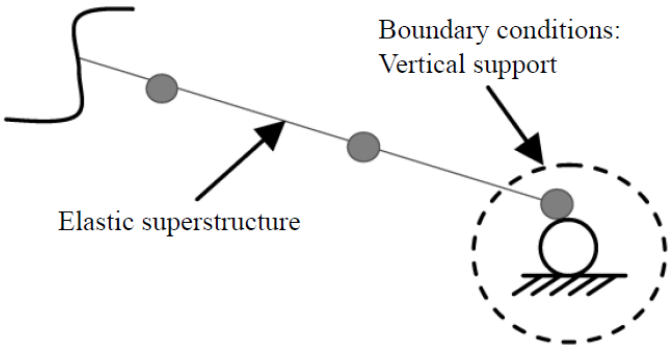

Figure 2.3. Roller abutment model[34]

In this model, if a rotational restraint is assigned in the longitudinal direction of the superstructure to illustrate the overturning resistance of the abutment, there is high possibility of overestimation of the strength of the bridge and underestimation of its ductility, particularly for single-column bents. The real behavior of the bridge lies between the restrained and unrestrained rotational degree of freedom. However, at least the roller abutment approach is needed whenever the nonlinear behavior in a bridge needs to be modelled.

2.5.3.2. Simplified abutment model

In simplified abutment model, the guideline suggests[34] a rigid element of length equal to the superstructure width, d_w, is connected to the superstructure centerline through a rigid joint. At both end of this rigid element, the longitudinal, transverse, and vertical nonlinear responses are modeled using link elements as shown in Figure 2.4. While modeling this rigid element, the gross section properties such as areas, inertias, and torsional constant are increased by a factor of 10^3 and mass and weight of the element is ignored by assigning a zero factor.

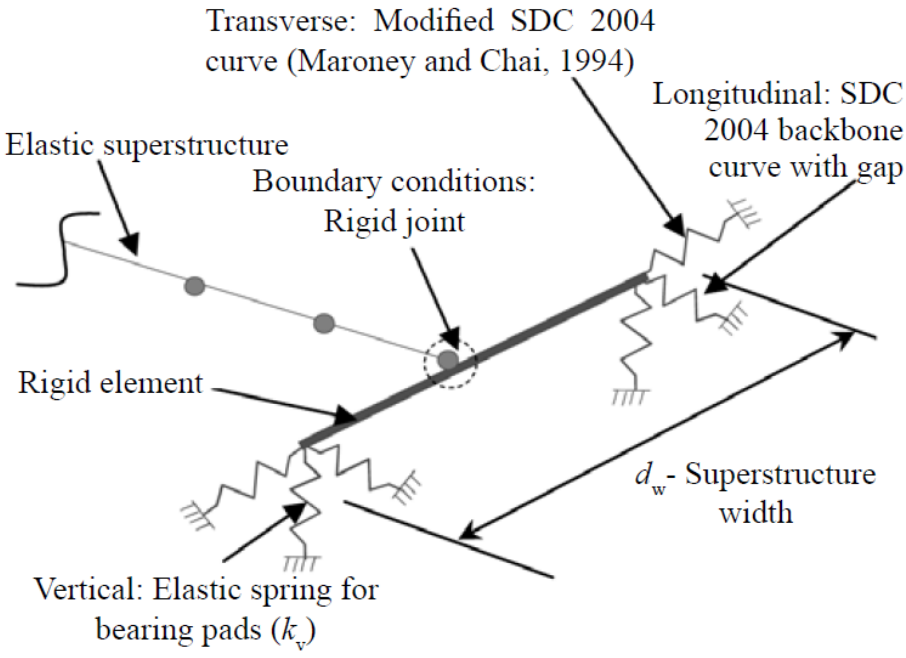

Figure 2.4. Simplified abutment model scheme[34]

At each end of the rigid element of length d_w, a series of elements are defined in longitudinal direction consisting of a rigid element, a gap element, and a zero-length element as shown in Figure 2.5. The shear and moment are released in the rigid element. The gap element allows the translation only in longitudinal direction and is assigned with the opening value in seat abutment. Section 6.3.1 of the Caltrans SDC 2019[46] can be used to define the zero-length element where an elastic-perfectly-plastic (EPP) backbone curve with abutment stiffness (K_{abut}) and ultimate strength (F_{bw}) is assigned to the zero-element length. This longitudinal response considers only the gap and embankment fill response, where the passive pressure is developed by the abutment back wall. And the shear resistance offered by bearing pads is ignored in this modeling approach.

To model the nonlinear behavior in transverse direction, the guideline[34] suggests a zero-length element to be defined at each end of the rigid element using an elastic-perfectly-plastic (EPP) backbone curve which can illustrate the backfill, wing wall, pile system response.

The guideline further suggests that the factors corresponding to wall effectiveness C_L of 2/3 and participation coefficients C_W of 4/3 are used with the stiffness of abutment and back wall strength calculated for the longitudinal direction to get the modified stiffness and back wall strength in transverse direction. The wing wall length is suggested to be assumed between 1/2-1/3 of the length of backwall. The brittle shear key resistance and the distribution of bearing pads are ignored in this model.

According to the guideline[34], the abutment response in vertical direction is modeled using an elastic spring at each end of the rigid link element, with a stiffness equivalent to the bearing pads stiffness k_v. Assuming the rigid soil condition, the distribution of bearing pads and vertical embankment stiffness is not considered in this modeling approach.

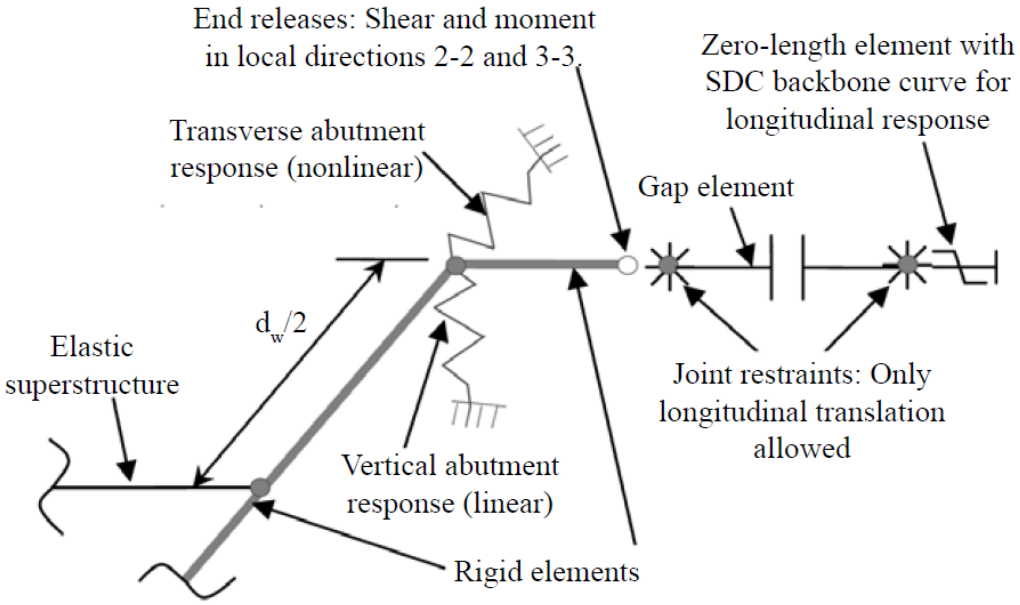

Figure 2.5. Series of elements for the longitudinal response in simplified abutment model[34]

Following are the major elements and steps needed to model the simplified abutment in the longitudinal direction of the bridge[34].

- Rigid element with shear and moment releases: Rigid element is created by assigning any cross section to the segment (such as column, deck, or cap beam), however, the property modifiers should be in the order of $10^2 - 10^3$ to gross section properties and 0 factor has to be provided to the mass and weight of the section in order to make the element rigid and massless respectively. The shear and moment releases are defined at the connection with the gap element, while a rigid connection is assigned at the joint connection with the first rigid element.
- Boundary conditions: longitudinal translation is allowed at each end of the gap element while the remaining degrees of freedom are assigned to be fixed.
- Gap element: A finite length nonlinear link element (NL-Link element) with 2 nodes is used to define a gap element. The length of gap element does not affect the response of the structure. In CSiBridge, the properties of gap element are used in linear and nonlinear cases. For linear analysis case, a high effective stiffness[47] and zero effective damping are defined. For nonlinear analysis cases, the gap size called "open" is defined as 2" and an infinite stiffness has been assigned. To avoid the convergence problems, it is recommended to use a stiffness value in the order of $10K_{abut}$.
- NL-Link element with longitudinal backbone curve: A NL-Link element is defined at the end of gap element, assigning a backbone curve as per the EPP (elastic-perfectly-plastic) behavior according to section 6.3.1 of SDC 2019[46]. Thus, after the closing of the gap element, the longitudinal behavior is governed by the backbone curve assigned to zero-length NL-link element.

2.5.3.3. Spring abutment model

Mackie and Stojadinovic [48] have proposed spring abutment model, a sophisticated and complex model to include the longitudinal, transverse, and vertical nonlinear abutment behavior, as well as a mass participation from the concrete abutment and mobilized embankment soil. A general scheme for this model is shown in Figure 2.6. In this modeling approach, the longitudinal response depends on the behavior of elastomeric bearing pads, gap, abutment back wall, abutment piles, and soil backfill material. Before the abutment gap closes, the force from deck is transferred through the elastomeric bearing pads to the stem wall and eventually to the piles and backfill, in a series. Once the gap closes, the forces are directly supported by the abutment back wall and mobilize the full passive backfill pressure. Each element of the abutment is modeled using a zero-length element to estimate their combined behavior. Seismic Design Criteria (SDC) can be used to determine the abutment stiffness (K_{abut}) and ultimate strength (F_{bw}) as explained in the simplified abutment modelling approach. Unlike the simplified abutment model, in spring abutment model, the number and distribution of the bearing pads are considered and assigned per the number and location of the girder and their thickness sizes per the specification. The yield and ultimate displacement of the bearing pads are suggested to be 150% and 300% of the shear strain. And to ensure that the shear failure of bearing pad occurs prior to its sliding, a dynamic coefficient of friction of 0.4 has been suggested for neoprene bearing on concrete. To consider the rotation of the deck about the vertical axis, a system of zero-length elements is placed at each of the two outermost bearing pads, modeling the abutment stiffness and strength.

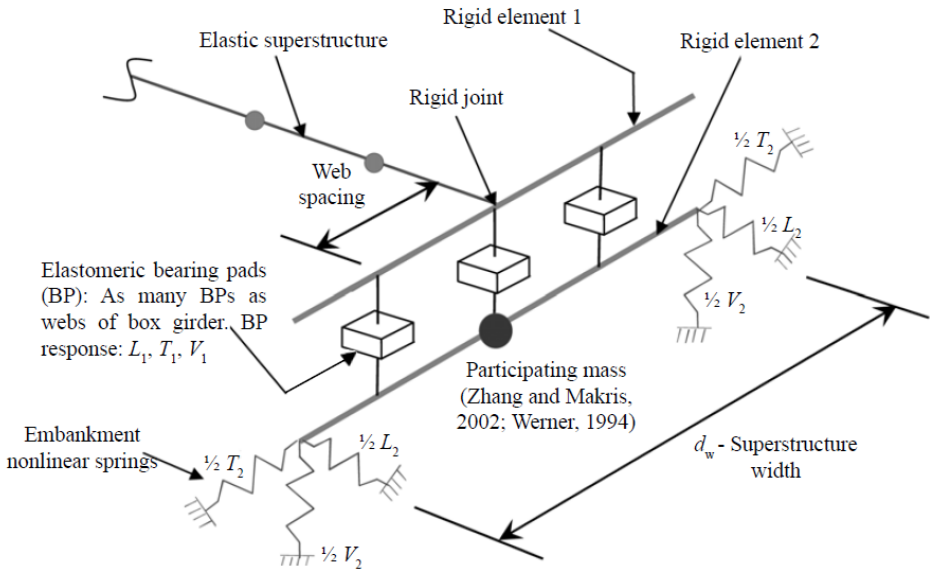

Bearing pads response:

- Longitudinal L_1: BP shear resistance and backwall gap contact element in parallel.
- Transverse T_1: BP shear resistance and brittle shear keys (extreme BPs only) in parallel.
- Vertical V_1: BP vertical stiffness and contact element for stem wall in parallel.

Embankment response:

- Longitudinal L_2: SDC (2004) backbone curve.
- Transverse T_2: Modified SDC (2004) backbone curve.
- Vertical V_2: Embankment vertical stiffness.

Figure 2.6. General scheme of spring abutment model[34]

In this modeling approach, the transverse response depends on the response of elastomeric bearing pads, exterior concrete shear keys, abutment piles, wing walls, and back-fill material. The transverse stiffness and strength of the backfill, wing wall, and pile system can be determined by modifying the SDC steps for the longitudinal direction. As per Maroney and Chai[49], the wing wall effectiveness C_L of 2/3 and participation coefficients C_W of 4/3 can be used. And the abutment stiffness (K_{abut}) and back wall strength (F_{bw}) obtained from SDC 2019 [46] or SDC 2004[36] are modified with these coefficients. The wing wall length can be approximated as 1/2-1/3 times the length of back wall. In this model the bearing pads and shear keys are modeled to behave in parallel and this combined behavior act in series with the transverse abutment stiffness and strength. For more details, the readers are suggested to refer the guideline[34].

In the current research work, simplified abutment model has been used.

2.6. Abutment Stiffness

The abutment stiffness can be modeled in three different forms: longitudinal stiffness, transverse stiffness, and vertical stiffness.

2.6.1. Longitudinal Stiffness

The passive pressure exerted by the backfill of the abutment, which resists the movement at the abutment, shows nonlinear variation with the longitudinal displacement of the abutment and depends on the material properties of the backfill. Seismic Design Criteria V2.0 [46] has suggested a bilinear force-deformation curve as shown in Figure 2.7 to model the nonlinear abutment-backfill.

This bilinear approximation of the backbone curve can be used in NTHA (nonlinear time history analysis). This bilinear model was developed based on experimental investigations and calibrated analytical models using engineered structural backfill compacted to a minimum relative compaction level of 95%.

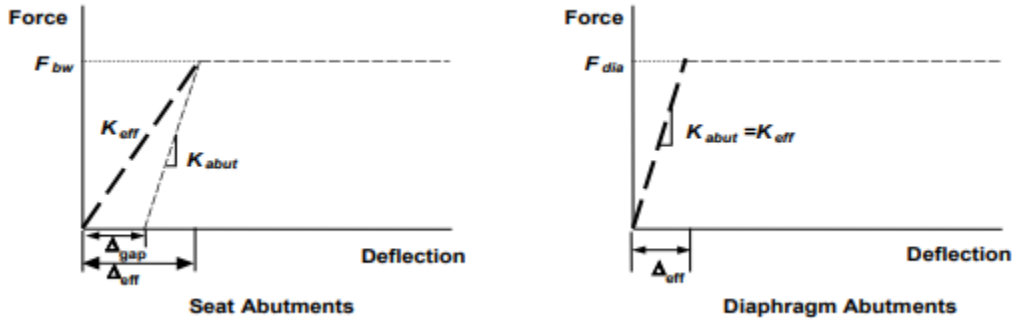

Figure 2.7. Nonlinear Abutment model[46]

The effective abutment stiffness, K_{eff}, as shown in Figure 2.7 is determined as:

$$K_{eff} = \frac{F_{abut}}{\Delta_{eff}} \quad (2.\ 2)$$

where

$$\Delta_{eff} = \begin{cases} \Delta_{gap} + \Delta_{abut} & (seat\ abutment) \\ \Delta_{abut} & (diaphragm\ abutment) \end{cases} \quad (2.3)$$

$$\Delta_{abut} = \frac{F_{abut}}{K_{abut}} \quad (2.4)$$

For seat-type abutment, SDC 2019[46] suggests that the expansion hinge gap, Δ_{gap}, is considered to estimate the effective abutment wall stiffness as shown in Figure 2.7. The idealized ultimate passive pressure force, F_{abut} can be calculated using equation (2.5), which is developed by fitting the nonlinear hyperbolic backbone curve by Shamsabadi et. al. [50] and pile cap test [51-54], followed by the bilinear approximation of the hyperbolic backbone curves.

$$F_{abut} = w_{abut}\left(\frac{5.5h_{abut}^{2.5}}{1+2.37h_{abut}}\right)R_{sk} \quad (2.5)$$

$$K_{abut} = w_{abut}(5.5h_{abut} + 20)R_{sk} \quad (2.6)$$

$$R_{sk} = e^{-\theta/45} \quad (2.7)$$

$$\theta \leq 66^{\circ} \quad (2.8)$$

where

K_{eff}= effective abutment longitudinal stiffness (kip/in)

F_{abut}= idealized ultimate passive capacity of the backfill of the abutment backwall or the diaphragm (kips). In Figure 2.7, $F_{abut} = F_{bw}$ for seat abutment and $F_{abut} = F_{dia}$ for diaphragm abutment.

Δ_{eff}=effective abutment longitudinal displacement when passive force reaches F_{abut} (in.)

Δ_{gap}= width of expansion gap in seat abutment (in.)

Δ_{abut}=abutment displacement at yield (in.)

K_{abut}=longitudinal stiffness of abutment as shown in Figure 2.7 (kip/in)

R_{sk}= skew reduction factor

θ= abutment skew angle (in degrees)

h_{abut}= height of backwall or diaphragm as shown in Figure 2.7 (ft); As shown in Figure 2.8, $h_{abut} = h_{bw}$ for seat abutments, h_{dia}^{**} for diaphragm abutments designed for full soil pressure, and as h_{dia}^{*} for diaphragm abutments not designed for full soil pressure.

w_{abut}= width of abutment along the skew direction (ft); $w_{abut} = w_{bw}$ for seat abutment and w_{dia} for the diaphragm abutment as shown in Figure 2.8.

For seat abutment type, $w_{bw} = d_w - 2 \times h_{abut}$; where d_w= superstructure deck width (ft)

In this bilinear model, the ultimate force was calibrated so that the potential energy stored in the backfill resulting from the translational motion of the superstructure is equivalent to the nonlinear hyperbolic force-displacement curve[55]. For skewed abutments, both ultimate capacity and stiffness decrease by a reduction factor, R_{sk}. This skew reduction factor was calibrated by Shamsabadi and Rollins[55] through the comparison with the experimental data obtained from full-scale abutment test with skew angles of 0°, 15°, 30° and 45° [52, 54], along with the Finite Element simulation for 60° skewed abutment. The skew reduction factor considers the increment in tendency of skew bridges to undergo rotation and translation because of the earthquake ground motion. This induced deformation causes a partial loss of contact between the abutment and the backfill, resulting in the reduction of abutment stiffness.

In seat abutment, the backwall is generally designed to break off, serving as a protective measure for the foundation from the inelastic behavior. For diaphragm abutments, the diaphragm above and below the soffit, is generally engineered to immediately engage the backfill subjected to longitudinal movement of the bridge. Consequently, the effective abutment area corresponds to the total area of the diaphragm. However, if the diaphragm is not designed to withstand the passive earth pressure exerted by the abutment backfill, the effective abutment area is restricted

to the portion of the diaphragm located above the fracture plane. The restriction on abutment backwall heights, ranging from 2 to 10 feet, is suggested based on the heights observed in experimentally tested or analytically simulated backwalls.

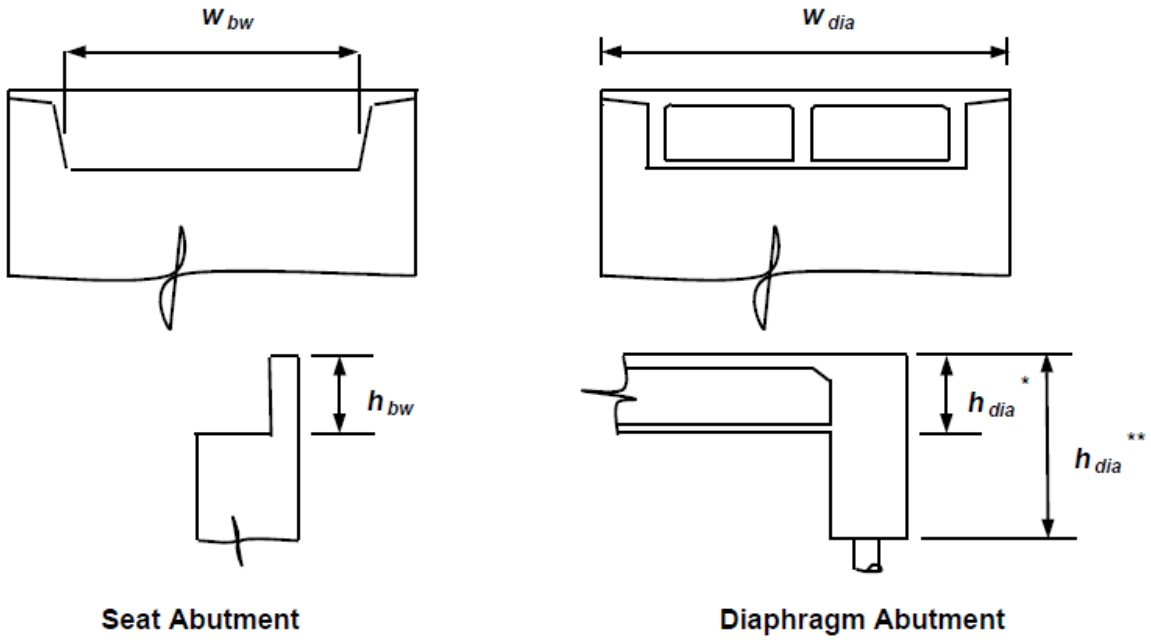

Figure 2.8. Effective area of Seat and Diaphragm Abutment (SDC 2.0[46])

2.6.2. Transverse Stiffness

SDC V2.0[46] suggests that in elastic demand assessment model the stiffness of a transverse spring at the abutment, K_{nom}, can be taken as 50% of the elastic transverse stiffness of the adjacent bent. SDC V1.3[36] suggests that the lateral capacity of seat abutments should not be considered effective for MCE (Maximum Considered Earthquake) unless the force-deflection characteristics and stiffness for each element that contributes the transverse resistance can be demonstrated.

In this research work, the wall effectiveness C_L of 2/3 and participation coefficients C_W of 4/3 were used with the stiffness of abutment and back wall strength, as explained in the

Simplified Abutment Model (in section 2.5.3.2.). In transverse direction, width of abutment, w_{abut}, was considered equal to the length of wing wall (w_{ww}), where the length of wing wall $w_{ww} = d_w/3$ per the simplified abutment model. Thus, in the transverse direction, the backwall strength and stiffness of abutment can be expressed as

$$F_{abut} = C_L \times C_L \times w_{ww} \left(\frac{5.5h_{abut}^{2.5}}{1+2.37h_{abut}}\right) R_{sk} \quad (2.\ 9)$$

$$K_{abut} = C_L \times C_L \times w_{ww}(5.5h_{abut} + 20)R_{sk} \quad (2.\ 10)$$

Since there is no gap in transverse direction, $\Delta_{gap} = 0$, thus, $\Delta_{eff} = \Delta_{abut}$ for seat abutment.

2.6.3. Vertical Stiffness

Simplified abutment modeling approach has been used in the current research work, which models the elastic stiffness of the bearing pad in the vertical direction. The vertical elastic stiffness, K_v, of the bearing pad is calculated using the following formula[38]

$$K_v = \frac{EA}{h} \quad (2.\ 11)$$

where K_v= vertical elastic stiffness (kip/in)

E= Young's modulus of the bearing pad material (ksi)

A=cross-section area of the bearing pad (sq.in)

h= height of the bearing pad (in)

The value of E =5ksi (taken from Lu et. al.[38]) and the cross section and height of the bearing pad has been taken from the as-built drawings of the bridges considered in the analysis.

2.7. Damping

2.7.1. Definition

The process of energy-dissipation that reduces the motion of vibration of a linear or nonlinear system when it is subjected to an exciting force or displacement is known as damping.

Material damping represents the energy dissipation process because of the deformation of a continuous medium. And radiation damping is the reduction of the vibration amplitude because of the dispersion of the energy wave in a large area. In bridge structure, the structural damping can be defined as the process of energy dissipation caused by the material damping in structural elements, inelastic cyclic behavior of the member, loss of friction at connection and interface, radiation damping in abutments and the backfill soil. Because of the small skew and short span in ordinary standard bridges, the radiation damping can be ignored[34].

Generally, the energy dissipation process is represented by viscous damping and it assumes that the existence of dissipative force is a function of velocity. This equivalent viscous damping force is considered to model the energy dissipation within the linear range of the structure. The damping property in nonlinear region is not specifically considered in dynamic analysis[41]. The equivalent viscous damping ratio in each mode of vibration of a structure is expressed in terms of mathematical equation to represent the real energy dissipation process. However, in most of the soil and structure, the energy is dissipated by yielding or plastic straining of the material, also known as hysterically.

2.7.2. Recommended Damping Ratio

For reinforced concrete bridges with substantial cracking that undergo small deformation or subjected to low intensity ground motion, the recommended damping value is 3-5% of the critical value. For pre-stressed deck section of bridges, the damping coefficient increases up to 5-7% of critical. In case of a yielding bridge with both pre-stressed and traditionally designed reinforced concrete deck, the hysteretic behavior and the structural damage happening in ductile elements because of the strong earthquake signals leads to a damping ratio at 7-10%.

Generally, a 5% damping ratio is used in the design codes. Therefore, 5% damping ratio has been used in the current research study. For the parametric study, damping ratio of 1%, 3%, and 7% have been considered to study the influence of damping ratio on inelastic displacement ratio.

2.7.3. Modeling of Damping in CSiBridge

In the current research, direct time history analysis has been used where viscous damping is needed and is defined by mass- and stiffness-proportional components. In the dynamic analysis cases of the bridge structure, it is recommended to specify Rayleigh (mass and stiffness proportional) damping coefficients directly, which needs the value of first two modal periods of the system. Once the bridge model is developed, a modal analysis has been performed to determine modal time periods. Same damping ratio was assigned for both the first and second modal periods when defining the linear and nonlinear transient analysis cases.

2.8. P-Delta Effects

P-delta (P-Δ) effect is a dynamic effect of column which occurs when an axial load of column acts upon a large lateral displacement and generates an additional moment. It is also known as second order effects and is considered a geometrically induced nonlinearity. P-Δ effect captures the amplification of the seismic demand on the column bents, which is primarily caused by the relative displacement between the column top and bottom. Thus, it helps to determine the structural instability hazard of the bridge. In time history analysis, P-Δ effect records the maximum displacement of a yielding system where a considerable amplification of the response is commonly expected for an adequate set of ground motion.

In CSiBridge, the direct integration method in nonlinear time history analysis offers two types of geometric nonlinearities: P-Δ and large displacement effects. P-Δ effects are computed

by solving the equation of equilibrium of the system by partially considering the deformed shape of a structure. In this case, the tensile force tries to resist the rotation of elements and stiffen the structure, on the other hand, the compressive force tries to increase the rotation of the elements and cause the structure to become unstable. In case of large displacements, all equations of equilibrium need to be built on the deformed geometrical shape of a structure that undergoes large displacement, especially large strains and rotations. This case needs more iteration than the P-Δ effects and is sensitive to the convergence tolerance defined by the user. The guideline[34] suggest that, P-Δ option is enough for typical bridges, especially when the material nonlinearity dominates the nonlinear behavior. The large displacement option is considered for structures that undergo large displacement and for buckling analysis, thus, it is not suggested for typical bridge analysis. In this research work, P-Δ effect option has been selected when performing the nonlinear time history analysis.

2.9. Time History Analysis

2.9.1. Purpose

Nonlinear time history analysis is suggested to determine the dynamic nonlinear response of a complex three-dimensional structure like bridge system. It considers the nonlinearities or the degradation of the strength of different elements of the bridge, and the ground motion intensity and its characteristics used in the analysis. Furthermore, the effect of added energy-dissipation devices in the structures can be determined using nonlinear time history analysis.

In time history analysis, the load applied is the ground motion acceleration or the foundation displacement, not externally applied loads at the joint or members of the structure. The design displacement is calculated directly from dynamic analysis using a set of ground motions. Because of the earthquake ground motion, a structure suddenly deforms, and the inertia

forces are developed in the structural members. Each of the bridge systems shows different predominating mode shapes and frequencies, which undergo excitation based on the earthquake ground motion. The response of the bridge system is significantly sensitive to those characteristics of the bridge.

The time history analysis needs high computational and analytical effort and it generates large amount of output information. The capacity of the main component of bridge system is assessed as a function of time, based on the nonlinear behavior evaluated for the elements and the materials. This assessment is performed for large number of input ground motions applied to the bridge structure, and the response of the structure is stored at every time step. Despite these challenges, the time history analysis method gives high quality results at each time step as it permits the redistribution of the internal forces within the structure. Furthermore, the seismic demand can be approximated using the statistical approximation, using the mean and the standard deviation values of the joint displacements to estimate the peak response expected for the bridge structure.

2.9.2. Implementation

In linear and nonlinear time history analysis, the direct integration method has been used in this work to obtain the solution of the differential equation of motion. In direct integration method for nonlinear time history analysis, all forms of nonlinearities (material and geometric) are considered in the numerical algorithm. Direct-integration in nonlinear time-history can be started from zero initial condition (unstressed state) or can be continued from the state at the end of a nonlinear case (pushover analysis or nonlinear dead load) or another direct-integration nonlinear transient analysis. The viscous proportional damping used in the nonlinear time history

analysis is calculated by CSiBridge when provided with the first and second time period and damping ratio.

3. MODELING MATRIX

The study of inelastic displacement ratio in realistic bridge structures has not been performed in the past. Therefore, this study performs the analysis of real bridge structure considering the nonlinearity in different components of the bridges, developing a more practical relationship between inelastic displacement ratio with the first mode of time period of different reinforced concrete box girder bridge structure.

This chapter provides a detailed explanation about the modeling matrix considered in this study. In the current bridge inventory, reinforced concrete (RC) highway bridges are the majority of the bridges. And this study is focused on reinforced concrete box girder bridges in California which is one of the most seismically active regions in the United States. The reinforced concrete box-girder bridges, their geometric and material properties, method of implementation in CSiBridge, selection of earthquake ground motion and parametric study are explained in the following sections.

3.1. Bridges

In order to investigate realistic bridge structures containing various components and nonlinear behavior, this study has considered six different reinforced concrete box girder bridges. Among these six bridges, two Ordinary Standard Bridges (OSB1 and OSB2) developed by Caltrans have been employed. Route 14 Left (R14L), Route 14 Right (R14R), La Veta and Adobe bridges are four other bridges considered in this study. For the boundary condition of column with the ground, both pinned and fixed connection have been considered. Therefore, a total of 12 bridge models have been developed and used in all the analysis presented in this report. The as-built drawings for these bridges were obtained from Caltrans where the unit of the

dimension measurement for OSB1 and OSB2 is in imperial system (ft) while for R14L, R14R, Adobe and La Veta the unit is in metric system (mm).

Three-dimensional (3D) models of the bridges were developed referring to the bridge drawings and the information available in CSiBridge input files of OSB1 bridge obtained directly from Caltrans. The abutment model of the OSB1 bridge has been modified as the simplified abutment model. Also, the rigid offset length in columns of OSB1 bridge modeled in this research work is different from that in the Caltrans CSiBridge model.

3.1.1. OSB1 Bridge

3.1.1.1. Geometric configuration

Ordinary Standard Bridge 1 (herein referred as OSB1) is a single two-column bent reinforced concrete box-girder bridge with two spans of 150 feet in length. Figure 3.1 and Figure 3.2 show the Plan and Elevation views of OSB1 bridge respectively. Although the column height has not been indicated clearly in the drawing, the column height is taken as 20 feet as mentioned by Lu et. al.[38]. The bent comprises two circular reinforced concrete columns with a diameter of 5’-6”, positioned at a spacing of 24 ft (center-to-center). These circular columns are reinforced with 36 #11 longitudinal bars and #8 transverse spirals at 6” of interval. The geometry and material strength for OSB1 bridge is listed in Table 3.1.

OSB1 bridge is a continuous cast-in-place post-tensioned concrete box girder bridge[47] with a total length of 300ft, total superstructure width of 47.5 feet, and depth of 6 feet. The cross-section detail of the deck and the column are shown in Figure 3.3 and Figure 3.4. Since the bent cap is integral with the superstructure deck section, its height is same as that of superstructure deck section. The width of the bent cap is 8’-8” obtained from the detailed drawing. The columns are supported by pile caps at the base, with provision for both shallow and deep foundation

details, and connected to the pile caps through pipe pins[47]. The connection of column with bent cap and deck section is assumed rigid (integral bent cap) at the top and both pinned and fixed connection has been modeled at the base.

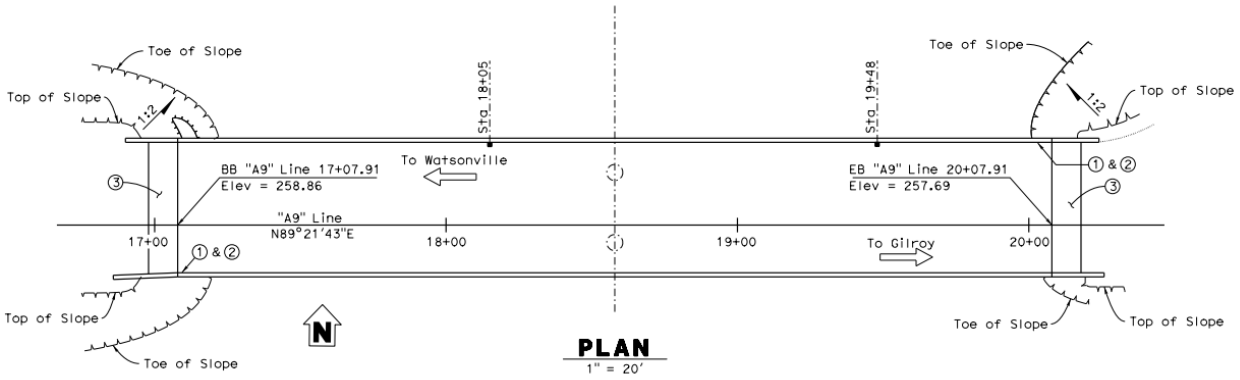

Figure 3.1. Schematic Plan View of OSB1 bridge (drawing provided by Caltrans)

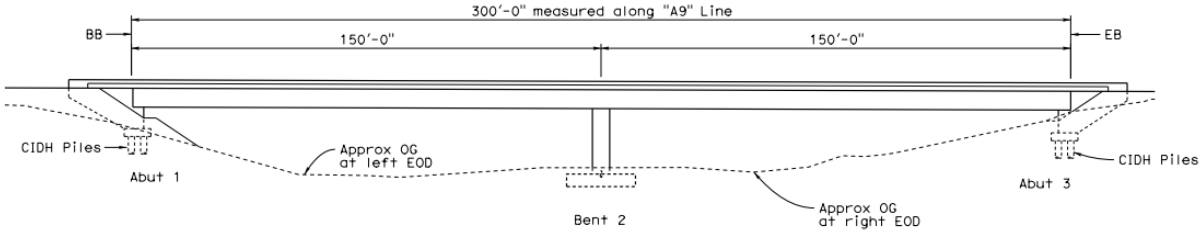

Figure 3.2. Schematic Elevation view of OSB1 (Caltrans)

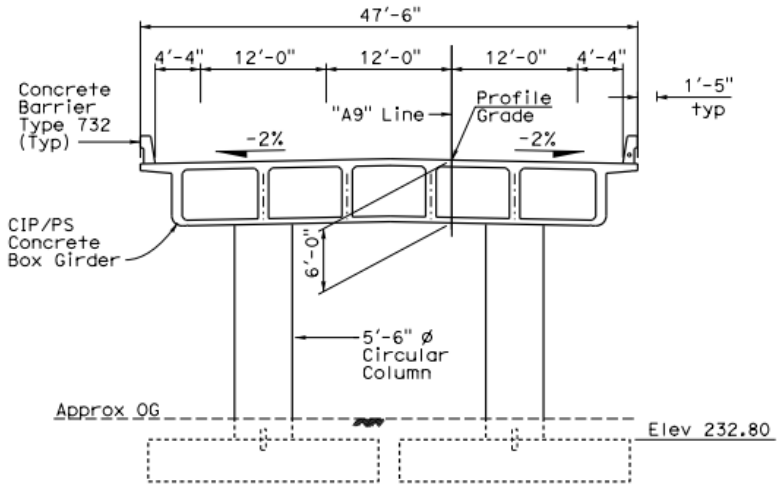

Figure 3.3. Cross-Section detail of OSB1 bridge deck (Caltrans)

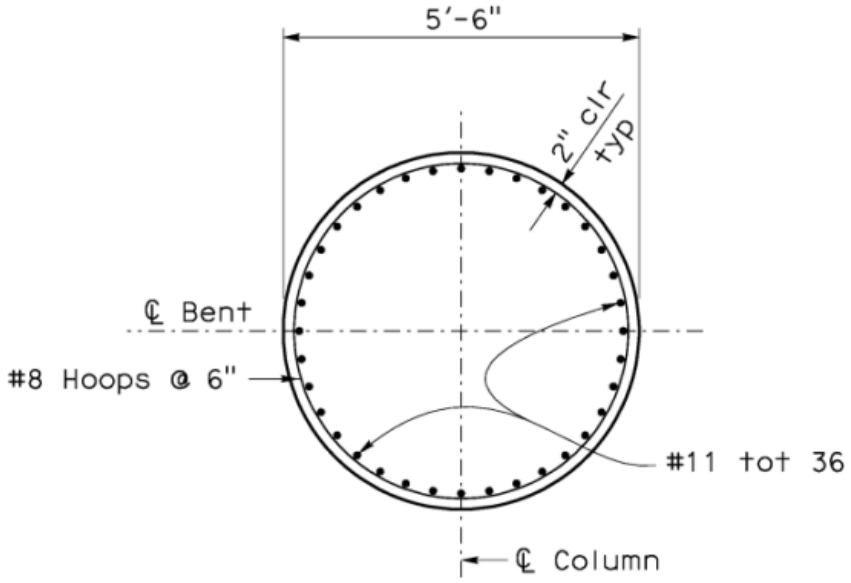

Figure 3.4. Cross-section detail of column of OSB1[38]

According to the detailed drawing, the abutments are standard seat-type abutments. Each is founded on a pile cap supported by a 7x2 pile group. Elastomeric bearings, measuring 18 inches square and 2.25 inches in height, are located under each of the six webs. Material properties specified for the bridge components include a compressive strength of 3.6 ksi for

structural concrete of the bridge, and a yield strength of 60 ksi for the reinforcement. The detail about the geometric and material properties of OSB1 bridge is tabulated in Table 3.1.

3.1.1.2. CSiBridge model

CSiBridge offers a single user interface to complete the modeling, analysis, design, load rating and reporting of different bridge structures. The CSiBridge OSB1 model was previously developed by Caltrans. The model was validated (discussed in next chapter) using the same model without making any changes. However, for the analysis purpose some of the changes were made to maintain the consistency between all bridges modeled in this work. The changes include no parametric variation defined in the exterior girders as defined in original CSiBridge model of OSB1 bridge, abutment modeling approach was modified according to simplified abutment mode, the rigid offset length between column top and deck, calculated by CSiBridge was used instead of 1.5ft as defined in the work of Mackie et. al.[47]. Also, rigid connection was provided between column top and bent cap. Figure 3.5 shows the three-dimensional model of OSB1 bridge, showing the superstructure deck section, bent, columns and the abutment model, Figure 3.6 shows its spine model and Figure 3.7 shows the detailed simplified abutment model created in CSiBridge for OSB1 bridge.

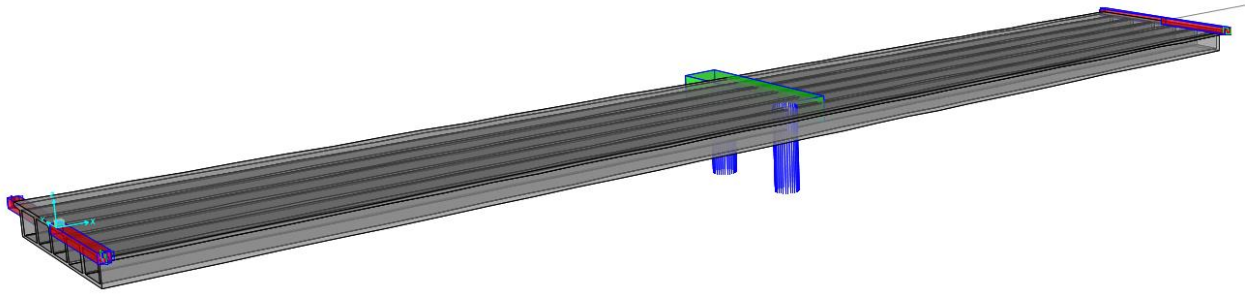

Figure 3.5. Three-dimensional model of OSB1 bridge created in CSiBridge

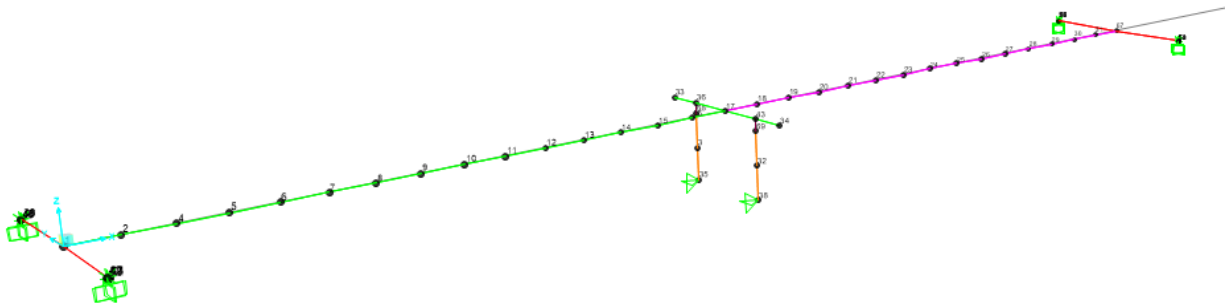

Figure 3.6. Spine model of OSB1 bridge created in CSiBridge

The abutment modeling approach was modified per the simplified abutment model as described in section 2.5.3.2. A massless rigid element of length 47.5 feet (equal to the superstructure deck width) was rigidly connected at each end of the deck section. Rigid connection was created by assigning constraints in all degrees of freedom (translational-U1, U2, U3 and rotational-R1, R2 and R3). At both end of this rigid bar, a series of elements were defined in the longitudinal direction consisting of a rigid element, a gap element and multilinear plastic link element as shown in Figure 3.7. In both rigid elements, the property modification factor of 0 was assigned to the mass and weight and a factor of 100 was assigned to the moment of inertia in CSiBridge to make them rigid.

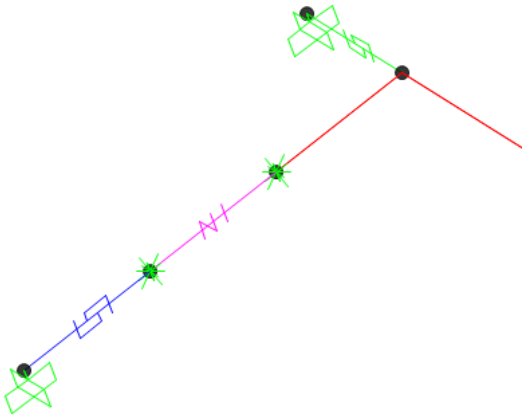

Figure 3.7. Simplified abutment model created in CSiBridge for OSB1 bridge

A gap element of finite length was defined in CSiBridge with nonlinear property in longitudinal degree of freedom (U1). It is connected to the rigid element at one end and with another link element at the other end. The definition of the characteristics of gap element in CSiBridge is used in linear and nonlinear cases. Referring to the work of Mackie et. al.[47], the effective stiffness for the linear analysis case was 2.4×10^6 kips/ft (2.0×10^5 kips/in) and zero damping while the gap and the stiffness for the nonlinear analysis case was 2" (obtained from As-built drawing) and 9407.5 kips/in. This stiffness is calculated to be 10 times the stiffness in the longitudinal direction as mentioned in section 2.5.3.2. The stiffness of abutment in longitudinal direction for OSB1 bridge was calculated as 940.75 kips/in as shown in Table 3.2. Both end nodes of the gap element had restraints in U2, U3 and all rotational degrees of freedom to allow the translation only in longitudinal direction.

The second link element was a multilinear plastic link element defined at the end of gap element used to define the nonlinear properties only in the longitudinal degree of freedom (U1). The backbone curve per elastic perfectly plastic behavior discussed in section 2.6.1 was assigned. The effective stiffness for the linear analysis case was 940.75 kips/in (i.e. $K_{abut}/2$)as calculated in Table 3.2. As shown in Figure 3.8, the nonlinear force-deformation relation was elastic-plastic (tension and compression) with a yield displacement of $\Delta_{abut} = 0.6"$ and yield force of $F_{abut}/2 = 565.62$kips, calculated in Table 3.2. The node connecting gap element and this link element has all degree of freedom restrained except for U1 (longitudinal translation).

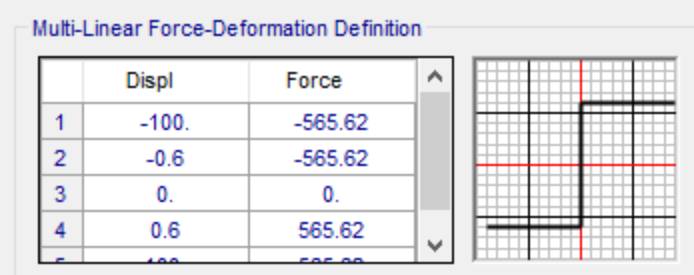

Figure 3.8. Properties of OSB1 abutment link in longitudinal direction (kips-in)

In transverse direction, another multilinear plastic link element was assigned at the end of rigid bar connected to the deck section to define the nonlinear properties in the transverse direction (i.e. U1 direction of the link element) and the elastic stiffness in the vertical direction (i.e. U2 direction of the link element). Like the longitudinal link element, the elastic perfectly plastic behavior of backbone curve was assigned in this transverse multilinear plastic link element. The effective stiffness for the linear analysis case was 373 kip/in as calculated in Table 3.3. As shown in Figure 3.9, the nonlinear force-deformation relation was elastic-plastic (tension and compression) with a yield displacement of 0.6” and yield force of 224.2kips, as calculated in Table 3.3.

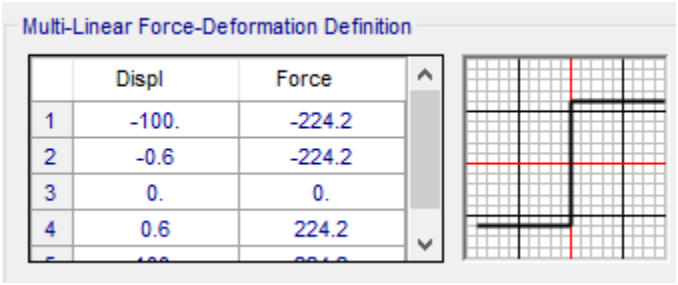

Figure 3.9. Properties of OSB1 abutment link in transverse direction (kips-in)

For vertical stiffness, the dimension of bearing pads is needed. The dimensions of bearing pad in OSB1 is a square of 18in×18in and height of 2.25in. Using the expression discussed in section 2.6.3, the vertical stiffness was calculated to be K_v=720 kip/in as listed in Table 3.3. This

linear stiffness was assigned as the effective stiffness for all analysis cases in U2 direction in the multilinear plastic link element assigned in the transverse direction.

OSB1 bridge column was modeled following the steps in section 2.3.4. Two different models were developed for pinned and fixed connection of column to the ground. For pinned connection of column to the ground, both columns were discretized into three elements as shown in Figure 3.10. The analytical plastic hinge length for OSB1 bridge column was calculated to be 2.8ft using the equation discussed in section 2.3.3. The top element of each column was 2.8ft long. The rigid offset calculated by CSiBridge was 2.783ft and therefore, the plastic hinge was assigned at a distance of 2.783ft from the node of deck line in spine model. Mackie et. al.[47] used the rigid offset of 1.5ft and the hinge was originally assigned at 1.5ft below the node defining the deck line. A cracked section property modifier of 0.35 was assigned to the lower two elastic elements while a factor of 3 has been assigned to the top element where plastic hinge was assigned.

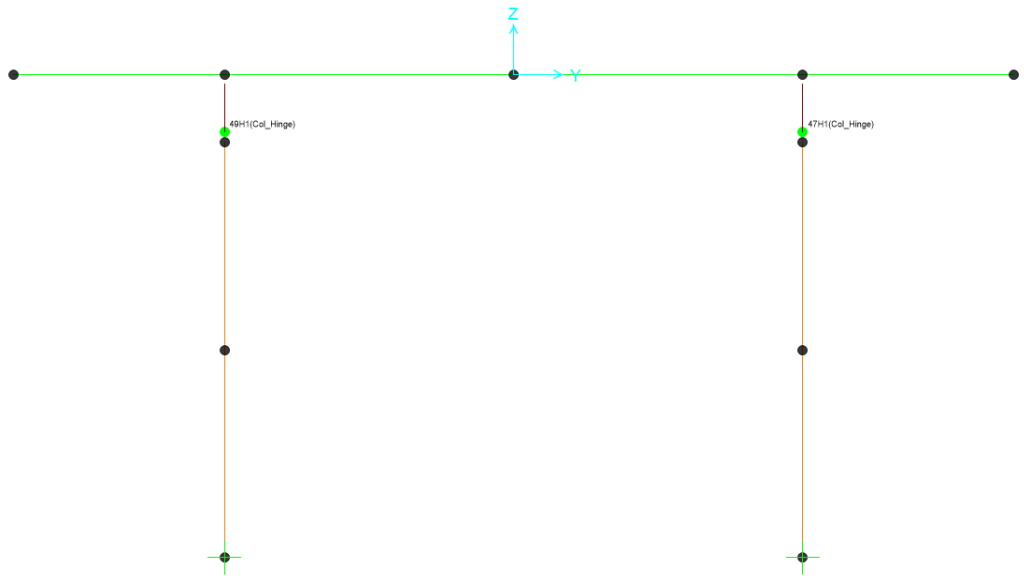

Figure 3.10. Assignment of plastic hinge in column with pinned connection to the ground in CSiBridge

For fixed connection of column to the ground, both columns were discretized into four elements as shown in Figure 3.11. The analytical plastic hinge length was 2.8ft. Both top and bottom elements of each column were 2.8ft long. A hinge was placed at the center of the bottom element, however, for the top element, the rigid offset calculated by CSiBridge was 2.783ft and therefore, the plastic hinge was assigned at a distance of 2.783ft from the node of deck line in spine model. A cracked section property modifier of 0.35 was assigned to the middle two elastic elements while a factor of 3 has been assigned to the top and bottom element where plastic hinges were assigned.

The joint between superstructure deck (spine model) and bent cap shown in Figure 3.6 and the joints between column and the bent cap shown in Figure 3.10 and Figure 3.11 were constrained in all degrees of freedom to make a rigid connection.

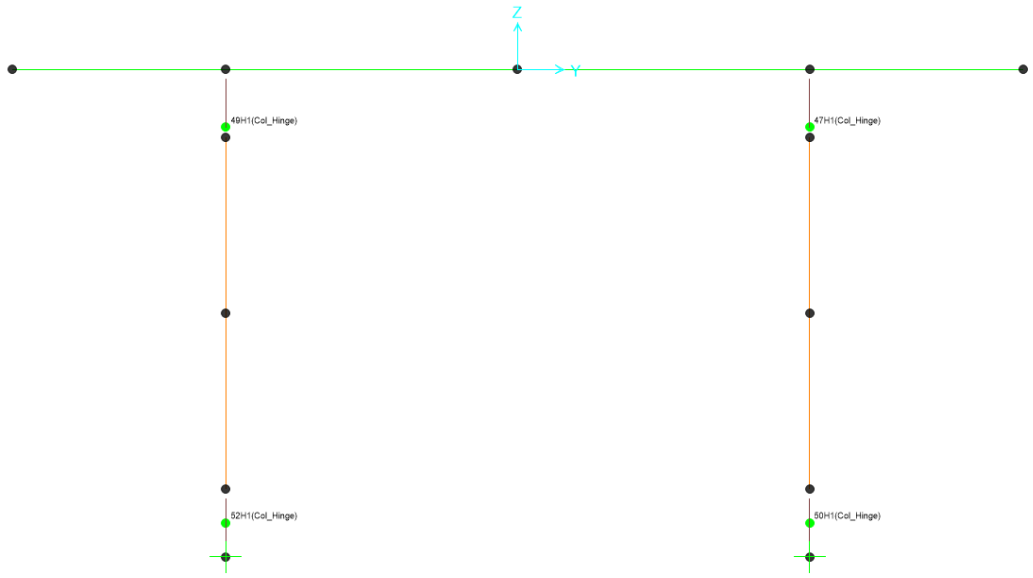

Figure 3.11. Assignment of plastic hinge in column with fixed connection to the ground in CSiBridge

3.1.2. OSB2 Bridge

3.1.2.1. Geometric configuration

Ordinary Standard Bridge 2 (OSB2) is a two-span reinforced concrete box girder bridge with a single column bent positioned at the center of the bridge total span. Figure 3.12 and Figure 3.13 show the schematic plan and elevation view of OSB2 bridge respectively. The height of column was taken as 20 feet referring to Lu et. Al.[38]. The bent consists of a single circular reinforced concrete column with a diameter of 5’-6”, positioned centrally within the bent. This circular column is reinforced with 44 #11 (bundle of 2) longitudinal bars and #8 transverse spirals at 6” intervals, as illustrated in Figure 3.15. The geometric and material specifications for the OSB2 bridge are detailed in Table 3.1.

The OSB2 bridge is characterized as a continuous cast-in-place post-tensioned concrete box girder bridge with three cells[47] . The total length of the bridge spans 300 feet, with a total superstructure width of 37.5 feet and a depth of 6 feet. The cross-section details of the deck and the column are depicted in Figure 3.14 and Figure 3.15, respectively. As the bent cap is integral with the superstructure deck section, its height is same as that of the superstructure deck section, while its width is 8’-8”, obtained from the detailed drawing. Elastomeric bearing pad measuring 1’-6” square and 2.25” high is positioned beneath each of the four webs. The connection of the column with the bent cap and deck section is rigid at the top. The abutments are standard seat-type abutments. Material properties specified for the bridge components include a compressive strength of 4 ksi for the structural concrete of the bridge and a yield strength of 60 ksi for the reinforcement. Further details regarding the geometric and material properties of the OSB2 bridge are presented in Table 3.1.

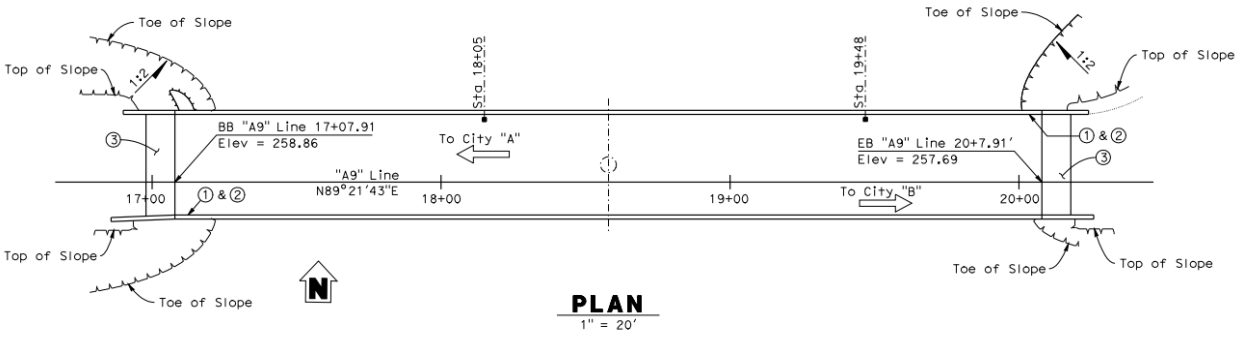

Figure 3.12. Schematic Plan view of OSB2 bridge (drawing provided by Caltrans)

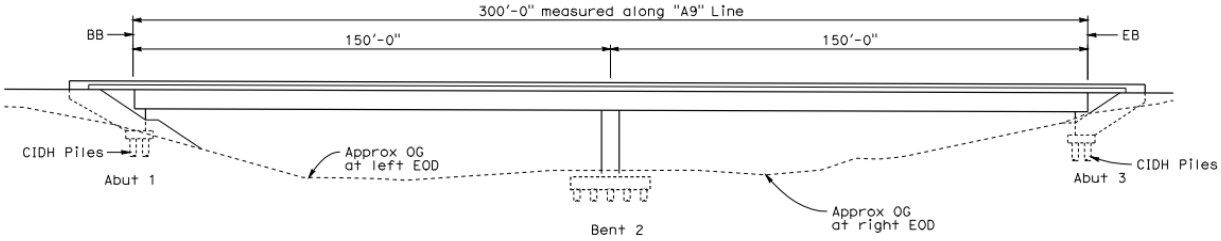

Figure 3.13. Schematic Elevation view of OSB2 bridge (Caltrans)

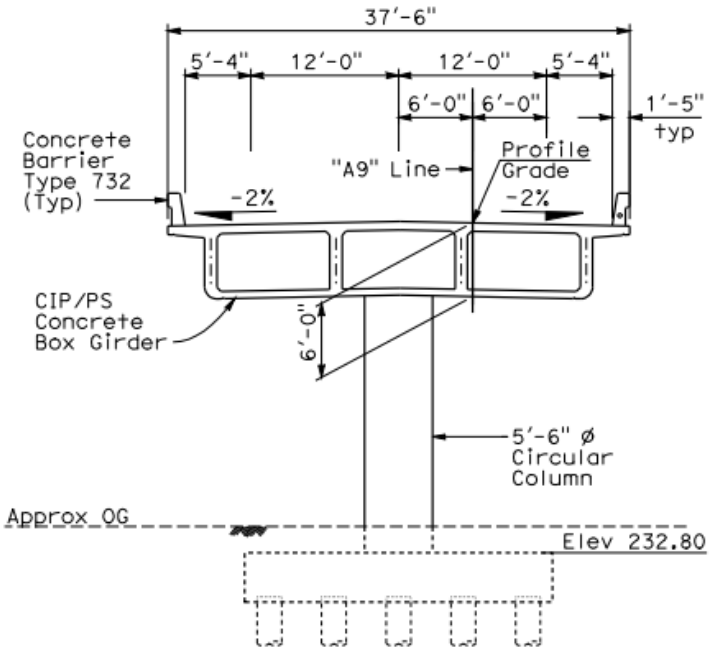

Figure 3.14. Cross-Section detail of OSB2 bridge deck (Caltrans)

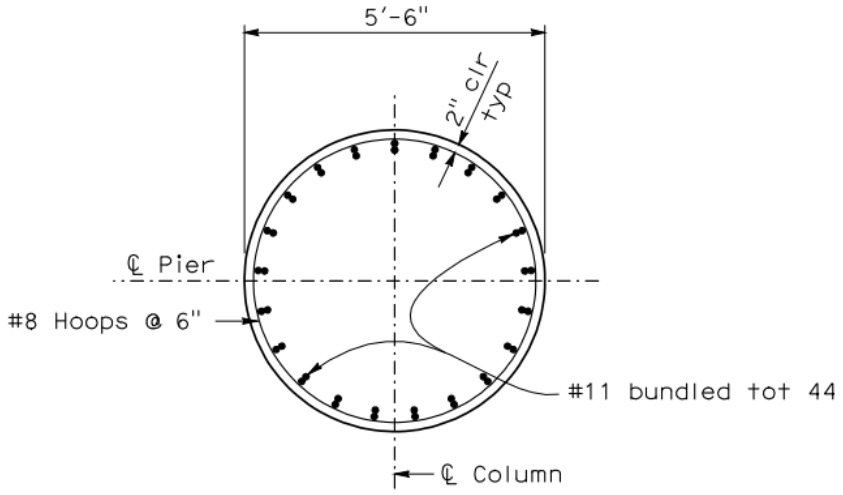

Figure 3.15. Cross-section detail of OSB2 bridge column (Caltrans)

3.1.2.2. CsiBridge model

Using the information about geometric configuration, a spine model of OSB2 bridge was created in CSiBridge as shown in Figure 3.16. The modeling approach was similar to OSB1 bridge.

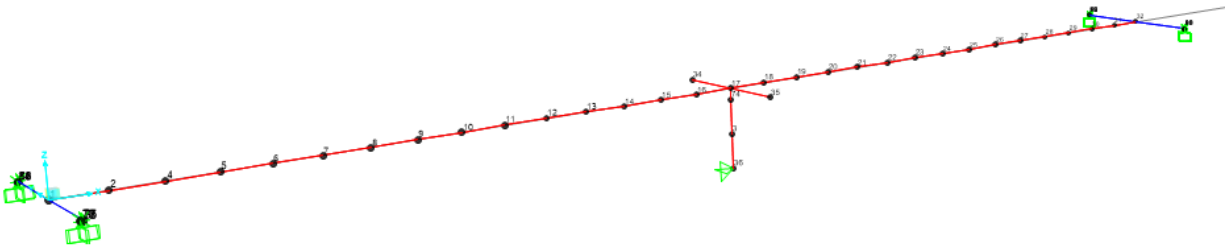

Figure 3.16. Spine model of OSB2 bridge created in CSiBridge

The nonlinear behavior of abutments was modeled using the same approach discussed for OSB1 bridge. A massless rigid element spanning a length of 37.5 feet was rigidly connected at each end of the deck section by assigning constraints in all degrees of freedom. At both ends of this rigid bar, a series of elements was defined longitudinally, comprising a rigid element, a gap element, and a multilinear plastic link element. The property modification factors for these rigid elements were the same as that explained in OSB1 bridge.

A finite length gap element with nonlinear properties in the longitudinal degree of freedom (U1) was defined. In the linear analysis case, the effective stiffness of the gap element was set to 2.0×10^5 kips/in with zero damping, same as that of OSB1 bridge. While for the nonlinear analysis a gap of 2" and stiffness of 6748 kips/in were assigned. This stiffness was calculated to be 10 times the stiffness in the longitudinal direction, as mentioned in section 2.5.3.2. Both end nodes of the gap element were restrained in U2, U3, and all rotational degrees of freedom.

The second link element is a multilinear plastic link element defined at the end of the gap element to define nonlinear behavior in the longitudinal degree of freedom (U1). For the linear analysis, the effective stiffness was 674.8 kips/in (i.e., $K_{abut}/2$) as computed in Table 3.2. As shown in Figure 3.17, the nonlinear force-deformation relationship using elastic-plastic behavior with a yield displacement of $\Delta_{abut} = 0.6$" and yield force of $F_{abut}/2 = 407.88$kips was assigned. The node connecting the gap element and this link element was subjected to restraints in all degrees of freedom except for U1 (longitudinal translation).

Multi-Linear Force-Deformation Definition

	Displ	Force
1	-100.	-407.88
2	-0.6	-407.88
3	0.	0.
4	0.6	407.88

Figure 3.17. Properties of OSB2 abutment link in longitudinal direction (kips-in)

Similar to OSB1 bridge, another multilinear plastic link element was assigned in the transverse direction to define nonlinear properties in the transverse direction (i.e. U1 direction of the link element) and elastic stiffness in the vertical direction (U2 direction of the link element). In U1 direction of this link element, the effective stiffness for the linear analysis was 295.2 kip/in

as computed in Table 3.3. While, for the nonlinear behavior, the elastic-plastic behavior (in tension and compression) with a yield displacement of 0.6 inches and a yield force of 177.5 kips, as shown in Figure 3.18 was assigned. The vertical stiffness was calculated using the dimensions of the bearing pad (a square of 18 inches × 18 inches and a height of 2.25 inches), which was calculated to be K_v = 720 kip/in, as tabulated in Table 3.3. This linear stiffness was assigned as the effective stiffness for all analysis cases in the U2 direction in the multilinear plastic link element.

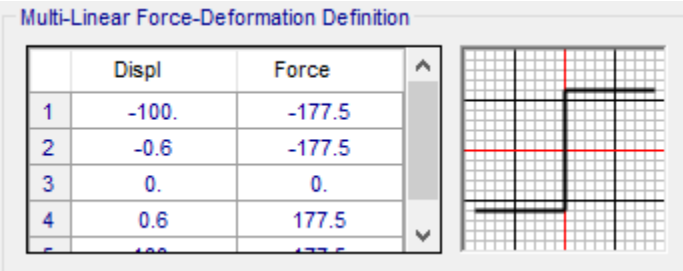

Figure 3.18. Properties of OSB2 abutment link in transverse direction (kips-in)

Similar to OSB1 bridge, two different models for pinned and fixed connection of column to the ground were created for OSB2 bridge. Since the height of the column, bent cap depth, and plastic hinge length are same for OSB 1 and OSB2, length of rigid offset, location of plastic hinges is same in both model, thus column modeling approach has not been discussed here for OSB2.

3.1.3. R14L Bridge

3.1.3.1. Geometric configuration

R14L bridge is a single two-column bent reinforced concrete box-girder bridge with two spans of 144.36ft and 141.08ft. Figure 3.19 and Figure 3.20 show the general configuration of Plan and Elevation view of R14L bridge respectively. The column height is not mentioned clearly in the drawing; thus, the column height is taken as 37.97 feet as mentioned in the work of

Aviram et. al.[56]. The bent comprises two circular reinforced concrete columns with diameter of 5.41', positioned at a distance of 10.51 ft and 32.82 ft along the length of bent cap. These circular columns are reinforced with 42#14 rebars (bundle of 2) longitudinal bars and #8 transverse spirals at 4.9" of interval. The geometry and material strength for R14L bridge are listed in Table 3.1.

R14L bridge has a total length of 285.43ft, superstructure width of 53.71ft with four cells and depth of 5.74 feet. The cross-section detail of the deck and the column are shown in Figure 3.21 and Figure 3.22. The bent cap is integral with the superstructure deck section; thus, its height is same as that of superstructure deck section. The width of the bent cap is 7.55' obtained from the detailed drawing.

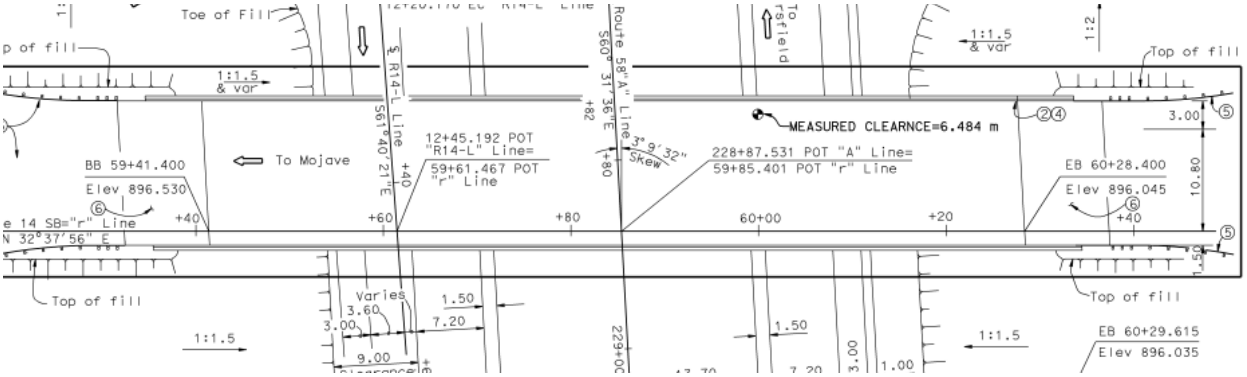

Figure 3.19. Schematic Plan view of R14L bridge (drawing provided by Caltrans)

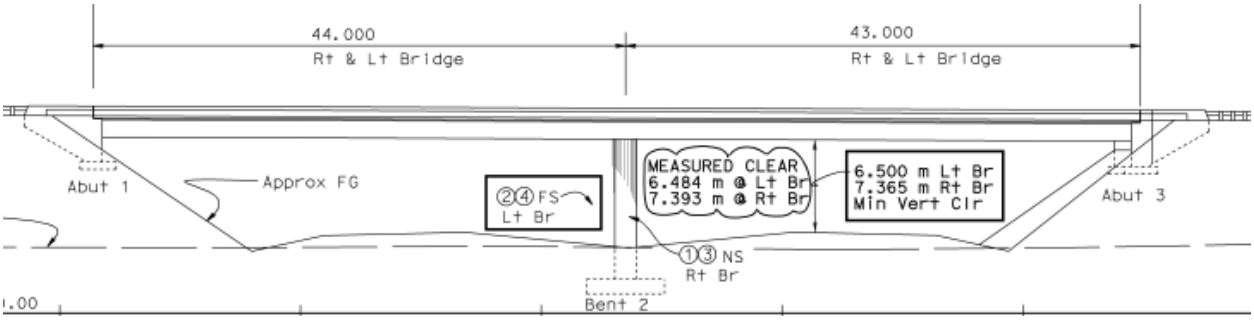

Figure 3.20. Schematic Elevation view of R14L bridge (Caltrans)

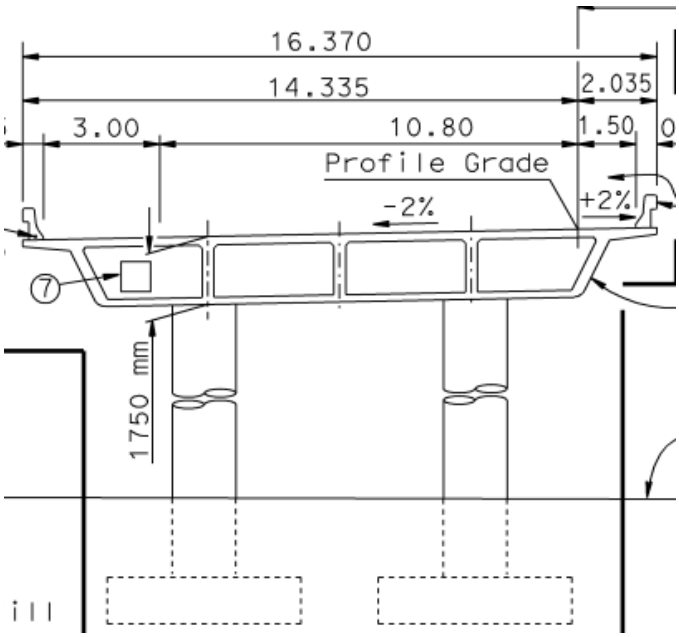

Figure 3.21. Cross-Section detail of R14L bridge deck (Caltrans)

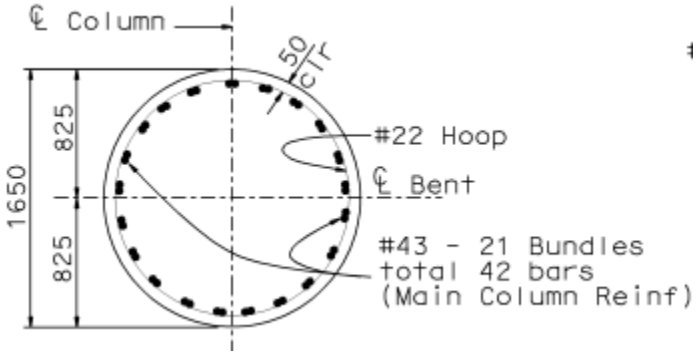

Figure 3.22. Cross-section detail of R14L bridge column (Caltrans)

According to the detailed drawing, the abutments are standard seat-type abutments. Bearing pads of size 15.75in×21.65in and height of 3.54in are located under each of the five webs. Material properties specified for the bridge components include a compressive strength of 4ksi for structural concrete of the bridge, and a yield strength of 60ksi for the reinforcement. The detail about the geometric and material properties of R14L bridge is tabulated in Table 3.1.

3.1.3.2. CSiBridge model

The connection of column with bent cap and deck section is assumed rigid because of the integral bent cap at the top and both pinned and fixed connection has been modeled at the base.

Figure 3.23 shows spine model for R14L bridge for the column with pinned connection to the ground.

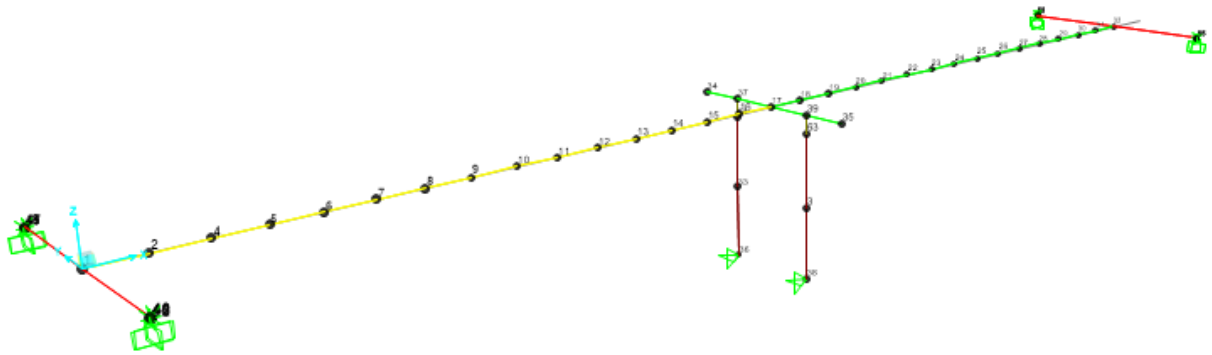

Figure 3.23. Spine model of R14L bridge created in CSiBridge

The abutment modeling approach was similar to OSB1 bridge. A massless rigid element of length 53.71 feet was rigidly connected at each end of the deck section. At both ends of this rigid bar, a series of longitudinal elements were defined in the bridge consisting of a rigid element, a gap element, and a multilinear plastic link element. The property modification factor for these rigid elements were same as that explained for OSB1 bridge.

A gap element of finite length with nonlinear properties in the longitudinal degree of freedom (U1) was defined. In the linear analysis case, the effective stiffness of the gap element was same as that of OSB1 bridge. However, for the nonlinear analysis a gap of 2" and stiffness of 10889.3 kips/in were assigned. Both end nodes of the gap element were restrained in U2, U3, and all rotational degrees of freedom. The second link element was defined at the end of the gap element to define nonlinear behavior in the longitudinal degree of freedom (U1). For the linear analysis, the effective stiffness was taken as 1088.93 kips/in (i.e., $K_{abut}/2$) as computed in Table 3.2. The nonlinear force-deformation relationship, as shown in Figure 3.24, using an elastic-plastic behavior with a yield displacement of $\Delta_{abut} = 0.58$" and yield force of $F_{abut}/2 =$

627.89kips was assigned. The node connecting the gap element and this link element was subjected to restraints in all degrees of freedom except for U1 (longitudinal translation).

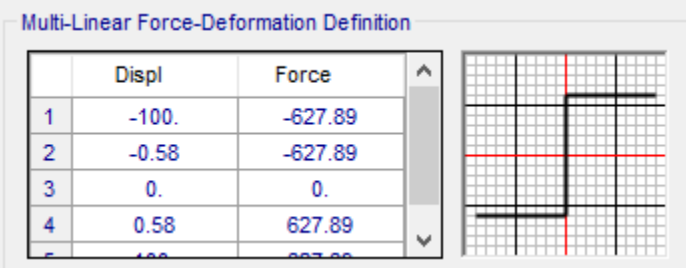

Figure 3.24. Nonlinear property of R14L bridge abutment in longitudinal direction (kips-in)

Similar to OSB1 bridge, the nonlinear properties in the transverse direction were defined by assigning another multilinear plastic link element in the transverse direction (U1 direction of the link element) and elastic stiffness in the vertical direction (U2 direction of the link element). In U1 direction of the link element, the effective stiffness for the linear analysis was 410.4 kip/in. The elastic-plastic behavior with a yield displacement of 0.58" and a yield force of 236.6kips, as shown in Figure 3.25 was assigned for the nonlinear behavior. Using the dimension of bearing pad, the elastic vertical stiffness was calculated as K_v = 481.2 kip/in. This linear stiffness was assigned as the effective stiffness for all analysis cases in the U2 direction of the transverse multilinear plastic link element.

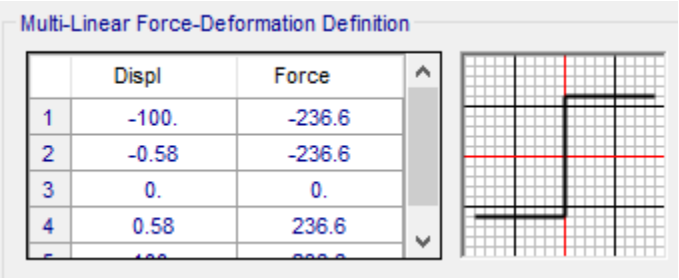

Figure 3.25. Nonlinear property of R14L bridge abutment in transverse direction (kips-in)

The column modeling approach for R14L bridge is same as OSB1 bridge. The length of analytical plastic hinge in the R14L bridge column was calculated to be 4.31ft. Thus, the top

element of each column was 4.31ft long. The length of rigid offset calculated by CSiBridge was 2.87ft and therefore, the plastic hinge was assigned at this distance from the node at deck line. A cracked section property modifier of 0.35 was assigned to the elastic elements while a factor of 3 was assigned to the top element in column with pinned base and top and bottom element in fixed base.

3.1.4. R14R Bridge

3.1.4.1. Geometric configuration

R14R bridge is a two-span reinforced concrete box girder bridge with a single column bent. R14L and R14R bridges have the same dimension and material strength except R14L is a two-column bent while R14R is a single column bent bridge and their cross-sections are also different. The total span length is 285.43ft. Figure 3.26 and Figure 3.20 show the schematic plan and elevation view of R14R bridge respectively. The height of column is 37.97ft and its diameter is 5.41'. This circular column was reinforced 42#14 rebars (bundle of 2) longitudinal bars and #8 transverse spirals at 4.9" of interval, as illustrated in Figure 3.27. The geometric and material specifications for the R14R bridge are tabulated in Table 3.1.

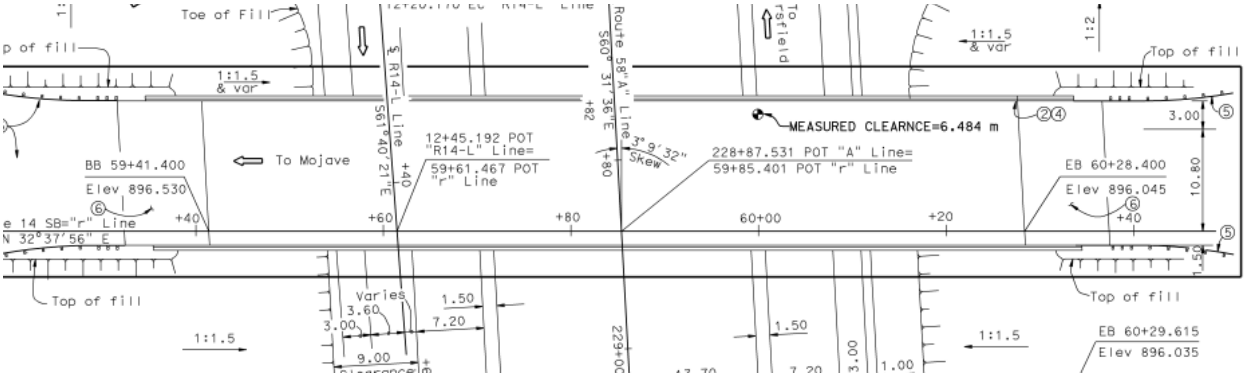

Figure 3.26. Schematic Plan view of R14R bridge (drawing provided by Caltrans)

Total superstructure width of R14R bridge is 41.9 feet with three cells and a depth of 5.74feet. The cross-section details of the column and deck are represented in Figure 3.27 and

Figure 3.28, respectively. The width of bent cap is taken to be 7.55 ft and the depth is 5.74 ft. Bearing pad measuring 15.75in×21.65in and height of 3.54in is located below each of the four webs. The connection of the column with the bent cap and deck section is rigid at the top. The abutments are standard seat-type abutments. The compressive strength of structural concrete is 4ksi and yield strength of reinforcement is 60ksi. Further details regarding the geometric and material properties of the R14R bridge are presented in Table 3.1.

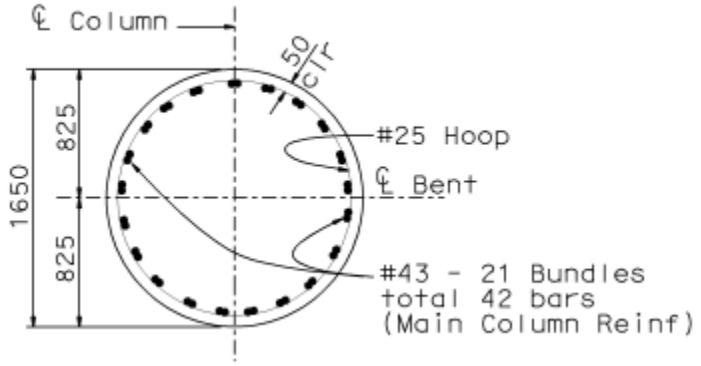

Figure 3.27. Cross-section detail of R14R bridge column (Caltrans)

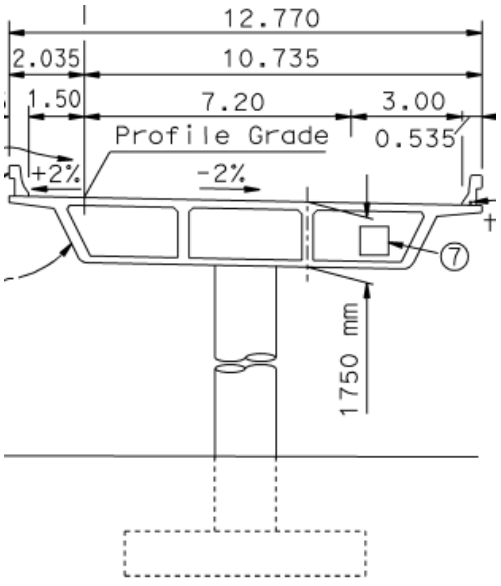

Figure 3.28. Cross-Section detail of R14R bridge deck (Caltrans)

3.1.4.2. CSiBridge model

Based on the information about geometric configuration, a spine model of R14R bridge was created in CSiBridge as shown in Figure 3.29. The modeling approach was similar to R14L bridge.

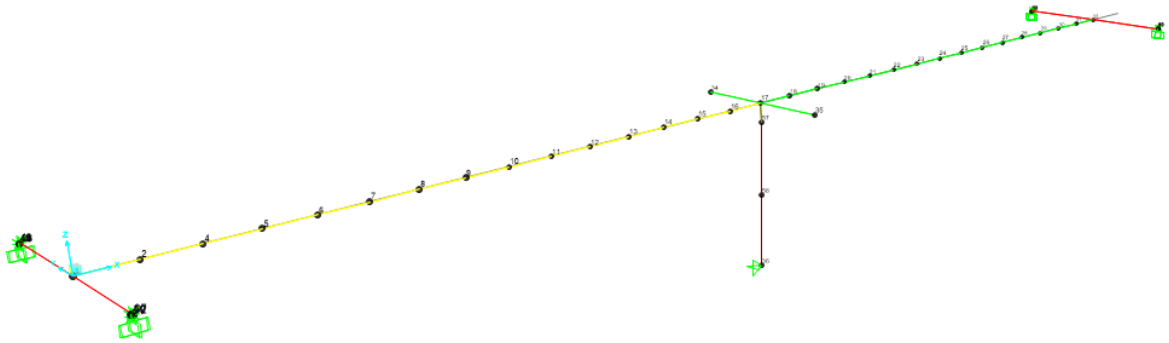

Figure 3.29. Spine model of R14R bridge created in CSiBridge

The nonlinear behavior of abutment was modeled using the same approach discussed for R14L bridge. A rigid element of length 41.9ft was rigidly connected at each end of the deck section. A gap element was defined with nonlinear properties in the longitudinal degree of freedom (U1). For the linear analysis case, the effective stiffness was set to 2.0×10^5 kips/in with zero damping, while for the nonlinear analysis a gap of 2" and stiffness of 7843.3 kips/in were assigned. Both ends of the gap element were restrained in U2, U3, R1, R2 and R3 degrees of freedom.

A multilinear plastic link element was defined at the end of the gap element. In linear analysis case, the effective stiffness was $K_{abut}/2$=784.33kips/in, on the other hand, the nonlinear force-deformation curve was defined with a yield displacement of $\Delta_{abut}= 0.58$" and yield force of $F_{abut}/2 = 452.26$kips as shown in Figure 3.30. The node that connects the gap element and this link element was subjected to restraints in all degrees of freedom except for U1 (longitudinal translation).

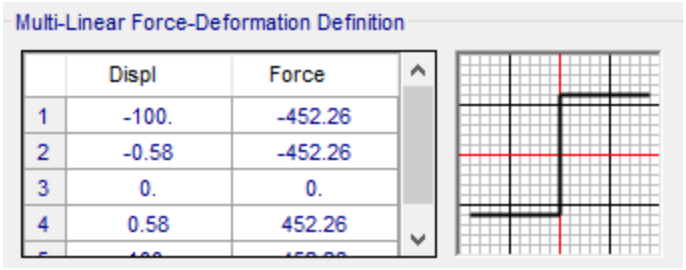

Figure 3.30. Nonlinear property of R14R bridge abutment in longitudinal direction (kips-in)

Similar to R14L bridge, another multilinear plastic link element was assigned in the transverse direction. In U1 direction of this link element, the effective stiffness for the linear analysis was 320.1 kip/in. While to model the nonlinear behavior, the elastic-plastic behavior with a yield displacement of 0.58 inches and a yield force of 184.6 kips, as shown in Figure 3.31 was assigned. Using the dimension of the bearing pad (15.75in×21.65in and height of 3.54in), the vertical stiffness was calculated to be K_v = 481.2 kip/in, as tabulated in Table 3.3. This linear stiffness was assigned as the effective stiffness for all analysis cases in the U2 direction in the multilinear plastic link element.

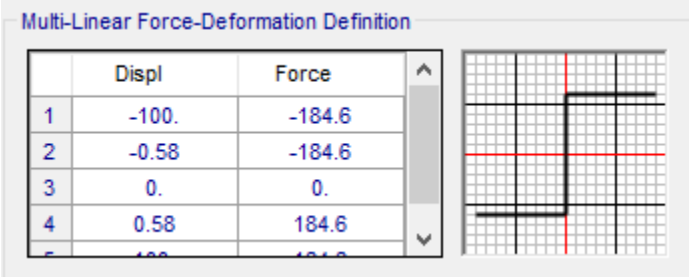

Figure 3.31. Nonlinear property of R14R bridge abutment in transverse direction (kips-in)

Similar to R14L bridge, two models for the pinned and fixed connection of column to the ground were created. Since the height of the column, bent cap depth reinforcement detailing are same for R14L and R14R, the plastic hinge, length of rigid offset, and location of plastic hinges are same in both model.

3.1.5. Adobe Bridge

3.1.5.1. Geometric configuration

Adobe bridge is a single two-column bent concrete box girder bridge with two spans of length 102.79ft and 100.3 ft. Figure 3.32 and Figure 3.33 show the general configuration of Plan and Elevation of Adobe bridge respectively. The column height is taken as 26.6 feet mentioned in [56]. The bent comprises two flare columns as per the drawing, however, for this research work circular reinforced concrete columns with diameter of 4', were considered. The location of columns was calculated to be at a distance of 11.83ft and 23.66ft along the length of bent cap which is equal to 35.49ft. These columns are reinforced with 20#10 longitudinal bars and #6 transverse spirals at 4.9" of interval. Adobe bridge has a total length of 203.08ft, superstructure width of 41.51ft with five cells and depth of 4.1 feet. The cross-section detail of the deck and the column are shown in Figure 3.34 and Figure 3.35. The depth of bent cap is same as that of superstructure deck section and the its width is 7'.

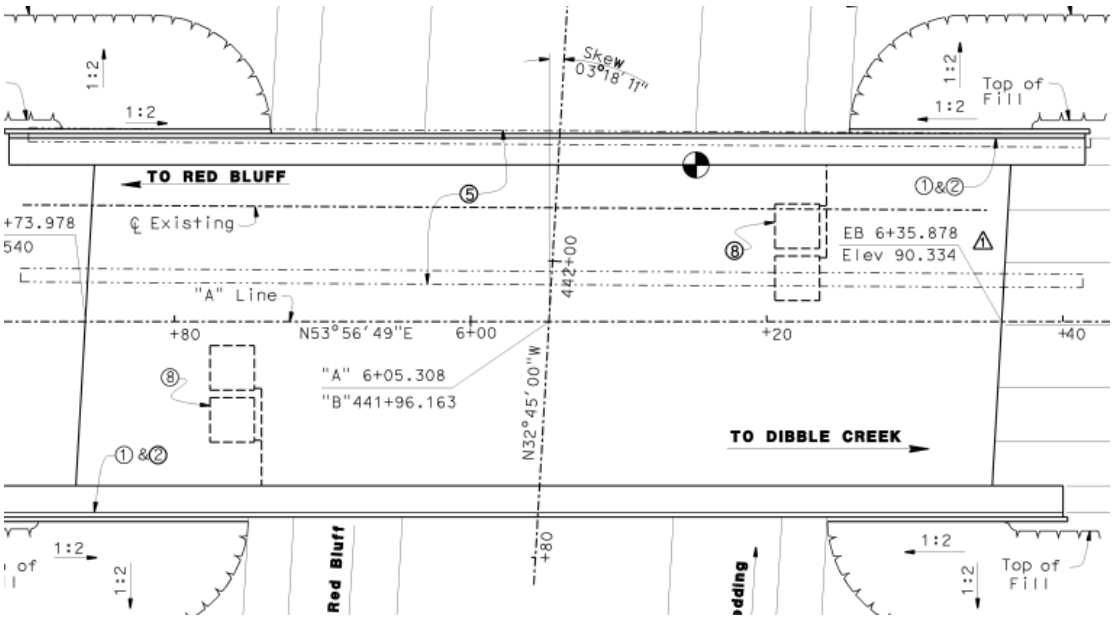

Figure 3.32. Schematic Plan view of Adobe bridge (drawing provided by Caltrans)

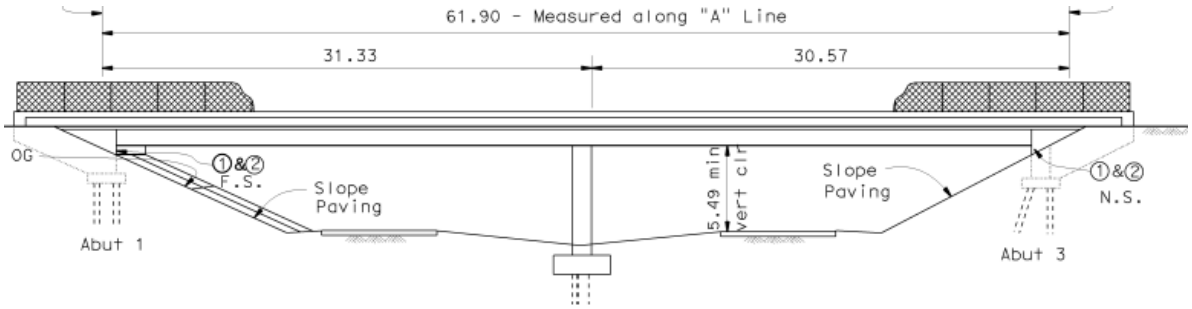

Figure 3.33. Schematic Elevation view of Adobe bridge (Caltrans)

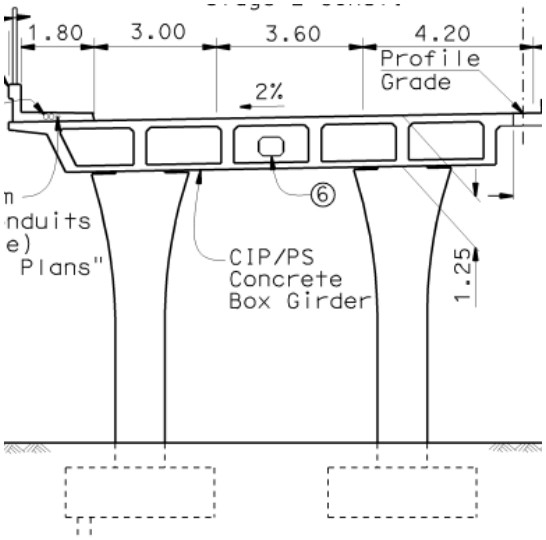

Figure 3.34. Cross-Section detail of Adobe bridge deck (Caltrans)

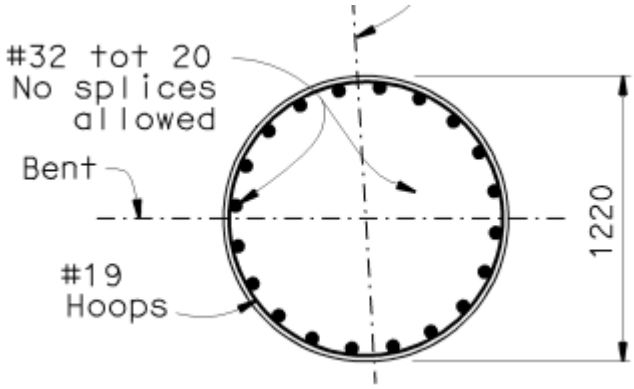

Figure 3.35. Cross-section detail of Adobe bridge column (Caltrans)

The abutments are standard seat-type abutments. Bearing pads of size 14.02in×14.02in and height of 2.36in are located under each of the six webs. The material properties for structural

concrete include a compressive strength of 4ksi, and a yield strength of 60ksi for the reinforcement.

3.1.5.2. CSiBridge model

Based on the geometric and material property, CSiBridge model of Adobe bridge was created. The bent was assumed integral to the deck and both pinned and fixed connection of column was modeled at the base. Figure 3.36 shows spine model of Adobe bridge with column fixed to the ground.

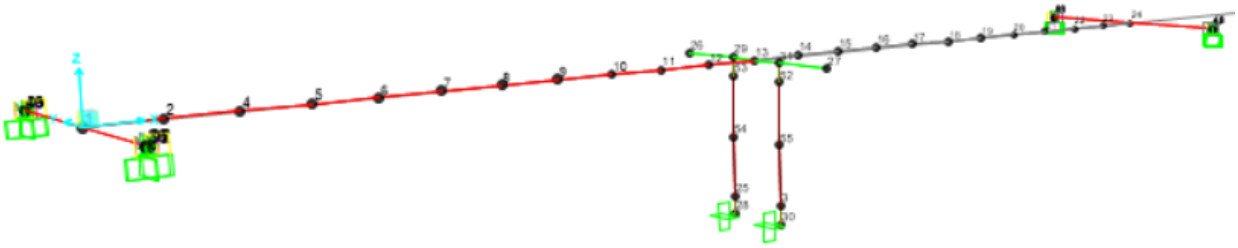

Figure 3.36. Spine model of Adobe bridge created in CSiBridge

Similar to OSB1 bridge, the simplified abutment model was developed. However, the length of massless rigid element for Adobe bridge was 41.51 feet, connected at each end of the deck section. The effective stiffness of the gap element for the nonlinear analysis was 7085.8 kips/in. For the second link element, the effective stiffness in linear analysis was taken as 708.58kips/in as computed in Table 3.2. However, for the nonlinear analysis, a yield displacement of $\Delta_{abut} = 0.41''$ and yield force of $F_{abut}/2 = 290.9$kips was used, as shown in Figure 3.37.

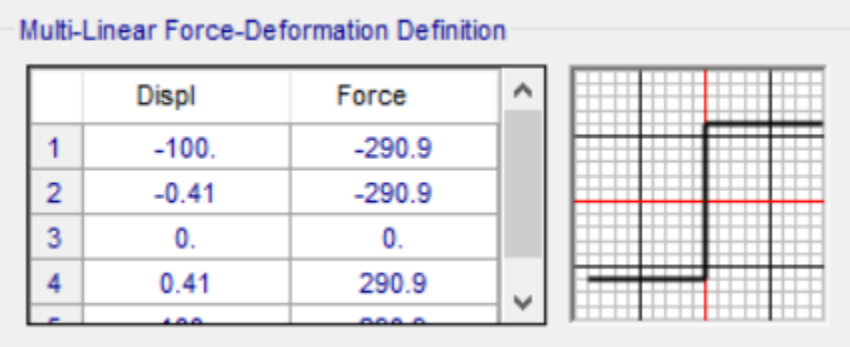

Figure 3.37. Nonlinear property of Adobe bridge abutment in longitudinal direction (kips-in)

Similar to OSB1 bridge, another multilinear plastic link element in the transverse direction was defined. In U1 direction of the link element, the effective stiffness for the linear analysis was 261.6 kip/in. The nonlinear property was assigned by defining elastic-plastic behavior with a yield displacement of 0.41" and a yield force of 107.4kips, as shown in Figure 3.38. Based on the dimension and material strength of bearing pad, the elastic vertical stiffness was calculated, K_v = 415.8 kip/in.

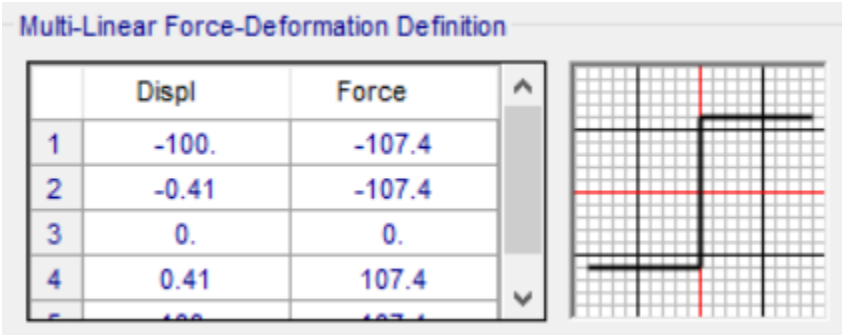

Figure 3.38. Nonlinear property of Adobe bridge abutment in transverse direction (kips-in)

The length of plastic hinge for Adobe bridge column was calculated to be 3.08ft and the length of rigid offset calculated by CSiBridge was 2.05ft. The modeling approach of Adobe bridge column was same as OSB1 bridge; therefore, it has not been explained in this section.

3.1.6. La Veta Bridge

3.1.6.1. Geometric configuration

La Veta bridge is a two-span concrete box girder bridge with two-column at bent. The span length is 154.86ft and 145.01ft. The schematic elevation of La Veta bridge is shown in Figure 3.39. The skewness in La Veta bridge in this work was not considered. The column height was taken as 25.4ft[56]. The bent consists of two flare columns as per the drawing, however, circular reinforced concrete columns with diameter of 5.58', were considered in this research work. The columns are located at a distance of 21.66ft and 43.33ft along the length of bent cap, which is 64.99ft long. These columns are reinforced with 44#11 longitudinal bars (bundles of 2) and #6 transverse spirals at 3.54" of interval. The geometry and material strength for La Veta bridge are listed in Table 3.1. The total length of bridge is 299.87ft, deck width of 75.49ft with six cells and depth of 6.23ft. For cross-section detail of the deck and column, Figure 3.40 and Figure 3.41 can be referred. The height of bent cap is same as the depth of superstructure and its width is 6.23'.

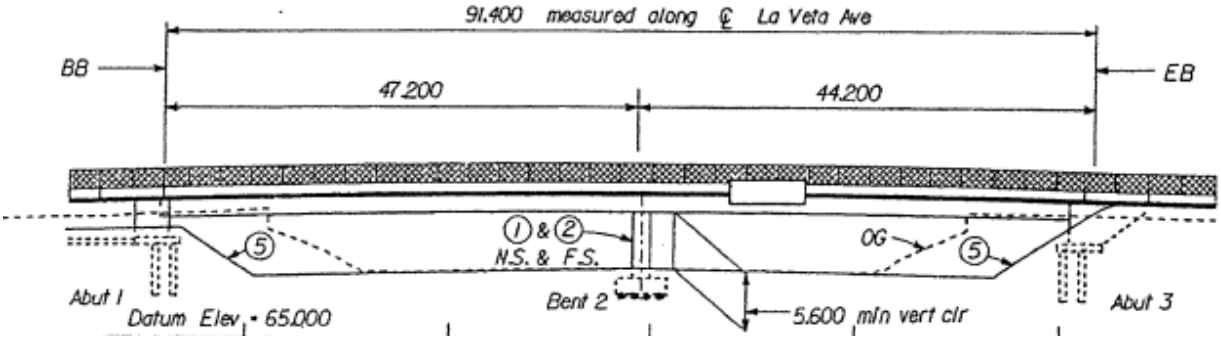

Figure 3.39. Schematic Plan view of La Veta bridge (drawing provided by Caltrans)

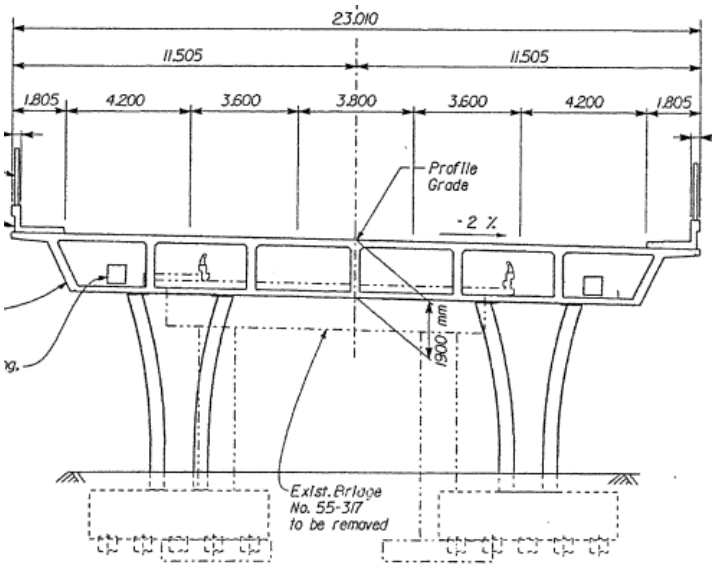

Figure 3.40. Cross-Section detail of La Veta bridge deck (Caltrans)

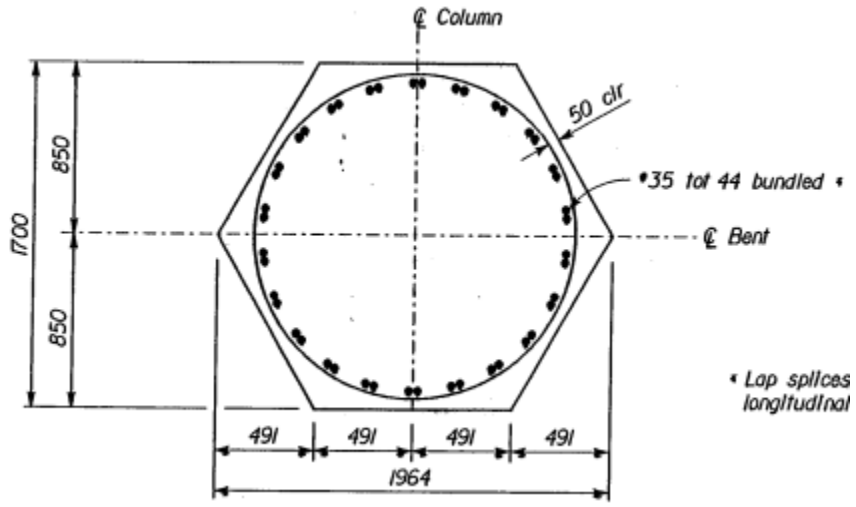

Figure 3.41. Cross-section detail of La Veta bridge column

The abutments are considered to be seat-type abutments. Bearing pads of size 15.75in×23.62in and height of 2.46in are located under each of the seven webs. The structural concrete has a compressive strength of 4ksi, and a yield strength of 60ksi for the reinforcement.

3.1.6.2. CSiBridge model

La Veta bridge has integral type of bent cap, thus, rigid connection was provided between bent and column and bent and superstructure. Figure 3.42 shows spine model for La Veta bridge for the column with pinned connection to the ground.

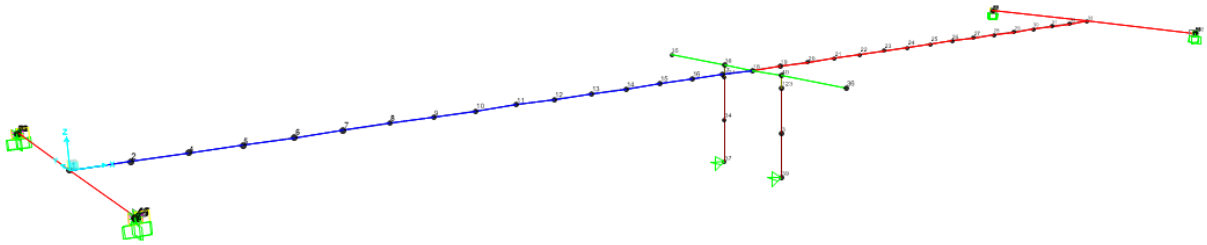

Figure 3.42. Spine model of La Veta bridge created in CSiBridge

Similar to OSB1 bridge model, the simplified abutment model was developed for La Veta bridge. A rigid element of length 75.49 feet was rigidly connected at each end of the deck section. The linear analysis case in gap element was same as that of OSB1 bridge, while for the nonlinear analysis a gap of 2" and stiffness of 17106.5 kips/in were assigned. For the linear analysis in multilinear plastic link element modeled at the end of the gap element, the effective stiffness was taken as 1710.65kips/in, while the nonlinear force-deformation relationship was assigned with a yield displacement of $\Delta_{abut} = 0.62"$ and yield force of $F_{abut}/2 = 1066.01$kips for the nonlinear analysis, as shown in Figure 3.43.

Multi-Linear Force-Deformation Definition

	Displ	Force
1	-100.	-1066.01
2	-0.62	-1066.01
3	0.	0.
4	0.62	1066.01

Figure 3.43. Nonlinear property of La Veta bridge abutment in longitudinal direction (kips-in)

In transverse direction, the effective stiffness of link element for the linear analysis was 607.1kip/in in U1 direction and for nonlinear analysis a yield displacement of 0.62” and a yield force of 378.3kips were assigned, as shown in Figure 3.44. Using the dimension and material strength of bearing pad, the vertical stiffness was estimated as K_v = 755.91 kip/in.

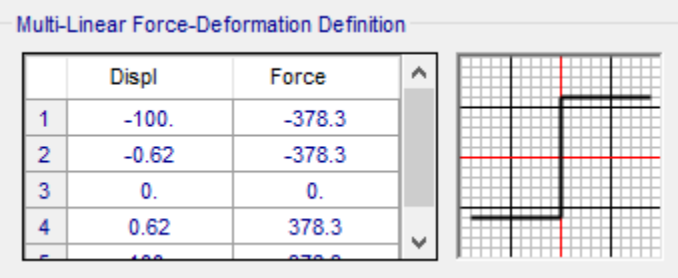

Figure 3.44. Nonlinear property of La Veta bridge abutment in transverse direction (kips-in)

Column with both pinned and fixed connection were modeled similar to OSB1 bridge. The length of analytical plastic hinge for La Veta bridge column was estimated to be 3.09ft and the length of rigid offset was 3.078ft. The modeling approach of column is similar to that of OSB1 bridge.

Table 3.1. Geometry and material strength of six different bridges

Geometry and Material	Unit	Bridge Name					
		R14_L	R14_R	Adobe	La Veta	OSB1	OSB2
Deck section							
Total length	ft	285.43	285.43	203.08	299.87	300.00	300.00
Number of spans	no.	2.00	2.00	2.00	2.00	2.00	2.00
Span 1	ft	144.36	144.36	102.79	154.86	150.00	150.00
Span 2	ft	141.08	141.08	100.30	145.01	150.00	150.00
Total deck width	ft	53.71	41.90	41.51	75.49	47.50	37.50
Deck depth	ft	5.74	5.74	4.10	6.23	6.00	6.00
Concrete material	ksi	4.00	4.00	4.00	4.00	3.60	4.00
Young's modulus	ksi	3605.00	3605.00	3605.00	3605.00	3420.00	3605.00
Cap Beam							
Cap beam width	ft	7.55	7.55	7.00	7.55	8.67	8.67
Cap beam depth	ft	5.74	5.74	4.10	6.23	6.00	6.00
Cap beam length	ft	43.32	31.64	35.49	64.99	41.50	31.50
Column							
Number of columns	no.	2.00	1.00	2.00	2.00	2.00	1.00
location of column 1	ft	10.51	15.82	11.83	21.66	8.75	15.75
location of column 2	ft	32.82		23.66	43.33	32.75	
Height of column	ft	37.97	37.97	26.60	25.40	20.00	20.00
Diameter	ft	5.41	5.41	4.00	5.58	5.50	5.50
Longitudinal rebar		42#14 (bundles of 2)	42#14 (bundles of 2)	20#10	44#11 (bundles of 2)	36#11 (bundles of 1)	44#11 (bundles of 2)
Transverse rebar		#7@4.9″	#7@4.9″	#6@4.9″	#6@3.54" spirals	#8@6″	#8@6″
concrete material	ksi	4.00	4.00	4.00	4.00	3.60	4.00
Young's modulus	ksi	3605.00	3605.00	3605.00	3605.00	3420.00	3605.00
fy of steel	ksi	60.00	60.00	60.00	60.00	60.00	60.00
Plastic hinge							
Length	ft	4.31	4.31	3.08	3.09	2.80	2.80

Note: The measurement in Table 3.1 is in imperial units

Table 3.2. Calculation of Longitudinal stiffness of the abutment

Bridge Dimension					Longitudinal stiffness							
Bridge	d_w (ft)	h_{abut} (ft)	w_{abut} (ft)	w_{ww} (ft)	K_{abut} (kip/in)	F_{abut} (kip)	Δ_{gap} (in)	Δ_{abut} (in)	Δ_{eff} (in)	K_{eff} (kip/in)	$\frac{F_{abut}}{2}$ (kip)	$\frac{K_{abut}}{2}$ (kip/in)
R14L	53.71	5.74	42.22	17.90	2177.85	1255.78	2.00	0.58	2.58	487.38	627.89	1088.93
R14R	41.90	5.74	30.41	13.97	1568.66	904.51	2.00	0.58	2.58	351.05	452.26	784.33
Adobe	41.51	4.10	33.31	13.84	1417.17	581.80	2.00	0.41	2.41	241.36	290.90	708.58
La Veta	75.49	6.23	63.02	25.16	3421.29	2132.02	2.00	0.62	2.62	812.77	1066.01	1710.65
OSB1	47.50	6.00	35.50	15.83	1881.50	1131.24	2.00	0.60	2.60	434.88	565.62	940.75
OSB2	37.60	6.00	25.60	12.53	1356.80	815.77	2.00	0.60	2.60	313.61	407.88	678.40

Table 3.3. Calculation of Transverse stiffness and Vertical stiffness

Transverse stiffness						Vertical Stiffness
Bridge	K_{abut} (kip/in)	F_{abut} (kip)	Δ_{eff} (in)	$\frac{F_{abut}}{2}$ (kip)	$\frac{K_{abut}}{2}$ (kip/in)	K_v (kip/in)
R14L	820.78	473.27	0.58	236.64	410.39	481.19
R14R	640.28	369.19	0.58	184.60	320.14	481.19
Adobe	523.28	214.83	0.41	107.41	261.64	415.80
La Veta	1214.24	756.67	0.62	378.33	607.12	755.91
OSB1	745.93	448.48	0.60	224.24	372.96	720.00
OSB2	590.46	355.01	0.60	177.50	295.23	720.00

3.2. Earthquake Ground Motion

This research was done for the bridges in California. Therefore, the earthquake events that happened in California in the last 55 years (1970 AD-2024 AD) were selected. The bridge structures are normally designed to function for 50-70 years, therefore, the earthquake ground motions occurred in 55 years were selected in this research work. To determine the mean magnitude and closest distance to rupture surface for earthquake events in California, USGS Disaggregation Hazard Tool has been used. From this hazard tool, the latitude was obtained as 36.374° and longitude as -119.27° for California. The site class of BC (Vs 30 760) was selected, and the probability of return period was selected to be 2% in 50 years (return period is 2475 years). From this Hazard tool, the mean earthquake was obtained to be 6.23 magnitude and the closest distance to rupture surface was obtained as 23.95km. Using these parameters, earthquake ground motions were selected from the PEER Ground motion Database.

The web-based PEER Ground motion Database (Pacific Earthquake Engineering Research center) is a platform to search, select, and download earthquake ground motion records. It provides unscaled and unrotated records. A set of 28 earthquake ground motions obtained from the PEER Ground motion Database was employed in the Nonlinear THA of the six bridges with two boundary condition of column with ground. The earthquake ground motions used are unscaled or with a scaling factor of 1. The name of earthquake, year, station name, and its characteristics like 5%-75% duration (duration from the 5% to 75% Arias intensity), 5%-95% duration (duration from the 5% to 95% Arias intensity), Arias intensity, magnitude, mechanism, R_{rup} (closest distance to rupture surface), R_{jb} (Joyner-Boore distance), and V_s30 (timed-average shear-wave velocity to a depth of 30 meters), considered in this research work are listed in Table 3.4. Each of the earthquakes considered in this study has three components:

two in horizontal direction and one in vertical direction. Joyner-Boore distance is defined as the shortest distance from a site to the surface projection of the rupture plane. Since the response of horizontal displacement has dominant responses in bridges, the vertical component has not been considered in this study. The file name for two-horizontal components and the direction in which they are applied are listed in Table 3.5, where U1 and U2 are the longitudinal and transverse direction of the bridge.

Table 3.4. List of 28 earthquake ground motion and their characteristics

S.N.	Earthquake Name	Year	Station Name	5-75% Duration (sec)	5-95% Duration (sec)	Arias Intensity (m/sec)	Magnitude	Mechanism	Rjb (km)	Rrup (km)	Vs30 (m/sec)
1	"Northridge-01"	1994	"LA - Hollywood Stor FF"	6.4	12	2	6.69	Reverse	19.7	24	316.5
2	"Loma Prieta"	1989	"Coyote Lake Dam - Southwest Abutment"	6	15.7	1.5	6.93	Reverse Oblique	20	20.3	561.4
3	"Superstition Hills-01"	1987	"Imperial Valley Wildlife Liquefaction Array"	7.3	15.2	0.3	6.22	strike slip	17.6	17.6	179
4	"Superstition Hills-02"	1987	"Plaster City"	9	13.3	0.6	6.54	strike slip	22.3	22.3	316.6
5	"N. Palm Springs"	1986	"Cranston Forest Station"	5.2	7.6	0.2	6.06	Reverse Oblique	27.2	27.5	425.2
6	"Chalfant Valley-02"	1986	"Lake Crowley - Shehorn Res."	3.8	9.8	0.1	6.19	strike slip	22.1	24.5	456.8
7	"Morgan Hill"	1984	"Agnews State Hospital"	23	40.9	0.1	6.19	strike slip	24.5	24.5	239.7
8	"Coalinga-01"	1983	"Cantua Creek School"	6.2	12.6	1.2	6.36	Reverse	23.8	24	274.7
9	"Imperial Valley-06"	1979	"El Centro Array #1"	7	19.5	0.3	6.53	strike slip	19.8	21.7	237.3
10	"San Fernando"	1971	"LA - Hollywood Stor FF"	5.2	13.4	0.7	6.61	Reverse	22.8	22.8	316.5

Table 3.4. List of 28 earthquake ground motion and their characteristics (continued)

S.N.	Earthquake Name	Year	Station Name	5-75% Duration (sec)	5-95% Duration (sec)	Arias Intensity (m/sec)	Magnitude	Mechanism	Rjb (km)	Rrup (km)	Vs30 (m/sec)
11	"Mammoth Lakes-01"	1980	"Mammoth Lakes H. S."	5.3	8.2	0.8	6.06	Normal Oblique	4.48	4.67	346.8
12	"Coyote Lake"	1979	"Coyote Lake Dam - Southwest Abutment"	2.7	8.5	0.4	5.74	strike slip	5.3	6.13	561.4
13	"Westmorland"	1981	"Brawley Airport"	3.6	8.8	0.3	5.9	strike slip	15.3	15.4	208.7
14	"Yountville"	2000	"APEEL 2 - Redwood City"	6.3	15.3	0	5	strike slip	94.2	94.5	133.1
15	"Santa Barbara"	1978	"Santa Barbara Courthouse"	4.3	7.5	0.2	5.92	Reverse Oblique	0	12.2	515
16	"San Juan Bautista"	1998	"Hollister - City Hall Annex"	9.8	19.8	0	5.17	strike slip	11.6	13.5	272.8
17	"Mohawk Val_ Portola"	2001	"Martis Creek Dam (Right Abtmnt)"	3.6	9.5	0	5.17	strike slip	67	67.1	553.3
18	"Oroville-01"	1975	"Oroville Seismograph Station"	1.5	3.4	0	5.89	Normal	7.79	7.99	680.4
19	"Sierra Madre"	1991	"Altadena - Eaton Canyon"	1.4	5.3	1.2	5.61	Reverse	8.57	13.2	375.2
20	"Whittier Narrows-01"	1987	"Alhambra - Fremont School"	2.3	5.7	0.9	5.99	Reverse Oblique	1.67	14.7	549.8
21	"Parkfield-02_ CA"	2004	"Shandon-1-story High School Bldg"	5.8	16.2	0.1	6	strike slip	12.6	13	357.4

Table 3.4. List of 28 earthquake ground motion and their characteristics (continued)

S.N.	Earthquake Name	Year	Station Name	5-75% Duration (sec)	5-95% Duration (sec)	Arias Intensity (m/sec)	Magnitude	Mechanism	Rjb (km)	Rrup (km)	Vs30 (m/sec)
22	"Joshua Tree_ CA "	1992	"Thousand Palms Post Office"	5.8	11.1	0.6	6.1	strike slip	17.2	17.9	333.9
23	"San Simeon_ CA"	2003	"Cambria - Hwy 1 Caltrans Bridge"	7.8	13.2	0.4	6.52	Reverse	6.97	7.25	362.4
24	"Chalfant Valley-01"	1986	"Benton"	5.7	18.5	0	5.77	strike slip	24.3	24.3	370.9
25	"Hector Mine"	1999	"12440 Imperial Hwy_ North Grn"	20.6	21.5	0	7.13	strike slip	177	177	276.4
26	"Cape Mendocino"	1992	"Cape Mendocino"	2.9	9.7	6	7.01	Reverse	0	6.96	567.8
27	"Livermore-01"	1980	"APEEL 3E Hayward CSUH"	3.6	10.3	0	5.8	strike slip	29.2	30.6	517.1
28	"Northern Calif-07"	1975	"Cape Mendocino"	4.3	5.7	0.1	5.2	strike slip	28.7	34.7	567.8

Table 3.5. Horizontal component of earthquake obtained from PEER Ground motion Database

S.N.	Earthquake Name	Horizontal-1 Acc. Filename (U1)	Horizontal-2 Acc. Filename (U2)
1	"Northridge-01"	RSN995_NORTHR_PEL090.AT2	RSN995_NORTHR_PEL360.AT2
2	"Loma Prieta"	RSN755_LOMAP_CYC195.AT2	RSN755_LOMAP_CYC285.AT2
3	"Superstition Hills-01"	RSN718_SUPER.A_A-IVW090.AT2	RSN718_SUPER.A_A-IVW360.AT2
4	"Superstition Hills-02"	RSN724_SUPER.B_B-PLS045.AT2	RSN724_SUPER.B_B-PLS135.AT2
5	"N. Palm Springs"	RSN516_PALMSPR_CFR225.AT2	RSN516_PALMSPR_CFR315.AT2
6	"Chalfant Valley-02"	RSN552_CHALFANT.A_A-SHE009.AT2	RSN552_CHALFANT.A_A-SHE099.AT2
7	"Morgan Hill"	RSN447_MORGAN_AGW240.AT2	RSN447_MORGAN_AGW330.AT2
8	"Coalinga-01"	RSN322_COALINGA.H_H-CAK270.AT2	RSN322_COALINGA.H_H-CAK360.AT2
9	"Imperial Valley-06"	RSN172_IMPVALL.H_H-E01140.AT2	RSN172_IMPVALL.H_H-E01230.AT2
10	"San Fernando"	RSN68_SFERN_PEL090.AT2	RSN68_SFERN_PEL180.AT2
11	"Mammoth Lakes-01"	RSN232_MAMMOTH.I_I-MLS254.AT2	RSN232_MAMMOTH.I_I-MLS344.AT2
12	"Coyote Lake"	RSN145_COYOTELK_CYC160.AT2	RSN145_COYOTELK_CYC250.AT2
13	"Westmorland"	RSN314_WESMORL_BRA225.AT2	RSN314_WESMORL_BRA315.AT2
14	"Yountville"	RSN1843_YOUNTVL_A02090.AT2	RSN1843_YOUNTVL_A02360.AT2

Table 3.5. Horizontal component of earthquake obtained from PEER Ground motion Database (continued)

S.N.	Earthquake Name	Horizontal-1 Acc. Filename (U1)	Horizontal-2 Acc. Filename (U2)
15	"Santa Barbara"	RSN136_SBARB_SBA132.AT2	RSN136_SBARB_SBA222.AT2
16	"San Juan Bautista"	RSN1756_SANJUAN_CHA090.AT2	RSN1756_SANJUAN_CHA180.AT2
17	"Mohawk Val_ Portola"	RSN1914_MOHAWK_2125B270.AT2	RSN1914_MOHAWK_2125A360.AT2
18	"Oroville-01"	RSN106_OROVILLE_A-ORV037.AT2	RSN106_OROVILLE_A-ORV307.AT2
19	"Sierra Madre"	RSN1641_SMADRE_ALT000.AT2	RSN1641_SMADRE_ALT090.AT2
20	"Whittier Narrows-01"	RSN589_WHITTIER.A_A-ALH180.AT2	RSN589_WHITTIER.A_A-ALH270.AT2
21	"Parkfield-02_ CA"	RSN4085_PARK2004_36535180.AT2	RSN4085_PARK2004_36535270.AT2
22	"Joshua Tree_ CA "	RSN6874_JOSHUA_5068045.AT2	RSN6874_JOSHUA_5068135.AT2
23	"San Simeon_ CA"	RSN3979_SANSIMEO_37737090.AT2	RSN3979_SANSIMEO_37737360.AT2
24	"Chalfant Valley-01"	RSN543_CHALFANT.B_B-BEN270.AT2	RSN543_CHALFANT.B_B-BEN360.AT2
25	"Hector Mine"	RSN1759_HECTOR_IMH090.AT2	RSN1759_HECTOR_IMH180.AT2
26	"Cape Mendocino"	RSN825_CAPEMEND_CPM000.AT2	RSN825_CAPEMEND_CPM090.AT2
27	"Livermore-01"	RSN210_LIVERMOR_A-A3E146.AT2	RSN210_LIVERMOR_A-A3E236.AT2
28	"Northern Calif-07"	RSN101_NCALIF.AG_D-CPM030.AT2	RSN101_NCALIF.AG_D-CPM120.AT2

3.3. Parametric Study

The model of six bridges with two boundary conditions of column were developed and the analysis was performed using the 28 earthquake ground motions for each of the bridges under 5% of damping as discussed in previous sections. As a parametric study, the influence of damping was studied for three other damping ratios 1%, 3% and 7%. Also, one span has been added in all the bridges to study the influence of span number on inelastic displacement ratio. The length of third span was same as the length of first span. Figure 3.45 shows the three-dimensional model of the three span OSB1 bridge.

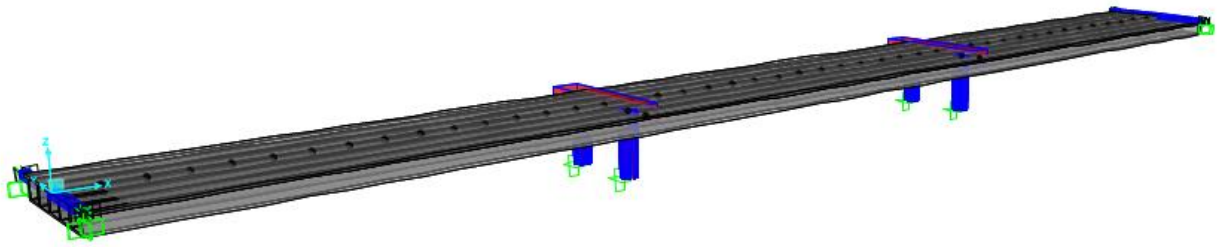

Figure 3.45. Three-dimensional model of OSB1 bridge with three spans for parametric study

4. MODEL VALIDATION AND ANALYSIS

This chapter explains the model validation using a single degree of freedom system (SDOF) and the OSB1 bridge model developed by Caltrans.

4.1. Model Validation

4.1.1. SDOF System

Chopra [41] has plotted the peak inelastic deformations (u_m) of an elastoplastic system and the elastic deformations (u_o or u_e) of the corresponding linear system when subjected to El Centro ground motion and the ratio u_m/u_e vs. the time period of SDOF systems for different normalized yield strength $\overline{f_y}$. These plots were used to validate the linear time history analysis and nonlinear time history analysis method in CSiBridge.

The normalized yield strength $\overline{f_y}$ of an elastoplastic system is defined as [41]

$$\overline{f_y} = \frac{f_y}{f_o} = \frac{u_y}{u_o} = \frac{u_y}{u_e} \tag{4. 1}$$

where f_o and u_o are the peak values of earthquake-induced resisting force and deformation of a linear system respectively and f_y and u_y are the yield force and yield displacement of its corresponding elastoplastic system.

First of all, a single degree of freedom system (SDOF) was created in CSiBridge using a multilinear elastic link element and a lumped mass (weight=300kips) was assigned at the top of the link element. Multilinear elastic link element was used to define the multi-linear force-deformation relation. By changing the time period of SDOF system (T=0.125,0.5 and 3 sec), elastic displacement (u_e) for each of the time period was calculated. Using different values of normalized yield strength $\overline{f_y}$, corresponding value of u_y was calculated for each time period. The elasto-perfectly-plastic behavior of link element was defined using the corresponding values of u_y and f_y for different time period. On performing nonlinear time history analysis, the maximum

inelastic displacement u_m was obtained. The ratio u_m/u_e was then plotted with the time period of SDOF system as shown in Figure 4.1. The analysis was conducted for 5% of damping ratio.

As observed in Figure 4.1, the ratio u_m/u_e for SDOF system calculated from linear time history analysis and nonlinear time history analysis performed in CSiBridge shows close agreement with the result in the literature[41]. This validates the SDOF system and more importantly the numerical methods being implemented for the study of inelastic displacement ratio of bridges.

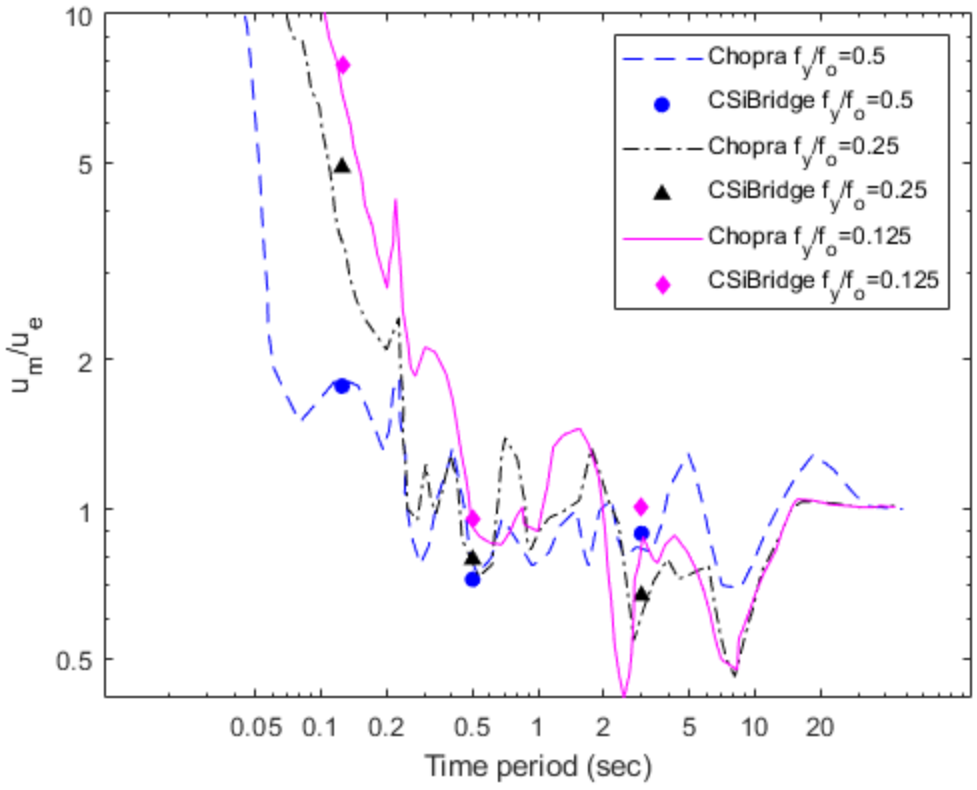

Figure 4.1. Comparison of the inelastic displacement ratios of 5% damping SDOF system with Chopra[41] under El Centro ground motion

4.1.2. MDOF System

The CSiBridge model of OSB1 bridge developed by Caltrans was analyzed for two different earthquake ground motions i.e. CLAYN1N1 and SANDN1N1 without any

modification. These earthquake ground motions were obtained from Caltrans and also reported in literature[47]. The time period of first six modes and inelastic displacement of center of mass (node connecting bent cap and deck section) when subjected to CLAYN1N1 and SANDN1N1 were obtained for the OSB1 bridge model and compared with the results reported by Mackie et. al. [47] in Table 4.1 and Table 4.2. It can be observed that the CSiBridge model results and the results reported in literature for OSB1 bridge match well. This validates the OSB1 bridge model and further analysis was performed with the modification in the OSB1 bridge as explained in section 3.1.1. CLAYN1N1P with a letter 'P' in the end was applied in the longitudinal direction of the bridge i.e. U1 direction and CLAYN1N1N with a letter 'N' in the end was applied in the transverse direction of the bridge i.e. U2 direction in the bridge model. For detailed information about these earthquake ground motions, the report by Mackie et.al. should be referred[47].

Table 4.1. Comparison of time period of first six modes of OSB1 bridge with literature

Mode	time period (sec)	
	Mackie et. al.[47]	Analysis
1	0.614	0.61054
2	0.609	0.60831
3	0.403	0.40246
4	0.352	0.35204
5	0.283	0.28312
6	0.157	0.15732

Table 4.2. Comparison of inelastic displacement of center of mass of OSB1 bridge with literature

Earthquake Name	Displacement (in.)			
	CLAYN1N1		SANDN1N1	
	U1 (P-090)	U2 (N-000)	U1 (P-090)	U2 (N-000)
Analysis	5.796	4.941	3.234	5.530
Mackie et. al.[47]		4.850	2.800	5.410

4.2. Analysis

The OSB1 bridge model was modified as explained in section 3.1.1 and OSB2, R14L, R14R, La Veta and Adobe bridges were developed with both pinned and fixed connection of column to the ground as explained in Chapter 3. And linear time history and nonlinear time history analysis were performed for the 28 earthquake ground motions mentioned in Section 3.2 to obtain the maximum elastic displacement u_e and the maximum inelastic displacement u_m of the complete bridge structure. Since the two components of each earthquake ground motions were applied in longitudinal (U1) and transverse direction (U2) of the bridge, the elastic and inelastic displacements were measured in both directions and the inelastic displacement ratio was computed in each direction. The mass proportional coefficient and stiffness proportional coefficient were determined using the time period of first mode and second mode of each bridge and the damping of 5% was used in the analysis. Further analysis was also performed for 1%, 3%, and 7% of damping ratio to study the influence of damping ratio and three number of spans for damping ratio of 5% to study the influence of number of spans. The analysis results for 5% of damping ratio for each of the bridge model are listed below.

4.2.1. OSB1 Bridge

The modal analysis of OSB1 bridge with pinned boundary condition provided the time periods of the first mode and the second mode of vibration as 0.46525sec and 0.41213 sec respectively. The maximum inelastic and elastic displacement demand on this bridge corresponding to the 28 earthquakes are listed in Table 4.3.

Table 4.3. Maximum inelastic and elastic displacement of OSB1 bridge with pinned boundary condition

Earthquake loading scenario		u_m(in.)		u_e(in.)		C_μ	
Longitudinal direction (U1)	Transverse direction (U2)	U1	U2	U1	U2	U1	U2
Northridge_01_U1	Northridge_01_U2	2.513	1.652	0.479	1.314	5.25	1.26
Loma_Prieta_U1	Loma_Prieta_U2	2.555	3.216	0.344	1.945	7.43	1.65
Superstition_Hills_01_U1	Superstition_Hills_01_U2	1.071	0.504	0.235	0.510	4.56	0.99
Superstition_Hills_02_U1	Superstition_Hills_02_U2	1.461	1.240	0.501	1.397	2.92	0.89
N_Palm_Springs_U1	N_Palm_Springs_U2	1.019	0.734	0.191	0.721	5.33	1.02
Chalfant_Valley_02_U1	Chalfant_Valley_02_U2	0.390	0.612	0.367	0.590	1.06	1.04
Morgan_Hill_U1	Morgan Hill_U2	0.683	0.140	0.104	0.136	6.55	1.02
Coalinga_01_U1	Coalinga_01_U2	2.912	2.457	0.589	2.275	4.94	1.08
Imperial_Valley_06_U1	Imperial_Valley_06_U2	1.022	0.311	0.253	0.303	4.04	1.03
San_Fernando_U1	San_Fernando_U2	2.302	0.679	0.468	0.614	4.92	1.11
Mammoth_Lakes_01_U1	Mammoth_Lakes_01_U2	0.812	0.878	0.643	1.147	1.26	0.77
Coyote_Lake_U1	Coyote_Lake_U2	0.911	1.382	0.390	1.582	2.33	0.87
Westmorland_U1	Westmorland_U2	0.967	0.499	0.313	0.476	3.09	1.05
Yountville_U1	Yountville_U2	0.157	0.075	0.017	0.075	9.38	1.00
Santa_Barbara_U1	Santa_Barbara_U2	0.809	0.939	0.273	0.772	2.96	1.22
San_Juan_Bautista_U1	San_Juan_Bautista_U2	0.883	0.195	0.128	0.184	6.92	1.06
Mohawk_Val_Portola_U1	Mohawk_Val_Portola_U2	0.111	0.058	0.019	0.058	5.78	1.00
Oroville_01_U1	Oroville_01_U2	0.090	0.082	0.068	0.081	1.32	1.00
Sierra_Madre_U1	Sierra_Madre_U2	2.280	1.306	1.552	1.092	1.47	1.20
Whittier_Narrows_01_U1	Whittier_Narrows_01_U2	2.805	1.120	0.708	0.702	3.96	1.59
Parkfield_02_CA_U1	Parkfield_02_CA_U2	0.451	0.404	0.238	0.403	1.90	1.00
Joshua_Tree_CA_U1	Joshua_Tree_CA_U2	1.237	0.633	0.347	0.621	3.57	1.02
San_Simeon_CA_U1	San_Simeon_CA_U2	1.414	0.444	0.576	0.385	2.45	1.15
Chalfant_Valley_01_U1	Chalfant_Valley_01_U2	0.300	0.196	0.098	0.196	3.07	1.00
Hector_Mine_U1	Hector_Mine_U2	0.374	0.064	0.053	0.064	7.04	1.00
Cape_Mendocino_U1	Cape_Mendocino_U2	4.684	1.499	2.413	1.795	1.94	0.84
Livermore_01_U1	Livermore_01_U2	0.324	0.158	0.172	0.158	1.88	1.00
Northern_Calif_07_U1	Northern_Calif_07_U2	0.122	0.160	0.072	0.160	1.68	1.00

For OSB1 bridge with fixed boundary condition, the time period of the first mode and second mode of vibration were obtained to be 0.41185sec and 0.32742sec respectively. The values of maximum inelastic and elastic displacement on this bridge for each of the 28 earthquake ground motions are listed in Table 4.4.

Table 4.4. Maximum inelastic and elastic displacement of OSB1 bridge with fixed boundary condition

Earthquake loading scenario		u_m(in.)		u_e(in.)		C_μ	
Longitudinal direction (U1)	Transverse direction (U2)	U1	U2	U1	U2	U1	U2
Northridge_01_U1	Northridge_01_U2	1.311	0.754	0.339	0.703	3.87	1.07
Loma_Prieta_U1	Loma_Prieta_U2	0.660	0.946	0.295	0.860	2.24	1.10
Superstition_Hills_01_U1	Superstition_Hills_01_U2	0.546	0.304	0.207	0.302	2.64	1.01
Superstition_Hills_02_U1	Superstition_Hills_02_U2	0.550	0.496	0.205	0.532	2.69	0.93
N_Palm_Springs_U1	N_Palm_Springs_U2	0.438	0.329	0.108	0.323	4.07	1.02
Chalfant_Valley_02_U1	Chalfant_Valley_02_U2	0.375	0.266	0.360	0.242	1.04	1.10
Morgan_Hill_U1	Morgan Hill_U2	0.250	0.082	0.050	0.082	5.02	1.00
Coalinga_01_U1	Coalinga_01_U2	1.171	1.299	0.318	0.979	3.68	1.33
Imperial_Valley_06_U1	Imperial_Valley_06_U2	0.447	0.215	0.243	0.213	1.84	1.01
San_Fernando_U1	San_Fernando_U2	0.651	0.348	0.455	0.347	1.43	1.00
Mammoth_Lakes_01_U1	Mammoth_Lakes_01_U2	0.798	0.530	0.499	0.598	1.60	0.89
Coyote_Lake_U1	Coyote_Lake_U2	0.760	0.810	0.244	0.640	3.12	1.27
Westmorland_U1	Westmorland_U2	0.573	0.320	0.223	0.314	2.57	1.02
Yountville_U1	Yountville_U2	0.117	0.018	0.009	0.018	12.56	1.00
Santa_Barbara_U1	Santa_Barbara_U2	0.345	0.462	0.163	0.526	2.11	0.88
San_Juan_Bautista_U1	San_Juan_Bautista_U2	0.257	0.103	0.064	0.102	4.01	1.00
Mohawk_Val_Portola_U1	Mohawk_Val_Portola_U2	0.094	0.025	0.017	0.025	5.41	1.00
Oroville_01_U1	Oroville_01_U2	0.098	0.118	0.061	0.118	1.61	1.00
Sierra_Madre_U1	Sierra_Madre_U2	1.385	0.348	0.848	0.288	1.63	1.21
Whittier_Narrows_01_U1	Whittier_Narrows_01_U2	1.060	0.874	0.697	0.778	1.52	1.12
Parkfield_02_CA_U1	Parkfield_02_CA_U2	0.287	0.182	0.227	0.181	1.26	1.01
Joshua_Tree_CA_U1	Joshua_Tree_CA_U2	0.726	0.469	0.260	0.474	2.79	0.99
San_Simeon_CA_U1	San_Simeon_CA_U2	0.659	0.302	0.530	0.247	1.24	1.22
Chalfant_Valley_01_U1	Chalfant_Valley_01_U2	0.323	0.102	0.082	0.102	3.94	1.00
Hector_Mine_U1	Hector_Mine_U2	0.173	0.055	0.038	0.055	4.61	1.01
Cape_Mendocino_U1	Cape_Mendocino_U2	3.616	1.845	2.160	1.242	1.67	1.49
Livermore_01_U1	Livermore_01_U2	0.229	0.195	0.087	0.196	2.63	1.00
Northern_Calif_07_U1	Northern_Calif_07_U2	0.143	0.214	0.079	0.214	1.81	1.00

4.2.2. OSB2 Bridge

The time period of the first mode and second mode of vibration of OSB2 bridge with pinned boundary condition were calculated to be 0.52635 sec and 0.39508 sec respectively. The maximum inelastic and elastic displacement demand of this bridge when subjected to different earthquakes are listed in Table 4.5.

Table 4.5. Maximum inelastic and elastic displacement of OSB2 bridge with pinned boundary condition

Earthquake loading scenario		u_m(in.)		u_e(in.)		C_μ	
Longitudinal direction (U1)	Transverse direction (U2)	U1	U2	U1	U2	U1	U2
Northridge_01_U1	Northridge_01_U2	2.747	1.781	0.507	1.956	5.42	0.91
Loma_Prieta_U1	Loma_Prieta_U2	2.406	3.165	0.331	3.169	7.27	1.00
Superstition_Hills_01_U1	Superstition_Hills_01_U2	1.251	0.441	0.264	0.441	4.74	1.00
Superstition_Hills_02_U1	Superstition_Hills_02_U2	1.643	1.350	0.534	1.496	3.07	0.90
N_Palm_Springs_U1	N_Palm_Springs_U2	1.096	0.895	0.185	0.896	5.92	1.00
Chalfant_Valley_02_U1	Chalfant_Valley_02_U2	0.437	0.566	0.340	0.564	1.29	1.00
Morgan_Hill_U1	Morgan Hill_U2	0.794	0.202	0.114	0.200	6.94	1.01
Coalinga_01_U1	Coalinga_01_U2	3.126	2.930	0.683	3.052	4.58	0.96
Imperial_Valley_06_U1	Imperial_Valley_06_U2	1.198	0.498	0.251	0.498	4.76	1.00
San_Fernando_U1	San_Fernando_U2	2.273	0.928	0.500	1.038	4.55	0.89
Mammoth_Lakes_01_U1	Mammoth_Lakes_01_U2	0.827	0.907	0.677	0.996	1.22	0.91
Coyote_Lake_U1	Coyote_Lake_U2	0.888	1.573	0.434	1.814	2.05	0.87
Westmorland_U1	Westmorland_U2	1.014	0.499	0.322	0.500	3.15	1.00
Yountville_U1	Yountville_U2	0.147	0.083	0.020	0.083	7.26	1.00
Santa_Barbara_U1	Santa_Barbara_U2	0.795	1.188	0.267	1.501	2.98	0.79
San_Juan_Bautista_U1	San_Juan_Bautista_U2	0.906	0.292	0.136	0.293	6.66	1.00
Mohawk_Val_Portola_U1	Mohawk_Val_Portola_U2	0.103	0.055	0.022	0.055	4.78	1.00
Oroville_01_U1	Oroville_01_U2	0.082	0.066	0.055	0.066	1.49	1.00
Sierra_Madre_U1	Sierra_Madre_U2	2.216	1.077	1.679	1.007	1.32	1.07
Whittier_Narrows_01_U1	Whittier_Narrows_01_U2	2.862	1.290	0.757	0.889	3.78	1.45
Parkfield_02_CA_U1	Parkfield_02_CA_U2	0.592	0.480	0.231	0.480	2.56	1.00
Joshua_Tree_CA_U1	Joshua_Tree_CA_U2	1.212	0.759	0.425	0.744	2.85	1.02
San_Simeon_CA_U1	San_Simeon_CA_U2	1.320	0.504	0.652	0.500	2.02	1.01
Chalfant_Valley_01_U1	Chalfant_Valley_01_U2	0.292	0.223	0.108	0.224	2.71	1.00
Hector_Mine_U1	Hector_Mine_U2	0.422	0.105	0.054	0.106	7.84	0.99
Cape_Mendocino_U1	Cape_Mendocino_U2	5.388	2.486	2.436	1.401	2.21	1.77
Livermore_01_U1	Livermore_01_U2	0.380	0.141	0.179	0.141	2.12	1.00
Northern_Calif_07_U1	Northern_Calif_07_U2	0.103	0.154	0.077	0.154	1.33	1.00

For OSB2 bridge with fixed boundary condition, modal analysis in CSiBridge calculated the time period of the first mode and second mode of vibration as 0.39479 sec and 0.39403 sec respectively. The values of maximum inelastic and elastic displacement in this bridge for each of the 28 earthquake ground motions are listed in Table 4.6.

Table 4.6. Maximum inelastic and elastic displacement of OSB2 bridge with fixed boundary condition

Earthquake loading scenario		u_m(in.)		u_e(in.)		C_μ	
Longitudinal direction (U1)	Transverse direction (U2)	U1	U2	U1	U2	U1	U2
Northridge_01_U1	Northridge_01_U2	1.450	1.012	0.336	1.322	4.32	0.77
Loma_Prieta_U1	Loma_Prieta_U2	0.752	1.127	0.281	1.279	2.68	0.88
Superstition_Hills_01_U1	Superstition_Hills_01_U2	0.549	0.498	0.219	0.469	2.50	1.06
Superstition_Hills_02_U1	Superstition_Hills_02_U2	0.590	1.119	0.228	1.038	2.59	1.08
N_Palm_Springs_U1	N_Palm_Springs_U2	0.500	0.724	0.113	0.679	4.44	1.07
Chalfant_Valley_02_U1	Chalfant_Valley_02_U2	0.400	0.399	0.402	0.390	1.00	1.02
Morgan_Hill_U1	Morgan Hill_U2	0.276	0.121	0.061	0.121	4.56	1.00
Coalinga_01_U1	Coalinga_01_U2	1.315	1.354	0.363	1.785	3.63	0.76
Imperial_Valley_06_U1	Imperial_Valley_06_U2	0.531	0.263	0.235	0.263	2.26	1.00
San_Fernando_U1	San_Fernando_U2	0.764	0.497	0.438	0.463	1.75	1.07
Mammoth_Lakes_01_U1	Mammoth_Lakes_01_U2	0.894	0.851	0.572	0.810	1.56	1.05
Coyote_Lake_U1	Coyote_Lake_U2	0.955	1.153	0.279	1.208	3.43	0.96
Westmorland_U1	Westmorland_U2	0.604	0.242	0.216	0.245	2.80	0.99
Yountville_U1	Yountville_U2	0.112	0.031	0.010	0.031	11.00	1.00
Santa_Barbara_U1	Santa_Barbara_U2	0.425	0.514	0.179	0.503	2.37	1.02
San_Juan_Bautista_U1	San_Juan_Bautista_U2	0.247	0.152	0.077	0.152	3.18	1.00
Mohawk_Val_Portola_U1	Mohawk_Val_Portola_U2	0.092	0.040	0.017	0.040	5.51	1.00
Oroville_01_U1	Oroville_01_U2	0.092	0.120	0.063	0.120	1.47	1.00
Sierra_Madre_U1	Sierra_Madre_U2	1.421	0.815	0.964	0.719	1.47	1.13
Whittier_Narrows_01_U1	Whittier_Narrows_01_U2	1.102	0.964	0.636	1.070	1.73	0.90
Parkfield_02_CA_U1	Parkfield_02_CA_U2	0.308	0.300	0.234	0.296	1.31	1.01
Joshua_Tree_CA_U1	Joshua_Tree_CA_U2	0.843	0.675	0.255	0.696	3.31	0.97
San_Simeon_CA_U1	San_Simeon_CA_U2	0.694	0.344	0.524	0.353	1.32	0.97
Chalfant_Valley_01_U1	Chalfant_Valley_01_U2	0.334	0.133	0.091	0.132	3.66	1.01
Hector_Mine_U1	Hector_Mine_U2	0.172	0.076	0.043	0.076	4.02	1.00
Cape_Mendocino_U1	Cape_Mendocino_U2	3.692	1.744	2.185	1.243	1.69	1.40
Livermore_01_U1	Livermore_01_U2	0.225	0.151	0.093	0.150	2.41	1.00
Northern_Calif_07_U1	Northern_Calif_07_U2	0.144	0.125	0.071	0.125	2.04	1.00

4.2.3. R14L Bridge

From the modal analysis, the time period of the first mode and second mode of vibration of R14L bridge with columns having pinned connection to the ground were obtained to be 0.49834 sec and 0.33449 sec respectively. The maximum inelastic and elastic displacement

demand on R14L bridge with pinned boundary condition corresponding to each earthquake ground motion are listed in Table 4.7.

Table 4.7. Maximum inelastic and elastic displacement of R14L bridge with pinned boundary condition

Earthquake loading scenario		u_m(in.)		u_e(in.)		C_μ	
Longitudinal direction (U1)	Transverse direction (U2)	U1	U2	U1	U2	U1	U2
Northridge_01_U1	Northridge_01_U2	3.013	1.639	0.452	1.641	6.66	1.00
Loma_Prieta_U1	Loma_Prieta_U2	2.377	2.975	0.350	2.356	6.80	1.26
Superstition_Hills_01_U1	Superstition_Hills_01_U2	2.139	0.574	0.238	0.433	8.98	1.32
Superstition_Hills_02_U1	Superstition_Hills_02_U2	1.553	1.973	0.480	1.387	3.24	1.42
N_Palm_Springs_U1	N_Palm_Springs_U2	0.483	0.988	0.181	0.766	2.67	1.29
Chalfant_Valley_02_U1	Chalfant_Valley_02_U2	0.567	0.648	0.391	0.638	1.45	1.02
Morgan_Hill_U1	Morgan Hill_U2	1.599	0.184	0.098	0.172	16.25	1.07
Coalinga_01_U1	Coalinga_01_U2	2.459	3.169	0.533	2.556	4.61	1.24
Imperial_Valley_06_U1	Imperial_Valley_06_U2	2.388	0.468	0.248	0.363	9.64	1.29
San_Fernando_U1	San_Fernando_U2	2.648	1.557	0.482	0.732	5.49	2.13
Mammoth_Lakes_01_U1	Mammoth_Lakes_01_U2	1.107	0.899	0.658	0.918	1.68	0.98
Coyote_Lake_U1	Coyote_Lake_U2	0.834	2.070	0.354	1.590	2.36	1.30
Westmorland_U1	Westmorland_U2	2.142	0.674	0.303	0.461	7.07	1.46
Yountville_U1	Yountville_U2	0.082	0.078	0.013	0.078	6.26	1.00
Santa_Barbara_U1	Santa_Barbara_U2	1.232	1.082	0.286	1.036	4.30	1.04
San_Juan_Bautista_U1	San_Juan_Bautista_U2	0.466	0.245	0.129	0.236	3.62	1.04
Mohawk_Val_Portola_U1	Mohawk_Val_Portola_U2	0.089	0.052	0.019	0.051	4.58	1.00
Oroville_01_U1	Oroville_01_U2	0.076	0.067	0.072	0.067	1.06	1.00
Sierra_Madre_U1	Sierra_Madre_U2	1.988	1.113	1.483	1.062	1.34	1.05
Whittier_Narrows_01_U1	Whittier_Narrows_01_U2	1.563	0.944	0.679	0.709	2.30	1.33
Parkfield_02_CA_U1	Parkfield_02_CA_U2	0.629	0.450	0.244	0.413	2.58	1.09
Joshua_Tree_CA_U1	Joshua_Tree_CA_U2	1.522	0.576	0.302	0.477	5.03	1.21
San_Simeon_CA_U1	San_Simeon_CA_U2	1.745	0.492	0.499	0.426	3.50	1.16
Chalfant_Valley_01_U1	Chalfant_Valley_01_U2	0.504	0.185	0.096	0.186	5.27	1.00
Hector_Mine_U1	Hector_Mine_U2	0.410	0.075	0.051	0.072	8.06	1.03
Cape_Mendocino_U1	Cape_Mendocino_U2	6.219	3.499	2.368	1.315	2.63	2.66
Livermore_01_U1	Livermore_01_U2	0.658	0.147	0.164	0.137	4.01	1.08
Northern_Calif_07_U1	Northern_Calif_07_U2	0.087	0.141	0.071	0.141	1.23	1.00

For R14L bridge with column having fixed connection to the ground, the time period of the first mode and second mode of vibration were obtained to be 0.45128 sec and 0.33443 sec

respectively. The values of maximum inelastic and elastic displacement on R14L bridge with fixed boundary condition for each of the 28-earthquake ground motion are listed in Table 4.8.

Table 4.8. Maximum inelastic and elastic displacement of R14L bridge with fixed boundary condition

Earthquake loading scenario		u_m(in.)		u_e(in.)		C_μ	
Longitudinal direction (U1)	Transverse direction (U2)	U1	U2	U1	U2	U1	U2
Northridge_01_U1	Northridge_01_U2	2.157	1.820	0.400	1.263	5.40	1.44
Loma_Prieta_U1	Loma_Prieta_U2	2.712	3.547	0.293	1.638	9.26	2.17
Superstition_Hills_01_U1	Superstition_Hills_01_U2	0.884	0.585	0.219	0.553	4.04	1.06
Superstition_Hills_02_U1	Superstition_Hills_02_U2	1.080	1.239	0.333	1.324	3.25	0.94
N_Palm_Springs_U1	N_Palm_Springs_U2	0.862	0.745	0.161	0.794	5.34	0.94
Chalfant_Valley_02_U1	Chalfant_Valley_02_U2	0.349	0.501	0.401	0.475	0.87	1.06
Morgan_Hill_U1	Morgan Hill_U2	0.572	0.127	0.095	0.125	6.02	1.01
Coalinga_01_U1	Coalinga_01_U2	2.905	2.753	0.433	1.957	6.72	1.41
Imperial_Valley_06_U1	Imperial_Valley_06_U2	0.798	0.269	0.265	0.250	3.02	1.08
San_Fernando_U1	San_Fernando_U2	2.158	0.873	0.467	0.612	4.62	1.43
Mammoth_Lakes_01_U1	Mammoth_Lakes_01_U2	0.718	0.946	0.687	1.219	1.05	0.78
Coyote_Lake_U1	Coyote_Lake_U2	0.912	1.484	0.289	1.492	3.15	0.99
Westmorland_U1	Westmorland_U2	0.960	0.486	0.275	0.380	3.49	1.28
Yountville_U1	Yountville_U2	0.146	0.067	0.011	0.065	12.82	1.02
Santa_Barbara_U1	Santa_Barbara_U2	0.783	0.897	0.262	0.667	2.99	1.34
San_Juan_Bautista_U1	San_Juan_Bautista_U2	0.838	0.240	0.112	0.194	7.51	1.24
Mohawk_Val_Portola_U1	Mohawk_Val_Portola_U2	0.098	0.057	0.016	0.057	6.05	1.00
Oroville_01_U1	Oroville_01_U2	0.075	0.083	0.066	0.084	1.14	1.00
Sierra_Madre_U1	Sierra_Madre_U2	2.241	1.451	1.301	0.989	1.72	1.47
Whittier_Narrows_01_U1	Whittier_Narrows_01_U2	2.830	1.553	0.622	0.766	4.55	2.03
Parkfield_02_CA_U1	Parkfield_02_CA_U2	0.433	0.382	0.247	0.377	1.75	1.01
Joshua_Tree_CA_U1	Joshua_Tree_CA_U2	1.339	0.775	0.277	0.564	4.82	1.37
San_Simeon_CA_U1	San_Simeon_CA_U2	1.352	0.436	0.438	0.382	3.09	1.14
Chalfant_Valley_01_U1	Chalfant_Valley_01_U2	0.264	0.173	0.110	0.172	2.40	1.01
Hector_Mine_U1	Hector_Mine_U2	0.325	0.070	0.048	0.070	6.70	1.00
Cape_Mendocino_U1	Cape_Mendocino_U2	5.474	2.203	2.347	1.736	2.33	1.27
Livermore_01_U1	Livermore_01_U2	0.309	0.151	0.123	0.150	2.52	1.01
Northern_Calif_07_U1	Northern_Calif_07_U2	0.120	0.162	0.072	0.161	1.67	1.01

4.2.4. R14R Bridge

The time period of the first mode and second mode of vibration were obtained to be 0.49522 sec and 0.31858 sec respectively for R14R bridge with pinned boundary condition. The maximum inelastic and elastic displacement demand in each direction is listed in Table 4.9.

Table 4.9. Maximum inelastic and elastic displacement of R14R bridge with pinned boundary condition

Earthquake loading scenario		u_m(in.)		u_e(in.)		C_μ	
Longitudinal direction (U1)	Transverse direction (U2)	U1	U2	U1	U2	U1	U2
Northridge_01_U1	Northridge_01_U2	3.291	1.409	0.472	1.591	6.98	0.89
Loma_Prieta_U1	Loma_Prieta_U2	2.557	2.637	0.351	2.260	7.28	1.17
Superstition_Hills_01_U1	Superstition_Hills_01_U2	2.226	0.543	0.249	0.429	8.92	1.27
Superstition_Hills_02_U1	Superstition_Hills_02_U2	1.371	1.768	0.533	1.373	2.57	1.29
N_Palm_Springs_U1	N_Palm_Springs_U2	0.468	0.935	0.181	0.761	2.58	1.23
Chalfant_Valley_02_U1	Chalfant_Valley_02_U2	0.528	0.660	0.377	0.640	1.40	1.03
Morgan_Hill_U1	Morgan Hill_U2	1.658	0.178	0.110	0.167	15.02	1.06
Coalinga_01_U1	Coalinga_01_U2	2.509	2.621	0.616	2.545	4.07	1.03
Imperial_Valley_06_U1	Imperial_Valley_06_U2	2.387	0.431	0.263	0.346	9.09	1.25
San_Fernando_U1	San_Fernando_U2	2.633	1.333	0.475	0.709	5.55	1.88
Mammoth_Lakes_01_U1	Mammoth_Lakes_01_U2	1.548	0.869	0.652	0.926	2.37	0.94
Coyote_Lake_U1	Coyote_Lake_U2	0.767	1.864	0.398	1.582	1.93	1.18
Westmorland_U1	Westmorland_U2	2.201	0.636	0.310	0.475	7.09	1.34
Yountville_U1	Yountville_U2	0.079	0.078	0.015	0.078	5.16	1.00
Santa_Barbara_U1	Santa_Barbara_U2	1.074	1.039	0.283	0.998	3.79	1.04
San_Juan_Bautista_U1	San_Juan_Bautista_U2	0.426	0.239	0.132	0.232	3.23	1.03
Mohawk_Val_Portola_U1	Mohawk_Val_Portola_U2	0.093	0.051	0.020	0.051	4.69	1.00
Oroville_01_U1	Oroville_01_U2	0.075	0.067	0.072	0.067	1.04	1.00
Sierra_Madre_U1	Sierra_Madre_U2	1.754	1.111	1.579	1.075	1.11	1.03
Whittier_Narrows_01_U1	Whittier_Narrows_01_U2	1.301	0.782	0.718	0.696	1.81	1.12
Parkfield_02_CA_U1	Parkfield_02_CA_U2	0.493	0.433	0.239	0.411	2.06	1.05
Joshua_Tree_CA_U1	Joshua_Tree_CA_U2	1.978	0.612	0.363	0.472	5.45	1.30
San_Simeon_CA_U1	San_Simeon_CA_U2	2.179	0.466	0.595	0.423	3.66	1.10
Chalfant_Valley_01_U1	Chalfant_Valley_01_U2	0.423	0.189	0.094	0.190	4.52	1.00
Hector_Mine_U1	Hector_Mine_U2	0.456	0.072	0.052	0.070	8.78	1.03
Cape_Mendocino_U1	Cape_Mendocino_U2	6.579	3.414	2.421	1.352	2.72	2.53
Livermore_01_U1	Livermore_01_U2	0.626	0.144	0.182	0.140	3.45	1.03
Northern_Calif_07_U1	Northern_Calif_07_U2	0.085	0.141	0.072	0.140	1.18	1.00

For R14R bridge with fixed boundary condition, the time period of the first mode and second mode of vibration were estimated to be 0.46335sec and 0.31581 sec respectively. And the maximum inelastic and elastic displacement of R14R bridge under the 28 earthquakes are listed in Table 4.10.

Table 4.10. Maximum inelastic and elastic displacement of R14R bridge with fixed boundary condition

Earthquake loading scenario		u_m(in.)		u_e(in.)		C_μ	
Longitudinal direction (U1)	Transverse direction (U2)	U1	U2	U1	U2	U1	U2
Northridge_01_U1	Northridge_01_U2	2.514	1.566	0.444	1.273	5.66	1.23
Loma_Prieta_U1	Loma_Prieta_U2	2.272	2.972	0.347	1.856	6.54	1.60
Superstition_Hills_01_U1	Superstition_Hills_01_U2	1.237	0.517	0.236	0.505	5.24	1.02
Superstition_Hills_02_U1	Superstition_Hills_02_U2	1.664	1.419	0.463	1.352	3.59	1.05
N_Palm_Springs_U1	N_Palm_Springs_U2	1.022	0.803	0.180	0.716	5.68	1.12
Chalfant_Valley_02_U1	Chalfant_Valley_02_U2	0.409	0.589	0.393	0.556	1.04	1.06
Morgan_Hill_U1	Morgan Hill_U2	0.830	0.152	0.099	0.131	8.36	1.16
Coalinga_01_U1	Coalinga_01_U2	3.208	2.464	0.514	2.172	6.24	1.13
Imperial_Valley_06_U1	Imperial_Valley_06_U2	1.154	0.298	0.246	0.287	4.70	1.04
San_Fernando_U1	San_Fernando_U2	2.577	0.692	0.484	0.585	5.32	1.18
Mammoth_Lakes_01_U1	Mammoth_Lakes_01_U2	0.889	0.870	0.661	1.132	1.34	0.77
Coyote_Lake_U1	Coyote_Lake_U2	0.825	1.588	0.342	1.530	2.41	1.04
Westmorland_U1	Westmorland_U2	1.000	0.462	0.301	0.452	3.32	1.02
Yountville_U1	Yountville_U2	0.122	0.072	0.013	0.072	9.62	1.01
Santa_Barbara_U1	Santa_Barbara_U2	0.825	1.010	0.287	0.737	2.88	1.37
San_Juan_Bautista_U1	San_Juan_Bautista_U2	0.802	0.218	0.128	0.181	6.28	1.20
Mohawk_Val_Portola_U1	Mohawk_Val_Portola_U2	0.103	0.056	0.019	0.057	5.40	1.00
Oroville_01_U1	Oroville_01_U2	0.072	0.080	0.071	0.080	1.02	0.99
Sierra_Madre_U1	Sierra_Madre_U2	2.221	1.166	1.455	1.049	1.53	1.11
Whittier_Narrows_01_U1	Whittier_Narrows_01_U2	2.792	1.105	0.670	0.692	4.17	1.60
Parkfield_02_CA_U1	Parkfield_02_CA_U2	0.754	0.391	0.244	0.389	3.08	1.00
Joshua_Tree_CA_U1	Joshua_Tree_CA_U2	1.346	0.702	0.300	0.597	4.49	1.17
San_Simeon_CA_U1	San_Simeon_CA_U2	1.314	0.431	0.477	0.372	2.75	1.16
Chalfant_Valley_01_U1	Chalfant_Valley_01_U2	0.313	0.190	0.098	0.187	3.20	1.02
Hector_Mine_U1	Hector_Mine_U2	0.530	0.063	0.051	0.062	10.47	1.01
Cape_Mendocino_U1	Cape_Mendocino_U2	5.039	1.736	2.367	1.757	2.13	0.99
Livermore_01_U1	Livermore_01_U2	0.513	0.154	0.159	0.154	3.22	1.00
Northern_Calif_07_U1	Northern_Calif_07_U2	0.085	0.157	0.072	0.157	1.17	1.00

4.2.5. Adobe Bridge

For Adobe bridge with pinned boundary condition, the time period of the first mode and second mode of vibration were determined to be 0.43955 sec and 0.27273 sec respectively. The maximum inelastic and elastic displacement demand in each direction for the 28 earthquake ground motions are listed in Table 4.11.

Table 4.11. Maximum inelastic and elastic displacement of Adobe bridge with pinned boundary condition

Earthquake loading scenario		u_m(in.)		u_e(in.)		C_μ	
Longitudinal direction (U1)	Transverse direction (U2)	U1	U2	U1	U2	U1	U2
Northridge_01_U1	Northridge_01_U2	2.688	1.553	0.348	1.234	7.72	1.26
Loma_Prieta_U1	Loma_Prieta_U2	2.106	2.943	0.301	1.376	7.01	2.14
Superstition_Hills_01_U1	Superstition_Hills_01_U2	2.078	0.904	0.211	0.585	9.82	1.55
Superstition_Hills_02_U1	Superstition_Hills_02_U2	1.698	1.632	0.215	1.297	7.90	1.26
N_Palm_Springs_U1	N_Palm_Springs_U2	0.669	0.952	0.109	0.820	6.16	1.16
Chalfant_Valley_02_U1	Chalfant_Valley_02_U2	0.392	0.465	0.407	0.460	0.96	1.01
Morgan_Hill_U1	Morgan Hill_U2	0.803	0.115	0.060	0.112	13.33	1.02
Coalinga_01_U1	Coalinga_01_U2	2.989	2.058	0.339	1.733	8.83	1.19
Imperial_Valley_06_U1	Imperial_Valley_06_U2	1.819	0.312	0.252	0.249	7.22	1.25
San_Fernando_U1	San_Fernando_U2	2.535	1.603	0.479	0.676	5.29	2.37
Mammoth_Lakes_01_U1	Mammoth_Lakes_01_U2	1.026	1.155	0.590	1.217	1.74	0.95
Coyote_Lake_U1	Coyote_Lake_U2	0.855	2.013	0.261	1.430	3.27	1.41
Westmorland_U1	Westmorland_U2	1.692	0.429	0.223	0.308	7.58	1.39
Yountville_U1	Yountville_U2	0.071	0.060	0.009	0.057	8.26	1.04
Santa_Barbara_U1	Santa_Barbara_U2	1.046	0.604	0.179	0.601	5.86	1.01
San_Juan_Bautista_U1	San_Juan_Bautista_U2	0.536	0.211	0.074	0.195	7.22	1.08
Mohawk_Val_Portola_U1	Mohawk_Val_Portola_U2	0.074	0.055	0.018	0.055	4.07	1.00
Oroville_01_U1	Oroville_01_U2	0.055	0.087	0.064	0.086	0.86	1.01
Sierra_Madre_U1	Sierra_Madre_U2	2.400	0.887	0.959	0.979	2.50	0.91
Whittier_Narrows_01_U1	Whittier_Narrows_01_U2	2.022	1.552	0.654	0.837	3.09	1.85
Parkfield_02_CA_U1	Parkfield_02_CA_U2	0.878	0.381	0.233	0.357	3.76	1.07
Joshua_Tree_CA_U1	Joshua_Tree_CA_U2	1.168	0.730	0.283	0.626	4.14	1.17
San_Simeon_CA_U1	San_Simeon_CA_U2	1.324	0.486	0.542	0.408	2.44	1.19
Chalfant_Valley_01_U1	Chalfant_Valley_01_U2	0.376	0.166	0.085	0.163	4.42	1.02
Hector_Mine_U1	Hector_Mine_U2	0.384	0.079	0.043	0.072	8.96	1.09
Cape_Mendocino_U1	Cape_Mendocino_U2	6.367	3.605	2.289	1.577	2.78	2.29
Livermore_01_U1	Livermore_01_U2	0.479	0.154	0.098	0.143	4.88	1.08
Northern_Calif_07_U1	Northern_Calif_07_U2	0.068	0.156	0.072	0.153	0.94	1.02

For Adobe bridge with fixed boundary condition, the time period of the first mode and second mode of vibration were calculated to be 0.39125sec and 0.25977sec respectively. And the maximum inelastic and elastic displacement of Adobe bridge with fixed boundary condition when subjected to the 28 earthquake ground motions are tabulated in Table 4.12.

Table 4.12. Maximum inelastic and elastic displacement of Adobe bridge with fixed boundary condition

Earthquake loading scenario		u_m(in.)		u_e(in.)		C_μ	
Longitudinal direction (U1)	Transverse direction (U2)	U1	U2	U1	U2	U1	U2
Northridge_01_U1	Northridge_01_U2	1.367	1.137	0.340	1.283	4.02	0.89
Loma_Prieta_U1	Loma_Prieta_U2	1.858	2.635	0.282	1.241	6.60	2.12
Superstition_Hills_01_U1	Superstition_Hills_01_U2	0.810	0.719	0.205	0.441	3.95	1.63
Superstition_Hills_02_U1	Superstition_Hills_02_U2	0.885	0.981	0.170	0.975	5.21	1.01
N_Palm_Springs_U1	N_Palm_Springs_U2	0.626	0.730	0.101	0.648	6.19	1.13
Chalfant_Valley_02_U1	Chalfant_Valley_02_U2	0.383	0.398	0.351	0.382	1.09	1.04
Morgan_Hill_U1	Morgan Hill_U2	0.346	0.121	0.056	0.117	6.14	1.03
Coalinga_01_U1	Coalinga_01_U2	2.541	2.472	0.291	1.728	8.74	1.43
Imperial_Valley_06_U1	Imperial_Valley_06_U2	0.714	0.281	0.232	0.250	3.07	1.12
San_Fernando_U1	San_Fernando_U2	1.992	0.779	0.477	0.439	4.18	1.77
Mammoth_Lakes_01_U1	Mammoth_Lakes_01_U2	0.586	0.746	0.440	0.770	1.33	0.97
Coyote_Lake_U1	Coyote_Lake_U2	0.903	1.209	0.206	1.172	4.39	1.03
Westmorland_U1	Westmorland_U2	0.842	0.276	0.231	0.244	3.64	1.13
Yountville_U1	Yountville_U2	0.111	0.034	0.008	0.031	13.36	1.11
Santa_Barbara_U1	Santa_Barbara_U2	0.643	0.629	0.152	0.490	4.23	1.28
San_Juan_Bautista_U1	San_Juan_Bautista_U2	0.713	0.166	0.069	0.146	10.31	1.14
Mohawk_Val_Portola_U1	Mohawk_Val_Portola_U2	0.077	0.040	0.017	0.037	4.55	1.07
Oroville_01_U1	Oroville_01_U2	0.059	0.116	0.069	0.117	0.86	0.98
Sierra_Madre_U1	Sierra_Madre_U2	1.839	1.023	0.793	0.673	2.32	1.52
Whittier_Narrows_01_U1	Whittier_Narrows_01_U2	2.471	1.164	0.711	1.059	3.48	1.10
Parkfield_02_CA_U1	Parkfield_02_CA_U2	0.375	0.301	0.225	0.284	1.67	1.06
Joshua_Tree_CA_U1	Joshua_Tree_CA_U2	1.306	0.712	0.269	0.683	4.85	1.04
San_Simeon_CA_U1	San_Simeon_CA_U2	0.875	0.477	0.499	0.346	1.76	1.38
Chalfant_Valley_01_U1	Chalfant_Valley_01_U2	0.332	0.135	0.082	0.127	4.07	1.06
Hector_Mine_U1	Hector_Mine_U2	0.230	0.078	0.032	0.072	7.14	1.08
Cape_Mendocino_U1	Cape_Mendocino_U2	4.818	2.629	2.087	1.213	2.31	2.17
Livermore_01_U1	Livermore_01_U2	0.293	0.157	0.085	0.149	3.45	1.05
Northern_Calif_07_U1	Northern_Calif_07_U2	0.095	0.118	0.089	0.116	1.06	1.02

4.2.6. La Veta Bridge

For La Veta bridge with pinned boundary condition, the time period of the first mode and second mode of vibration, obtained from modal analysis were 0.48833 sec and 0.33823 sec respectively. The maximum inelastic and elastic displacement demand in La Veta bridge subjected to the 28-earthquake ground motion are listed in Table 4.13.

Table 4.13. Maximum inelastic and elastic displacement of La Veta bridge with pinned boundary condition

Earthquake loading scenario		u_m(in.)		u_e(in.)		C_μ	
Longitudinal direction (U1)	Transverse direction (U2)	U1	U2	U1	U2	U1	U2
Northridge_01_U1	Northridge_01_U2	2.836	2.419	0.417	1.474	6.80	1.64
Loma_Prieta_U1	Loma_Prieta_U2	1.871	3.431	0.325	2.068	5.76	1.66
Superstition_Hills_01_U1	Superstition_Hills_01_U2	1.330	0.579	0.213	0.416	6.24	1.39
Superstition_Hills_02_U1	Superstition_Hills_02_U2	1.888	1.529	0.398	1.347	4.74	1.14
N_Palm_Springs_U1	N_Palm_Springs_U2	0.848	0.979	0.172	0.746	4.92	1.31
Chalfant_Valley_02_U1	Chalfant_Valley_02_U2	0.370	0.682	0.396	0.637	0.93	1.07
Morgan_Hill_U1	Morgan Hill_U2	0.855	0.182	0.098	0.154	8.72	1.18
Coalinga_01_U1	Coalinga_01_U2	3.449	2.650	0.471	2.488	7.33	1.07
Imperial_Valley_06_U1	Imperial_Valley_06_U2	1.312	0.385	0.249	0.325	5.28	1.18
San_Fernando_U1	San_Fernando_U2	2.811	1.202	0.475	0.695	5.92	1.73
Mammoth_Lakes_01_U1	Mammoth_Lakes_01_U2	0.917	0.921	0.669	0.943	1.37	0.98
Coyote_Lake_U1	Coyote_Lake_U2	0.884	2.112	0.309	1.563	2.86	1.35
Westmorland_U1	Westmorland_U2	1.323	0.567	0.289	0.495	4.59	1.15
Yountville_U1	Yountville_U2	0.109	0.079	0.012	0.079	9.09	1.00
Santa_Barbara_U1	Santa_Barbara_U2	1.489	1.127	0.277	0.931	5.37	1.21
San_Juan_Bautista_U1	San_Juan_Bautista_U2	0.604	0.249	0.120	0.222	5.02	1.12
Mohawk_Val_Portola_U1	Mohawk_Val_Portola_U2	0.109	0.052	0.018	0.051	6.24	1.01
Oroville_01_U1	Oroville_01_U2	0.086	0.068	0.063	0.067	1.35	1.01
Sierra_Madre_U1	Sierra_Madre_U2	2.525	1.258	1.356	1.080	1.86	1.16
Whittier_Narrows_01_U1	Whittier_Narrows_01_U2	2.580	1.167	0.641	0.670	4.02	1.74
Parkfield_02_CA_U1	Parkfield_02_CA_U2	0.756	0.433	0.246	0.403	3.07	1.07
Joshua_Tree_CA_U1	Joshua_Tree_CA_U2	1.510	0.680	0.282	0.521	5.36	1.30
San_Simeon_CA_U1	San_Simeon_CA_U2	1.314	0.512	0.425	0.412	3.09	1.24
Chalfant_Valley_01_U1	Chalfant_Valley_01_U2	0.398	0.207	0.105	0.197	3.80	1.05
Hector_Mine_U1	Hector_Mine_U2	0.535	0.077	0.050	0.067	10.79	1.16
Cape_Mendocino_U1	Cape_Mendocino_U2	5.618	2.636	2.348	1.441	2.39	1.83
Livermore_01_U1	Livermore_01_U2	0.551	0.148	0.139	0.143	3.97	1.03
Northern_Calif_07_U1	Northern_Calif_07_U2	0.100	0.141	0.073	0.140	1.36	1.00

For the fixed boundary condition of La Veta bridge, the time period of the first mode and second mode of vibration were estimated to be 0.40306 sec and 0.33822 sec respectively. And the maximum inelastic and elastic displacement of this bridge under the 28 earthquake motions are tabulated in Table 4.14.

Table 4.14. Maximum inelastic and elastic displacement of La Veta bridge with fixed boundary condition

Earthquake loading scenario		u_m(in.)		u_e(in.)		C_μ	
Longitudinal direction (U1)	Transverse direction (U2)	U1	U2	U1	U2	U1	U2
Northridge_01_U1	Northridge_01_U2	1.822	1.383	0.343	1.368	5.31	1.01
Loma_Prieta_U1	Loma_Prieta_U2	1.135	2.315	0.285	1.307	3.98	1.77
Superstition_Hills_01_U1	Superstition_Hills_01_U2	0.806	0.590	0.213	0.529	3.78	1.12
Superstition_Hills_02_U1	Superstition_Hills_02_U2	0.697	1.116	0.230	1.155	3.03	0.97
N_Palm_Springs_U1	N_Palm_Springs_U2	0.894	0.831	0.111	0.734	8.05	1.13
Chalfant_Valley_02_U1	Chalfant_Valley_02_U2	0.493	0.388	0.422	0.393	1.17	0.99
Morgan_Hill_U1	Morgan Hill_U2	0.322	0.128	0.067	0.126	4.81	1.01
Coalinga_01_U1	Coalinga_01_U2	1.756	1.329	0.363	1.832	4.84	0.73
Imperial_Valley_06_U1	Imperial_Valley_06_U2	0.591	0.265	0.251	0.268	2.35	0.99
San_Fernando_U1	San_Fernando_U2	0.942	0.642	0.460	0.507	2.05	1.27
Mammoth_Lakes_01_U1	Mammoth_Lakes_01_U2	0.752	0.897	0.623	0.887	1.21	1.01
Coyote_Lake_U1	Coyote_Lake_U2	0.838	1.384	0.263	1.265	3.19	1.09
Westmorland_U1	Westmorland_U2	0.874	0.255	0.220	0.239	3.97	1.07
Yountville_U1	Yountville_U2	0.115	0.002	0.009	0.002	12.48	0.99
Santa_Barbara_U1	Santa_Barbara_U2	0.612	0.542	0.187	0.512	3.27	1.06
San_Juan_Bautista_U1	San_Juan_Bautista_U2	0.395	0.170	0.080	0.166	4.91	1.03
Mohawk_Val_Portola_U1	Mohawk_Val_Portola_U2	0.089	0.044	0.017	0.044	5.24	1.00
Oroville_01_U1	Oroville_01_U2	0.091	0.118	0.065	0.117	1.39	1.00
Sierra_Madre_U1	Sierra_Madre_U2	1.532	0.956	1.015	0.805	1.51	1.19
Whittier_Narrows_01_U1	Whittier_Narrows_01_U2	1.529	1.186	0.620	1.065	2.46	1.11
Parkfield_02_CA_U1	Parkfield_02_CA_U2	0.305	0.329	0.238	0.312	1.28	1.05
Joshua_Tree_CA_U1	Joshua_Tree_CA_U2	1.503	0.742	0.269	0.680	5.59	1.09
San_Simeon_CA_U1	San_Simeon_CA_U2	0.961	0.388	0.523	0.364	1.84	1.06
Chalfant_Valley_01_U1	Chalfant_Valley_01_U2	0.282	0.141	0.094	0.141	3.02	1.00
Hector_Mine_U1	Hector_Mine_U2	0.242	0.081	0.044	0.082	5.49	0.99
Cape_Mendocino_U1	Cape_Mendocino_U2	4.134	2.106	2.281	1.285	1.81	1.64
Livermore_01_U1	Livermore_01_U2	0.312	0.149	0.102	0.146	3.05	1.02
Northern_Calif_07_U1	Northern_Calif_07_U2	0.131	0.131	0.069	0.133	1.90	0.99

5. RESULTS AND DISCUSSION

This chapter discusses the results on inelastic displacement ratio of bridges modeled in this research work and compares the result against the traditionally accepted AASHTO R_d equation. The limitation of the current approach has been discussed and a new equation has been suggested based on the fitting of the obtained inelastic displacement ratios. This chapter also presents the parametric study on the effect of column height, superstructure deck width, number of spans, damping ratio and boundary condition of column on inelastic displacement ratio of the bridge.

5.1. Comparison with AASHTO R_d Equation

As explained in section 4.2, OSB1, OSB2, R14L, R14R, La Veta, and Adobe bridges with pinned and fixed connection of column to the ground were analyzed using the 28-earthquake ground motion and considering damping ratio of ζ=5%. Each of the earthquake ground motion has two components and they were applied in longitudinal and transverse direction of the bridge respectively as discussed previously. The nonlinear time history analysis and linear time history analysis were performed for all bridges considered and all of the 28 earthquake ground motions to obtain the maximum elastic and maximum inelastic displacement demand in those bridges. The inelastic displacement ratios were then computed in each longitudinal and transverse directions as tabulated in Table 4.3 to Table 4.14. These inelastic displacement ratios were then plotted in y-axis (as shown in Figure 5.1) vs. time period of the first mode of vibration in x-axis in order to compare the results with the AASHTO R_d equation.

For each of the bridges considered, the mean and standard deviation (SD) of inelastic displacement ratios corresponding to all earthquake ground motions in both directions, were computed. Mean + SD and mean + 3×SD were further calculated and plotted in Figure 5.1.

As shown in equation 1.5, AASHTO R_d equation can be expressed as $R_d = 0.167 + 1.042/T$ when the ductility $\mu = 6$ and $T^* = 1.25$. In this research work, a detailed analysis was performed for each of the bridge, thus, $\mu = 6$ was adopted (suggested by AASHTO[31]) and a general equation, $C_\mu = 0.167 + a/T$, maintaining the consistency with AASHTO R_d, was used to fit the data set of mean, mean + SD and mean + 3×SD individually. In this general equation, a is only the variable, since the term 0.167 was kept unchanged to that of AASHTO R_d. The value of a was determined using Curve Fitter application available in MATLAB. The time period of the bridges modeled here only ranged between 0.35-0.55sec and no data sets were available for time period less than 0.35sec and greater than 0.55sec. Also, the general equation of C_μ was considered based on AASHTO R_d, rather than obtaining the best fit equation from the data sets. Therefore, the correlation coefficients for the fit equation for mean, mean + SD and mean + 3×SD were found to be low and it does not have any significance in this work, therefore, the correlation coefficients are not discussed here.

In Figure 5.1, it can be observed that the fit equation for mean inelastic displacement ratio i.e. $C_\mu = 0.167 + 1.094/T$ is almost close to the AASHTO R_d equation, which means AASHTO R_d equation predicts the average inelastic displacement ratio of bridges subjected to different magnitude of earthquake ground motion. However, it significantly underpredicts C_μ for most of the earthquake ground motion if they are considered individually. Therefore, two different equations were developed using the data set of mean + SD and mean + 3×SD to consider the variability in the inelastic displacement ratio for different characteristics of earthquake ground motions. These equations $C_\mu = 0.167 + 2.142/T$ and $C_\mu = 0.167 + 4.239/T$ developed based on mean + SD and mean + 3×SD respectively, gives better estimate of inelastic displacement ratio for bridges in a seismically active region like California.

Figure 5.1 implies that AASHTO R_d equation or mean equation: $C_\mu = 0.167 + 1.094/T$ can only estimate the mean inelastic displacement ratio, while mean + SD equation: $C_\mu = 0.167 + 2.142/T$, and mean + 3×SD equation: $C_\mu = 0.167 + 4.239/T$ consider the variability in the inelastic displacement ratio due dynamic nature of the bridge system as well as wide range of earthquake ground motion. In statistics, mean + SD considers the variability of about 68% and mean + 3SD considers the variability of 99.7% within a normal distribution. Therefore, mean + SD equation can be used to consider 68% of variability and mean + 3×SD equation can be used to consider 99.7% of the variability.

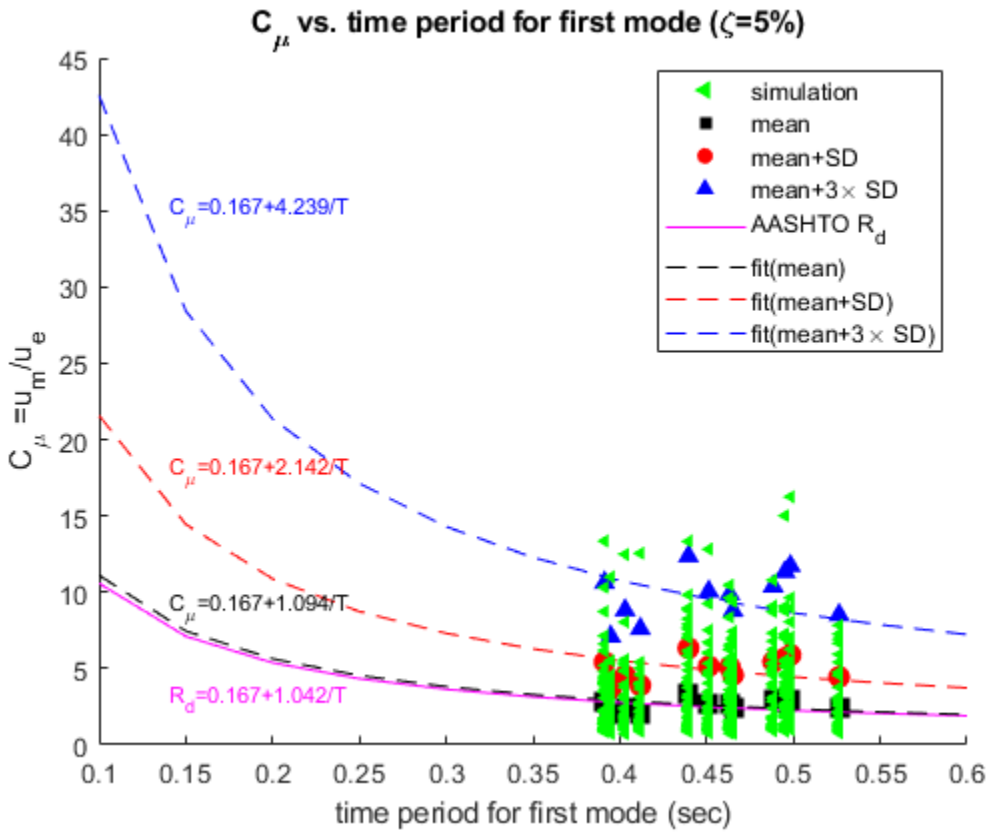

Figure 5.1. Inelastic displacement ratio vs. time period of first mode of two span bridges for damping ratio of 5%

5.2. Parametric Study

In this section, the factors that influence the inelastic displacement ratio are studied in detail. The factors include boundary condition of column to the ground, column height, superstructure deck width, number of spans, and damping ratio.

5.2.1. Influence of Connection of Column to the Ground

The analysis result presented in section 4.2 has been re-plotted in Figure 5.2 to study the influence of pinned connection and fixed connection of column to the ground on inelastic displacement ratio. It can be observed that the fit equation for mean values of inelastic displacement ratio in pinned connection of bridges is $C_\mu = 0.167 + 1.296/T$ while for fixed connection is $C_\mu = 0.167 + 1.024/T$. This shows that the inelastic displacement ratio in bridges whose column has pinned connection is higher than in bridges with column fixed to the ground.

In pinned connection, the column base is only restrained in translation degrees of freedom (U1, U2, and U3), however, the column is unrestrained against the rotational degree of freedom (R1, R2, and R3). Therefore, column is flexible and can undergo larger rotation when subjected to earthquake ground motion or other loading condition. However, when column has fixed connection to the ground, it is restrained against all degree of freedom (translation and rotation). The rigid connection at the base prevents it from rotation which reduces the flexibility of the column, thus, increasing the stiffness. Increased stiffness causes reduction in displacement demand in the structure. Alternatively, as observed in Figure 5.2, the time period of first mode is higher for pinned connection than for fixed connection. And stiffness is inversely proportional to the square of the time period. This also implies that the stiffness for column with pinned connection is lower than for the fixed connection. Therefore, due to increase in flexibility or

decrease in stiffness, the column with pinned connection to the ground causes higher inelastic displacement ratio as compared to the fixed connection.

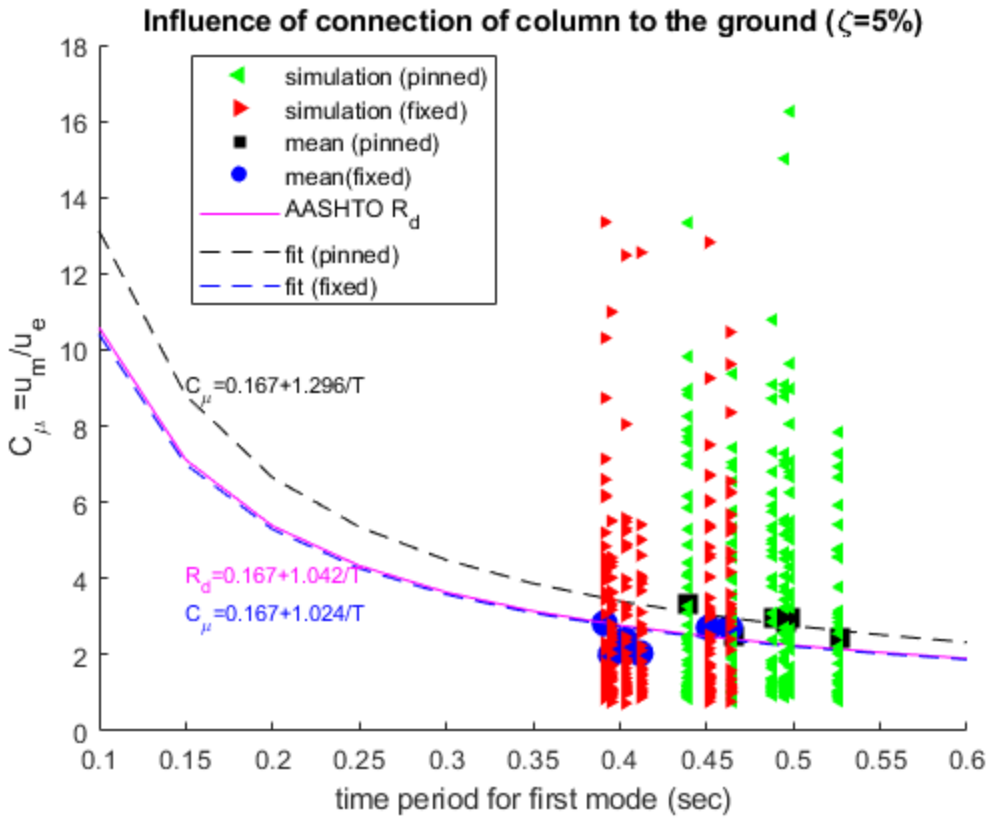

Figure 5.2. Influence of boundary condition of column on inelastic displacement ratio for damping ratio of 5%

5.2.2. Influence of Column Height

The height of column of the bridges considered in this study ranges from 20ft to 40ft. Therefore, the analysis results presented in section 4.2 were divided into two sets, one data set for column having height between 20ft to 30ft and another data set for column having height between 30ft to 40ft. These data sets are plotted in Figure 5.3to study the influence of column height on inelastic displacement ratio of bridges. The fit equation for mean C_μ for column height ranging 20ft-30ft is $C_\mu = 0.167 + 1.026/T$ and for column height ranging 30ft-40ft is $C_\mu = 0.167 + 1.258/T$. These equations suggest that the inelastic displacement ratio in bridges

increases with the increase in column height. The stiffness of column is inversely proportional to the cubic of the height of the column. If the material of concrete column and cross-section of the column remains unchanged, the stiffness of column decreases with the increase in column height. The decrease in stiffness causes an increase in displacement of column. Because of this reason, the inelastic displacement ratio is higher in bridge having higher column height.

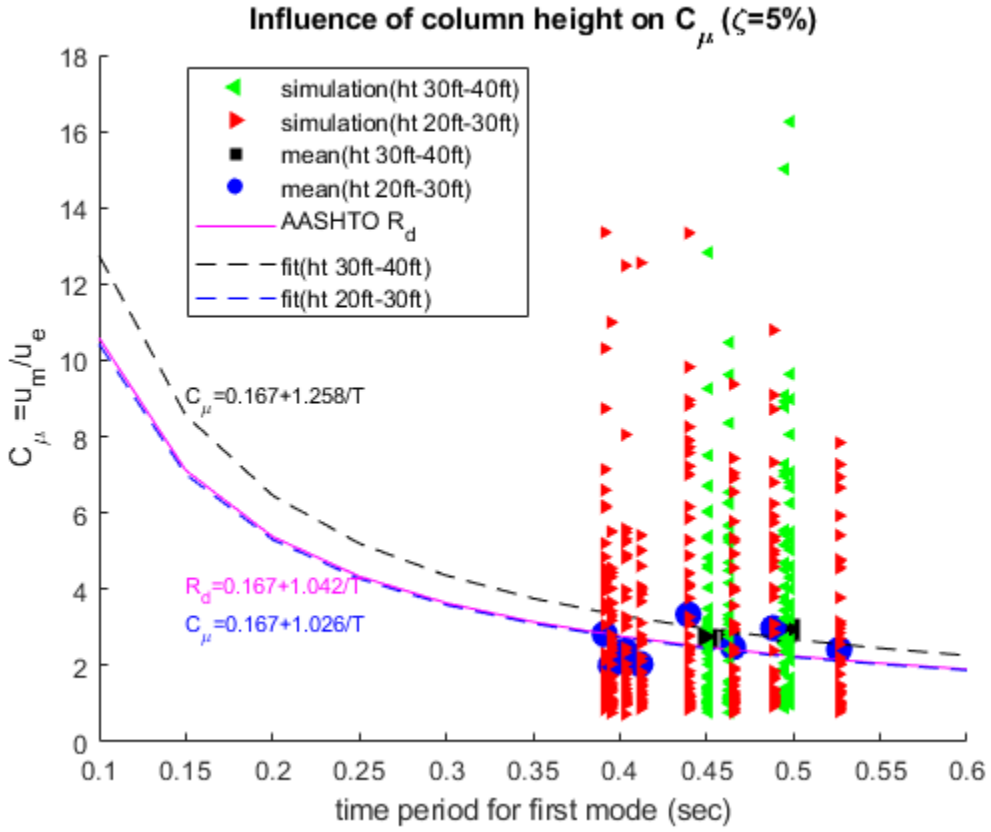

Figure 5.3. Influence of column height on inelastic displacement ratio for damping ratio of 5%

5.2.3. Influence of Deck Width

The width of the superstructure deck section of the box girder bridges considered in this study varies from 30ft to 80ft. The analysis results presented in section 4.2 were separated into two data sets: one is based on the width of deck ranging within 30ft-50ft and the other consists of the data for the deck width between 50ft-80ft. These data sets are plotted in Figure 5.4 to study how inelastic displacement ratio varies with changing the deck width. The mean inelastic

displacement ratio for both data sets were calculated at different time period and fit equation for the mean C_μ were calculated. When the deck width ranges from 30ft-50ft, the fit equation is $C_\mu = 0.167 + 1.059/T$ while for the deck width between 50ft-80ft is $C_\mu = 0.167 + 1.169/T$. These equations suggest that inelastic displacement ratio increases with increase in deck width.

The stiffness is directly proportional to the moment of inertia of a cross-section of any member. If width increases, the stiffness also increases and reduces the elastic displacement. However, width also increases the weight of the deck section which causes increase in earthquake force and thus, increases inelastic displacement. For example, the deck width of R14L bridge is 53.71ft while R14R bridge is 41.9ft. As observed in Table 4.7 and Table 4.8, the elastic displacement corresponding to most of earthquake ground motion for R14R bridge (with smaller width) is greater than that for R14L bridge (with larger width). However, the inelastic displacement for most of the earthquake ground motion for R14R bridge is smaller than that for R14L bridge. Therefore, the increase in deck width causes increase in inelastic displacement ratio.

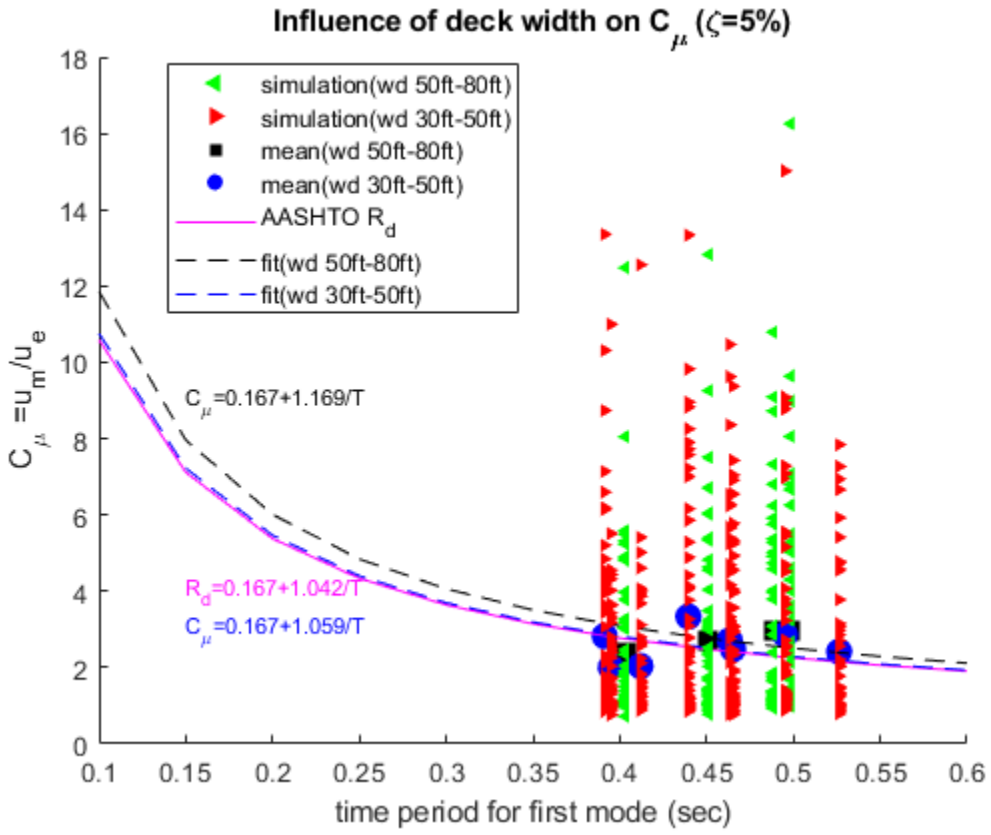

Figure 5.4. Influence of deck width on inelastic displacement ratio for damping ratio of 5%

5.2.4. Influence of Number of Spans

In order to study the influence of number of spans of bridges on inelastic displacement ratio, 12 models were created (six bridges with pinned and fixed connection) having three spans as explained in section 3.3 with damping ratio of 5%. The analysis results for two span bridges (presented in Figure 5.1) and three span bridges are plotted in Figure 5.5. The mean values of C_μ were computed for both cases and the fit equations were obtained in each case. The fit equation for bridges with two spans is $C_\mu = 0.167 + 1.094/T$ while for three spans bridges is $C_\mu = 0.167 + 0.863/T$. These equations suggest that the inelastic displacement ratio decreases with increase in number of spans in bridges.

From the analysis results, it was observed that the elastic displacement of bridges with three spans is greater than that for bridges with two spans. The displacement of overall bridge

system actually depends upon the connection between different span. When one span undergoes deformation, it can influence the deformation behavior of adjacent span through dynamic interactions. Such interaction can contribute to increase in elastic displacement in three-span bridges as compared to two-span bridges. It was also observed that the inelastic displacement in three span bridges were greater than two span bridges for most of the earthquake ground motion. However, the proportion of increment in both elastic and inelastic displacement was not same. In other word, the influence of number of spans on elastic and inelastic displacement is not the same. The spreadsheet for the elastic and inelastic displacement for three span bridges is not shown in this report.

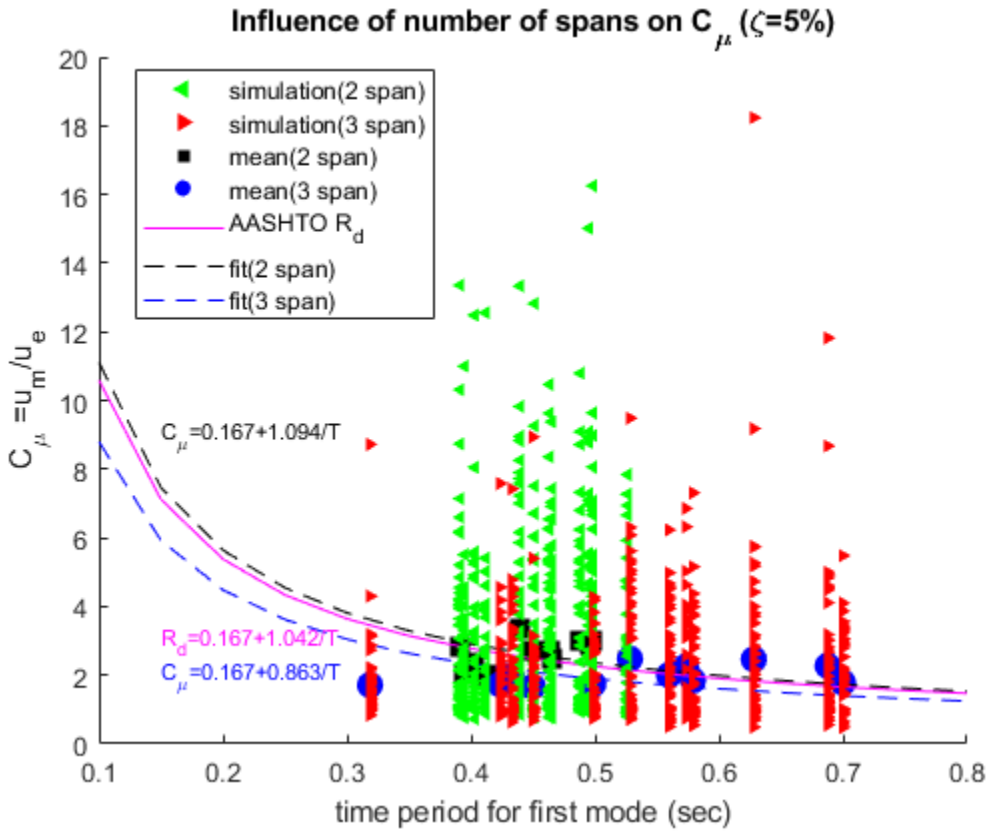

Figure 5.5. Influence of number of spans on inelastic displacement ratio for damping ratio of 5%

5.2.5. Influence of Damping

The linear and nonlinear time history analysis of six bridges with both pinned and fixed boundary conditions were performed for a damping ratio of 1%, 3% and 7% to study the influence of damping ratio on the inelastic displacement ratio. The analysis results are plotted in Figure 5.6, Figure 5.7 and Figure 5.8. The mean C_μ were computed for each of the cases and their respective fit equations were developed in MATLAB. The fit equations for 1%, 3% 5% and 7% of damping ratio are $C_\mu = 0.167 + 1.023/T$, $C_\mu = 0.167 + 1.077/T$, $C_\mu = 0.167 + 1.094/T$ and $C_\mu = 0.167 + 1.097/T$ respectively. These equations suggest that the inelastic displacement ratio increases with increase in damping ratio of the bridge system.

From the analysis result, it was observed that the elastic displacement increases with decrease in damping ratio (i.e. $u_o\ for\ \zeta = 1\% > u_o\ for\ \zeta = 3\%$, $u_o\ for\ \zeta = 3\% > u_o\ for\ \zeta = 5\%\ and\ u_o\ for\ \zeta = 5\% > u_o\ for\ \zeta = 7\%$)which is in agreement with Chopra [41]. This is because the damping dissipates the energy from the system. When a bridge system is subjected to earthquake ground motion, higher damping values reduce the magnitude of vibrations and thus reduces the response of the structure or the displacement. The inelastic displacements were also observed to be increasing with decrease in damping ratio. However, the proportion of this increment in elastic and inelastic displacement was not the same. In other words, the influence of damping in inelastic displacement is not similar to the influence of damping in elastic displacement.

To obtain a reduction factor similar to AASHTO $R_D = (0.05/\xi)^{0.4}$ when a bridge has different damping ratio than 5%, the values of a in equation $C_\mu = 0.167 + a/T$ that was used to fit the mean values of C_μ for different damping ratio were determined and plotted with respect to the damping ratio in Figure 5.9. A general fit equation $R_D = (b/\zeta)^d$ was used to fit a vs. ζ. The

best fit equation was obtained to be $R_D = (0.4888/\zeta)^{-0.037}$ as observed in Figure 5.9which can be rewritten as $R_D = (\zeta/0.4888)^{0.037}$. This equation is instead an amplification factor and shows that the inelastic displacement ratio increases with increase in damping ratio which is opposite the notion of AASHTO R_D.

The discrepancy between AASHTO R_D and R_D equation suggested in this study can be attributed to the type of system considered for the corresponding study. AASHTO R_D was developed based on the response of single degree of freedom which did not consider the nonlinearity in different component of bridges individually. However, in the present research work complete geometry of bridge and the material strength were considered in addition to the nonlinear behavior in column and the bridge abutment. Therefore, R_D equation suggested in this work is more practical.

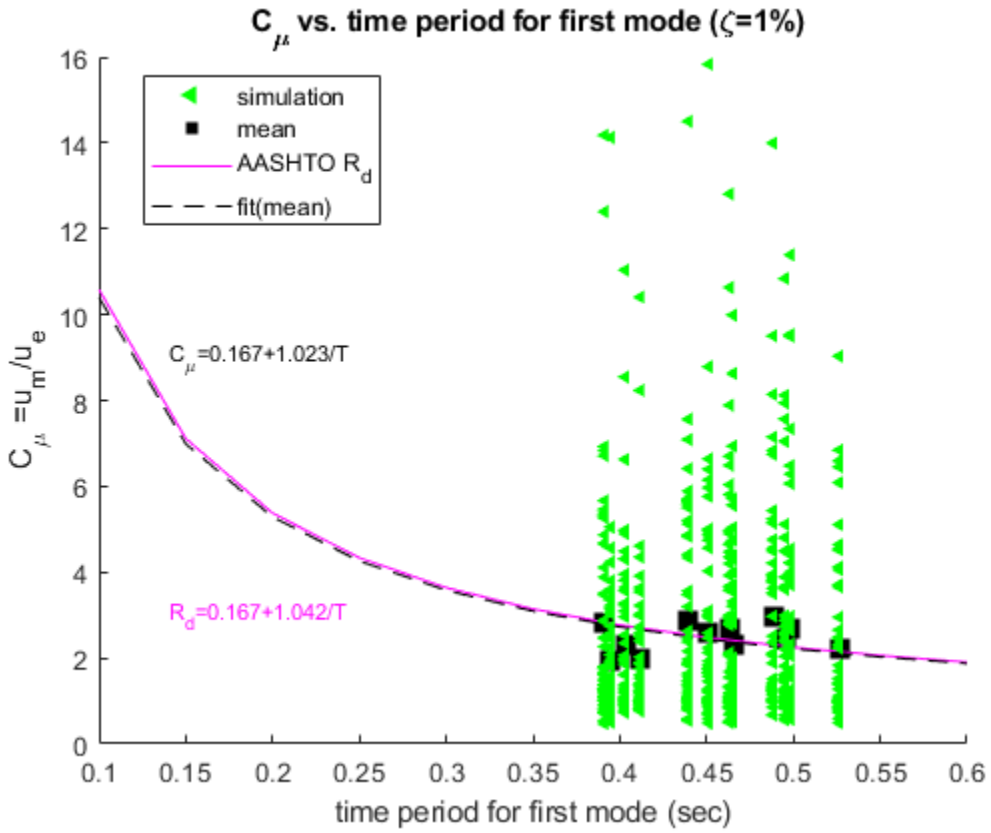

Figure 5.6. Inelastic displacement ratio for all bridges with 1% of damping ratio

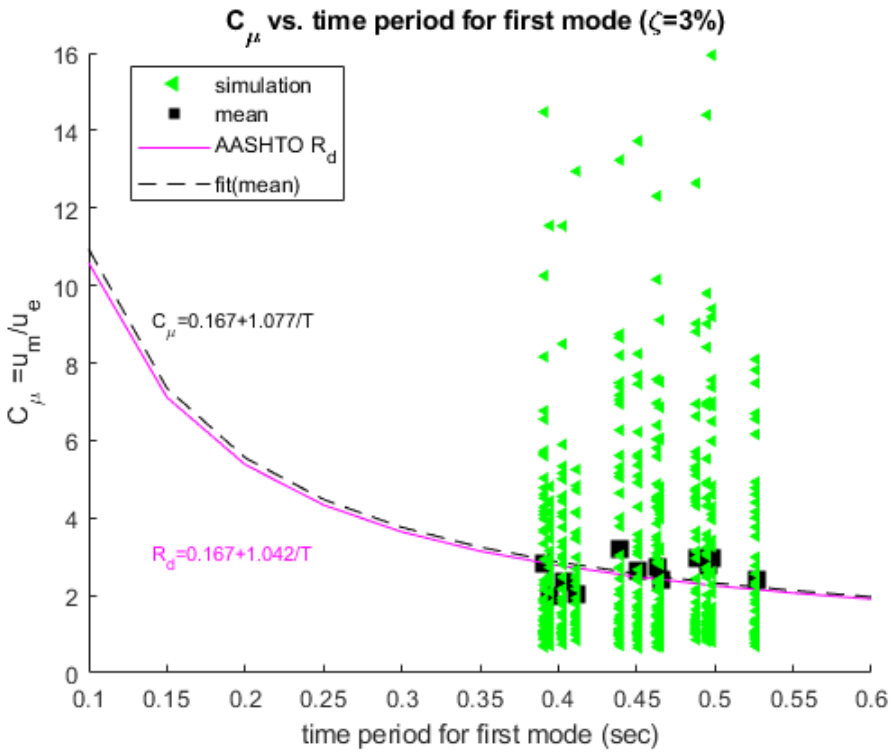

Figure 5.7. Inelastic displacement ratio for all bridges with 3% of damping ratio

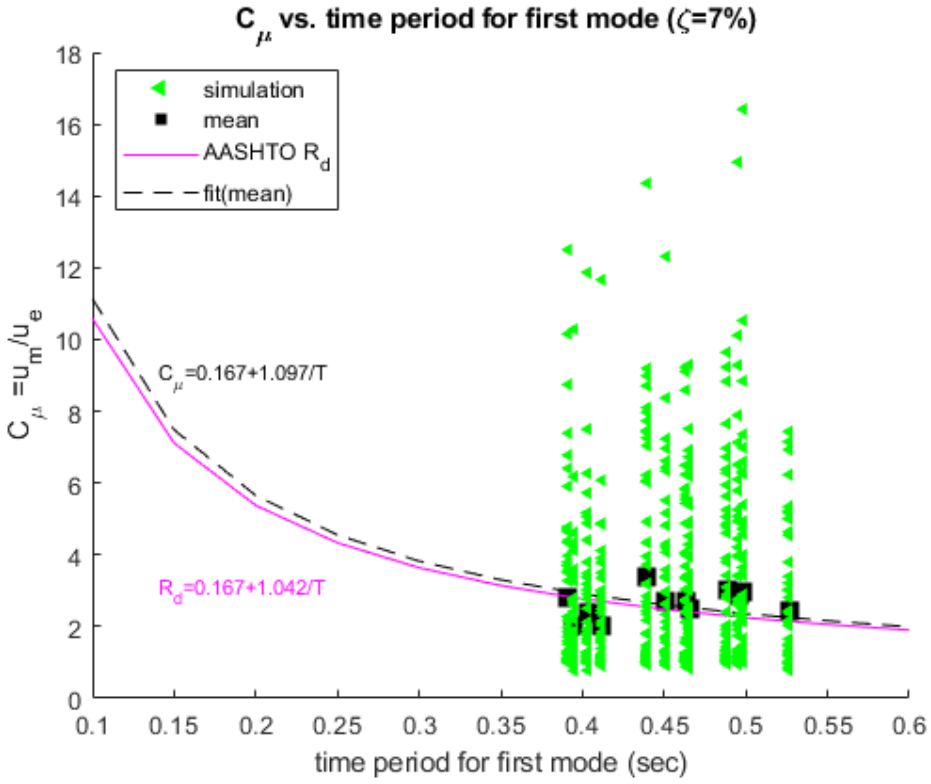

Figure 5.8. Inelastic displacement ratio for all bridges with 7% of damping ratio

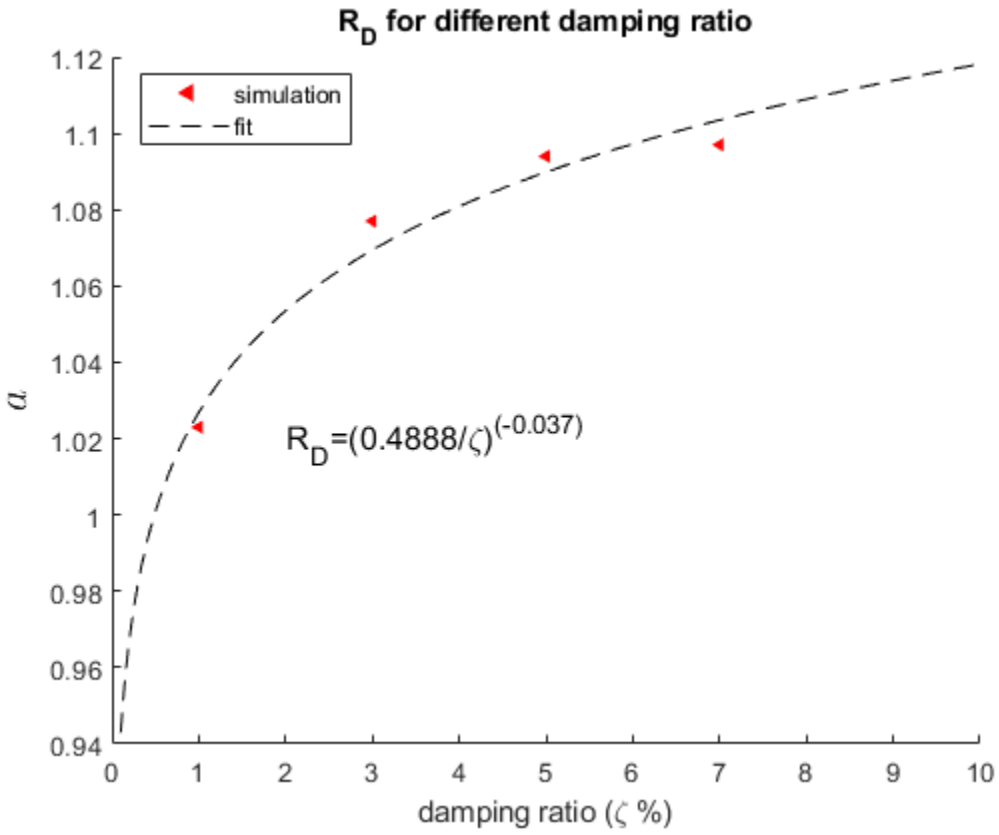

Figure 5.9. Influence of factor a with damping ratio

6. CONCLUSION

Six different reinforced concrete box girder bridges were modeled to develop the relationship between earthquake induced inelastic displacement ratio in bridges and time periods of their first modes of vibration. Both pinned and fixed connection of the column to the ground and 28 earthquake ground motions recorded in California in the past 55 years were considered. Two horizontal components of each of these earthquakes were applied in the longitudinal and transverse direction of the bridges. In reality, columns and abutments of the bridge structures show nonlinear behavior when subjected to earthquake events. Therefore, the nonlinear behavior was modeled in these two components while rest of the structural components like superstructure deck section and the bent cap were modelled elastically. The relationship developed from the mean values of inelastic displacement ratio corresponding to different earthquake events was found to close to the AASHTO R_d. However, AASHTO R_d can not predict the inelastic displacement ratio for wide range of earthquake ground motion, which is the limitation of the current approach. To address this variability in inelastic displacement ratio due to dynamic nature of bridge and wide range of earthquake ground motion, two additional equations were developed based on mean + SD and mean + 3×SD i.e. $C_\mu = 0.167 + 2.142/T$ and $C_\mu = 0.167 + 4.239/T$ respectively, which can better predict the inelastic displacement ratio.

From the parametric study, the following conclusions can be drawn.

- Connection of column to the ground: In case of the bridge column having pinned connection to the ground results in greater inelastic displacement ratio as compared to the fixed connection to the ground which. This is because of the increase in flexibility of the column due to the rotation of column and results in increase in displacement ratio.

- Column height: The inelastic displacement ratio has been increasing with the increase in the bridge column height. With the increase of column height, its stiffness decreases which results in increase in displacement, therefore, increasing the inelastic displacement ratio.
- Superstructure deck width: In case of increasing the deck width, the elastic displacement is observed to be decreasing since the stiffness of deck section increases, however, the width also increases the weight of superstructure deck which results in increases in earthquake force as well as inelastic displacement. Therefore, it can be concluded that the inelastic displacement ratio has a direct relation with the width of the deck section.
- Number of spans: An increase in the number of spans increases the elastic as well as inelastic displacement, however, with different proportions. The inelastic displacement ratio was found to be decreasing with increase in the number of spans. Therefore, it can be concluded that C_μ is inversely proportional to the number of spans.
- Damping ratio: Increasing the damping ratio increases the energy dissipation, reduces the vibration and thus, decreases the elastic displacement. The influence was in case of inelastic displacement, however, the proportion of this increment was not the same. Therefore, it can be concluded that the magnitude of influence of damping in elastic and inelastic displacement are different. And increasing the damping ratio increases the inelastic displacement ratio unlike to that suggested by AASHTO. Amplification factor $R_D = (0.4888/\zeta)^{-0.037}$ has been suggested from this research work, which needs to be multiplied with the parameter a in equation $C_\mu = 0.167 + a/T$ instead

of using $R_D = (0.05/\xi)^{0.4}$, a reduction factor suggested by AASHTO with $R_d = 0.167 + 1.042/T$ when the damping ratio is different than 5%.

Conclusively, in this research work, the limitation of AASHTO R_d across a wide range of earthquake ground motion was outlined, and two equations based on mean + SD and mean + 3×SD were proposed, which gives better estimate of C_μ in reinforced concrete box girder bridges. An appropriate amplification factor was suggested for different damping ratios of bridges and detailed parametric study on factors affecting C_μ was performed. Therefore, the objectives of this research works were achieved.

7. FUTURE WORKS

The following works can be performed in future to further advance this research area.

- Since this work is limited to reinforced concrete box girder bridges, detailed study on other different type of bridges including slab bridge, T-girder bridge, Arch bridge, and Truss bridge can be performed.
- Since simplified abutment modeling technique has been used in this work, therefore, a comparative study can be performed using other abutment modeling method like roller abutment and spring abutment.
- 28 earthquake ground motions were considered in this work. More earthquakes from different sites can be considered to study the influence of different soil condition, magnitude of earthquake, etc.

REFERENCES

[1] J. Zhang, S.-Y. Xu, and Y. Tang, "Inelastic displacement demand of bridge columns considering shear-flexure interaction," *Earthquake engineering & structural dynamics,* vol. 40, no. 7, pp. 731-748, 2011, doi: 10.1002/eqe.1056.

[2] J. P. Moehle, "Displacement-based design of RC structures subjected to earthquakes," *Earthquake spectra,* vol. 8, no. 3, pp. 403-428, 1992, doi: 10.1193/1.1585688.

[3] A. Whittaker, M. Constantinou, and P. Tsopelas, "Displacement estimates for performance-based seismic design," *Journal of Structural Engineering,* vol. 124, no. 8, pp. 905-912, 1998.

[4] ATC, "Tentative Provisions for the Development of Seismic Regulations for Buildings," *Report ATC 3-06,* 1978.

[5] ATC, "Structural Response Modification Factors," *Report ATC-19,* 1995.

[6] E. Miranda, "Evaluation of site-dependent inelastic seismic design spectra," *Journal of Structural Engineering,* vol. 119, no. 5, pp. 1319-1338, 1993.

[7] A. Banerjee and V. K. Gupta, "A statistical study of inelastic displacement ratio spectrum for existing structures," *Earthquake Engineering and Resilience,* vol. 1, no. 4, pp. 454-479, 2022.

[8] SEAOC, "Vision 2000- A framework methodology for performance-based earthquake engineering.," Structural Engineers Associations of California, 1995.

[9] E. Rosenblueth and I. Herrera, "On a kind of hysteretic damping," *Journal of the Engineering Mechanics Division,* vol. 90, no. 4, pp. 37-48, 1964.

[10] P. Gulkan and M. A. Sozen, "Inelastic Responses of Reinforced Concrete Structure to Earthquake Motions," *Journal Proceedings,* vol. 71, pp. 604-610, 1974.

[11] W. D. Iwan, "Estimating inelastic response spectra from elastic spectra," *Earthquake Engineering & Structural Dynamics,* vol. 8, no. 4, pp. 375-388, 1980.

[12] ATC, "Seismic Evaluation and Retrofit of Concrete Buildings," *Report ATC-40,* 1996.

[13] S. A. Freeman, "Evaluations of existing buildings for seismic risk-A case study of Puget Sound Naval Shipyard," in *Proc. 1st U.S. Nat. Conf. Earthquake Engrg.*, Earthquake Engineering Research Institute, Berkeley, Calif, 1975.

[14] S. A. Freeman, "Development and use of the capacity spectrum method," in *Proc. 6th U.S. Nat. Conf. Earthquake Engrg.*, Earthquake Engineering Research Institute, Oakland, Calif (on CD-ROM), 1998.

[15] N. M. Newmark and W. J. Hall, "Seismic Design Criteria for Nuclear Reactor Facilities," in *Proceedings of the Fourth World Conference on Earthquake Engineering*, Santiago, Chile, 1969, vol. II, pp. B4-37-B4-50.

[16] E. Miranda, "Inelastic displacement ratios for structures on firm sites," *Journal of structural engineering,* vol. 126, no. 10, pp. 1150-1159, 2000.

[17] E. Miranda, "Estimation of inelastic deformation demands of SDOF systems," *Journal of Structural Engineering*, vol. 127, no. 9, pp. 1005-1012, 2001.

[18] M. Rahnama and H. Krawinkler, *Effects of soft soil and hysteresis model on seismic demands*. John A. Blume Earthquake Engineering Center Standford, 1993.

[19] G. D. P. K. Seneviratna and H. Krawinkler, *Evaluation of inelastic MDOF effects for seismic design*. John A. Blume Earthquake Engineering Centre, Department of Civil Environmental Engineering, Stanford University, 1997.

[20] FEMA, "NEHRP Guidelines for the Seismic Rehabilitation of Buildings," *Reports FEMA 273 (Guidelines) and FEMA 274 (Commentary),* 1997.

[21] FEMA, "Prestandard and commentary for the seismic rehabilitation of buildings," *Report No. FEMA-356,* 2000.

[22] FEMA, "Improvement of nonlinear static seismic analysis procedures," *Report No. FEMA 440,* 2005.

[23] A. S. Veletsos and N. M. Newmark, "Effect of inelastic behavior on the response of simple systems to earthquake motions," in *Proceedings of the Second World Conference on Earthquake Engineering*, Japan, 1960, vol. 2, pp. 895-912.

[24] A. S. Veletsos, N. M. Newmark, and C. V. Chelapati, "Deformation spectra for elastic and elastoplastic systems subjected to ground shock and earthquake motions," in *Proceedings of the third world conference on earthquake engineering*, Auckland-Wellington, New Zealand, 1965, vol. 2, pp. 663-682.

[25] A. S. Veletsos and W. P. Vann, "Response of ground-excited elastoplastic systems," *Journal of the Structural Division,* vol. 97, no. 4, pp. 1257-1281, 1971.

[26] R. Riddell, *Statistical analysis of the response of nonlinear systems subjected to earthquakes*. University of Illinois at Urbana-Champaign, 1979.

[27] J. Ruiz-García and E. Miranda, "Inelastic displacement ratios for evaluation of existing structures," *Earthquake Engineering & Structural Dynamics,* vol. 32, no. 8, pp. 1237-1258, 2003.

[28] G. D. Hatzigeorgiou and D. E. Beskos, "Inelastic displacement ratios for SDOF structures subjected to repeated earthquakes," *Engineering structures,* vol. 31, no. 11, pp. 2744-2755, 2009.

[29] Y.-f. Wu, A.-q. Li, and H. Wang, "Inelastic displacement spectra for Chinese highway bridges characterized by single-degree-of-freedom bilinear systems," *Advances in Structural Engineering,* vol. 22, no. 14, pp. 3066-3085, 2019.

[30] Y. Bozorgnia, M. M. Hachem, and K. W. Campbell, "Deterministic and probabilistic predictions of yield strength and inelastic displacement spectra," *Earthquake spectra,* vol. 26, no. 1, pp. 25-40, 2010, doi: 10.1193/1.3281659.

[31] AASHTO, "AASHTO Guide specifications for LRFD seismic bridge design," American Association of State Highway and Transportation Officials, 2011.

[32] T. Huff and S. Pezeshk, "Inelastic Displacement Spectra for Bridges Using the Substitute-Structure Method," *Practice Periodical on Structural Design and Construction,* vol. 21, no. 2, p. 04015020, 2016.

[33] T. Huff, "Inelastic Seismic Displacement Amplification for Bridges: Dependence upon Various Intensity Measures," *Practice periodical on structural design and construction,* vol. 23, no. 1, 2018, doi: 10.1061/(ASCE)SC.1943-5576.0000355.

[34] A. Aviram, K. R. Mackie, and B. Stojadinović, *Guidelines for nonlinear analysis of bridge structures in California*. Pacific earthquake engineering research center, 2008.

[35] R. Omrani *et al.,* "Guidelines for nonlinear seismic analysis of ordinary bridges: Version 2.0," *State of California Department of Transportation,* 2015.

[36] Caltrans, "Seismic Design Criteria Version 1.3," Caltrans, 2004.

[37] Caltrans, "Bridge Design Practice 5.6," Caltrans, 2022, vol. Chapter 5.6.

[38] J. Lu, A. Elgamal, and K. R. Mackie, "Parametric study of ordinary standard bridges using OpenSees and CSiBridge," University of California, San Diego, 2015.

[39] Caltrans, "Seismic Design Criteria Version 1.7," Caltrans, 2013.

[40] ATC, "ATC-32 Improved Seismic Design Criteria for California Bridges: Provisional Recommendations," California Department of Transportation, Redwood City, California, 1996.

[41] A. K. Chopra, W. J. Hall, Ed. *Dynamics of Structures: Theory and Applications to Earthquake Engineering*, third ed. New Jersey: Prentice Hall, 2006.

[42] I. P. Lam and G. R. Martin, "Seismic design for highway bridge foundations," U.S. Dept. of Transportation, Federal Highway Administration, Research, Development, and Technology, 1986.

[43] A. Kotsoglu and S. Pantazopoulou, "Modeling of embankment flexibility and soil-structure interaction in integral bridges," in *Proceedings of First European Conference on Earthquake Engineering and Seismology*, Geneva, Switzerland, 2006.

[44] S. D. Werner, "Study of Caltrans' seismic evaluation procedures for short bridges," in *Proceedings of the 3rd Annual Seismic Research Workshop*, Sacramento, California, 1994.

[45] A. Bozorgzadeh, S. A. Ashford, and J. I. Restrepo, "Effect of backfill soil type on stiffness and ultimate capacity of bridge abutments," in *The 14th World Conference on Earthquake Engineering*, Beijing, China, 2008.

[46] Caltrans, "Caltrans Seismic Design Criteria Version 2.0," Caltrans, 2019.

[47] K. R. Mackie, M. H. Scott, K. Johnsohn, M. Al-Ramahee, and M. Steijlen, "Nonlinear time history analysis of ordinary standard bridges," California. Dept. of Transportation. Division of Engineering Services, 2017.

[48] K. Mackie and B. Stojadinovic, "Seismic vulnerability of typical multiple-span California highway bridges," in *Proceedings of the Fifth National Seismic Conference on Bridges & Highways*, San Francisco, 2006.

[49] B. H. Maroney and Y. H. Chai, "Seismic design and retrofitting of reinforced concrete bridges," in *Proceedings of 2nd International Workshop, Earthquake Commission of New Zealand*, Queenstown, 1994.

[50] A. Shamsabadi, P. Khalili-Tehrani, J. P. Stewart, and E. Taciroglu, "Validated simulation models for lateral response of bridge abutments with typical backfills," *Journal of Bridge Engineering*, vol. 15, no. 3, pp. 302-311, 2010.

[51] B. Maroney, "Large scale bridge abutment tests to determine stiffness and ultimate strength under seismic loading," *Ph. D. Dissertation, Univ. of California*, 1995.

[52] J. P. Stewart *et al.*, "Full scale cyclic testing of foundation support systems for highway bridges. Part II: Abutment backwalls," University of California, Los Angeles, CA, 2007.

[53] K. M. Rollins and R. T. Cole, "Cyclic lateral load behavior of a pile cap and backfill," *Journal of geotechnical and geoenvironmental engineering*, vol. 132, no. 9, pp. 1143-1153, 2006.

[54] K. M. Rollins and S. J. Jessee, "Passive force-deflection curves for skewed abutments," *Journal of Bridge Engineering*, vol. 18, no. 10, pp. 1086-1094, 2013.

[55] A. Shamsabadi and K. M. Rollins, "Three-dimensional nonlinear continuum seismic soil-structure interaction analysis of skewed bridge abutments," in *Proc. 8th European Conference on Numerical Methods in Geotechnical Engineering*, Delft, The Netherlands, 2014.

[56] A. Aviram, K. R. Mackie, and B. Stojadinovic, "Effect of abutment modeling on the seismic response of bridge structures," *Earthquake engineering and engineering vibration*, vol. 7, no. 4, pp. 395-402, 2008.